UiT The Arctic University of Norway

FACULTY OF SCIENCE AND TECHNOLOGY

Department of Geosciences

The geochemical signature of Cu mineralisation preserved in stream sediments from the Alta-Kvænangen Tectonic Window, Northern Norway

Johan Bang Hilmo

Master's thesis in Geology, GEO-3900

June 2021

Abstract

The Paleoproterozoic Greenstone Belts of Fennoscandia are metamorphosed and deformed volcanic and sedimentary basins with a high metallic ore potential. One of those, the Alta-Kvænangen Tectonic Window (AKTW), is exposed as a window below the Caledonides of Northern Norway. The Kåfjord area located within the AKTW hosts numerous known Cu occurrences. The Cu mineralisation in Kåfjord occurs mostly in the form of quartz-carbonate-sulphide veins hosted by magmatic and sedimentary lithologies.

While there is a demand for new ore deposits that can support the green energy transition, undiscovered deposits are partly or completely buried which has made exploration in recent years less efficient and more expensive. Streams carry material from their upstream drainage area, and therefore stream sediments can be used for exploration geochemistry to assess nearby mineralisation. The purpose of this master thesis is to identify the geochemical footprint and multi-element dispersion patterns of the Cu mineralisation in stream sediments sampled from streams draining the known Cu deposits in Kåfjord. Identification and analysis of the distribution of chemical elements will contribute to a more efficient targeting of Cu occurrences in the Fennoscandian Shield.

Stream sediments from three streams draining; (1) the sediment-hosted Cu mineralisation, (2) the mafic rock-hosted Cu mineralisation and (3) both the sediment- and mafic rock-hosted Cu mineralisation have shown different geochemical footprints. The bulk chemical composition of stream sediments exhibit a correlation between Cu and elements associated with the hydrothermal mineralisation in all three streams. Additionally, content of Cu in stream sediments seems to be associated with the respective lithologies hosting the mineralisation. Carbonate grains separated from stream sediments have isotopic compositions resembling the carbonates associated with both sediment- and mafic rock-hosted Cu mineralisation.

LA-ICP-MS analyses of individual grains separated from stream sediments resulted in multi-element data sets with minor and trace element compositions of specific minerals. The hydrothermal signature of sulphides separated from stream sediments is characterised by high contents of Ag and Se, but low concentrations of Ga. Furthermore, the hydrothermal signature of sulphides seem to be preserved in mineral aggregates derived from the oxidation of

sulphides, in so-called Fe-oxy-hydroxides. Thus, Fe-oxy-hydroxides can have the potential to be used as indicators for Cu mineralisation in the Kåfjord area.

Acknowledgements

This project, part of MinExTarget, has been funded and made possible my EiT Raw materials. I am very grateful to participate in such an interesting project.

I would like to thank my thesis advisors for all the support and guidance this past year. Sabina Strmic Palinkaš for your immense knowledge in the field and for taking time to discuss and answer my questions. Your incredible enthusiasm is very much appreciated. My co-supervisor Harald Hansen for your guidance during fieldwork and final suggestions.

I would like to thank my colleagues at UiT and from MinExTarget for their generous assistance. Carly Faber for helping me separate minerals and preparing mineral mounts, without you it would have taken much longer. Fredrik Sahlström for your guidance and discussions regarding the SEM. Yulia Mun for all the help throughout this past year. Hugh O'Brian from GTK for doing the LA-ICP-MS analyses and processing the immense data set. Thank you, Karina, Ingvild, Matteus and Trine at department laboratory, for your help and assistance.

Finally, I would like to thank my fellow students for the good company and encouragement during my time in Tromsø. A special thanks to my office mate and business partner, Sondre, for all our on- and off-topic discussions.

Johan Bang Hilmo

Tromsø, June 2021

Table of Contents

1 Introduction

1.1 Context of the study

The northern Fennoscandian Shield hosts numerous greenstone belts (Figure 1A). These deformed and metamorphosed volcano-sedimentary basins have been recognized as locations with a high metallic ore potential (e.g. Eilu, 2012). The Alta-Kvænangen Tectonic Window (AKTW) is one of the Paleoproterozoic Greenstone Belts, appearing as a north-western continuation of the Kautokeino Greenstone Belt (KKGB) and can be traced underneath the Caledonian nappes on aeromagnetic anomaly maps (Figure 1B) (e.g. Nasuti et al., 2015).

The AKTW hosts historical copper mines. The mines are located on the western side of Kåfjorden and the mineralisation occurs mostly in quartz-carbonate veins hosted by basaltic to gabbroic rocks and by dolostone and shale lithologies (Vik, 1985). Although there are several known copper deposits in the area that have been mined in the past, the copper deposits have not been a subject for detailed geochemical studies.

While there is a demand for new ore deposits that can support the green energy transition, undiscovered ore deposits are partly or completely buried which has made exploration in recent years less efficient and more expensive. Exploration geochemistry investigates the enrichment or depletion of elements to identify potential ore deposits. The use of stream sediment geochemistry for exploration purposes may be ideal in many scenarios because of the minimal environmental impact and the continuous improvement of analytical methods. However, reliable indicators for mineralisation can in many areas be difficult to identify (e.g. Hulkki et al., 2018).

The study is part of MinExTarget: Enhanced Use of Heavy Mineral Chemistry in Exploration Targeting, a project funded by EIT Raw Materials aimed at developing and introducing a new exploration tool which provides more efficient targeting in the early stages of mineral exploration. The concept is that the primary sources of geochemical and mineralogical anomalies can be better targeted and qualified by the determination of mineral associations and concentrations of trace elements together with stable isotope compositions in selected types of heavy mineral grains.

This thesis is one of two master projects offered within the framework of MinExTarget the academic year 2020-2021. Sondre Stenvold Simonsen has conducted a study on the primary mineralisation in the same area in the thesis entitled “Geochemistry of sediment- and mafic

rock-hosted Cu deposits in the Kåfjord area, Alta-Kvænangen Tectonic Window, Northern Norway", while this study is focusing on the associated stream sediments.

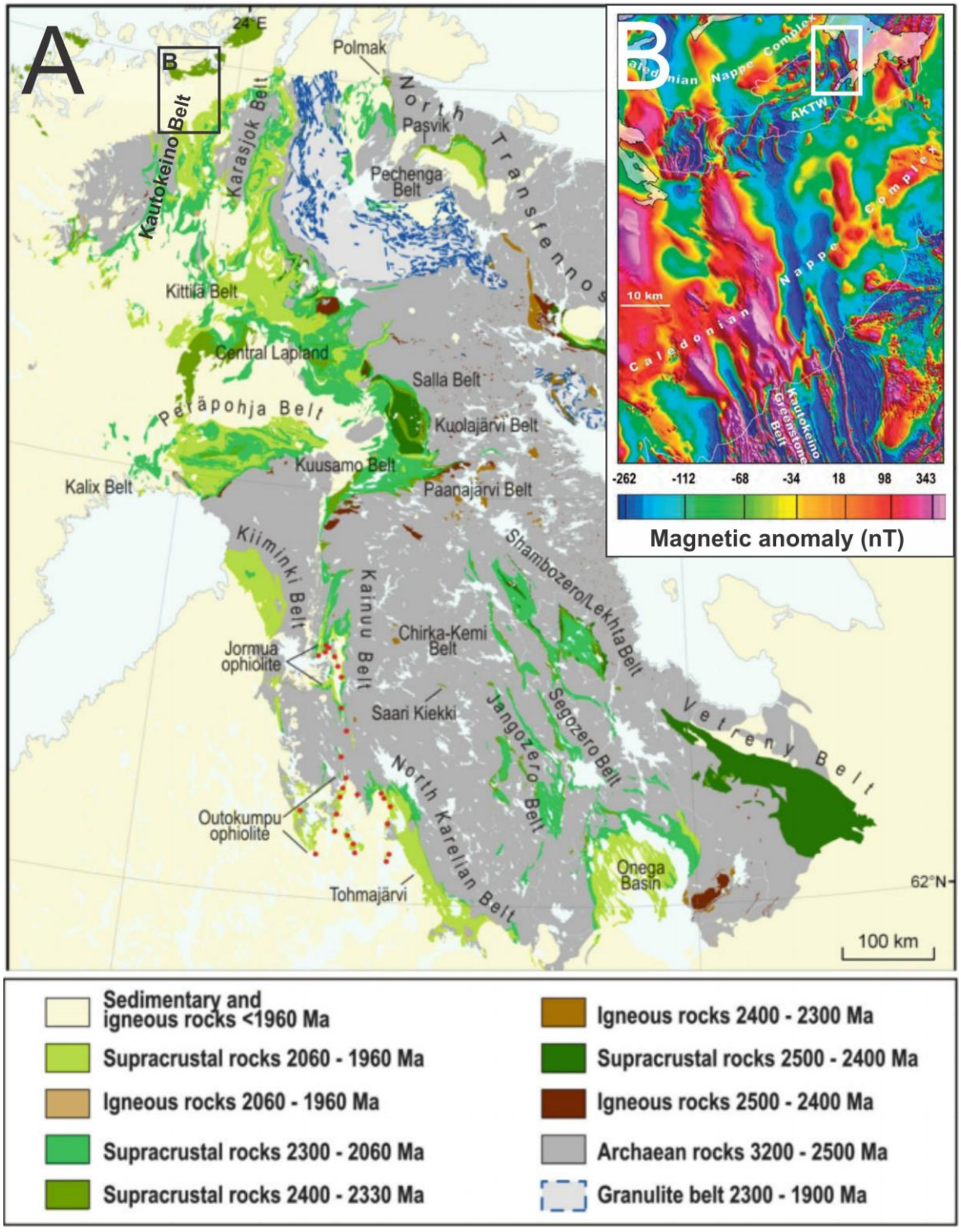

Figure 1: A: Geological map of the northern part of the Fennoscandian Shield highlighting the Paleoproterozoic rocks. Modified from Melezhik & Hanski (2013) *and based on* Koistinen et al. (2001). *B: Aeromagnetic anomaly map over the AKTW and the northern part of the KKGB. The positive magnetic anomalies of the KKGB can be traced beneath the Caledonian Nappe Complex into the AKTW. White frame marks the study area. Originally from* Nasuti et al. (2015)*, modified in* Melezhik et al. (2015)

1.2 Purpose of the study

The primary goal of this study is to determine if the geochemical footprint of the sediment- and mafic rock-hosted Cu mineralisation of the Alta-Kvænangen Tectonic Window can be identified in stream sediments, and if so to characterise that footprint and to define its multi-element dispersion pattern. Bulk chemistry of stream sediments that drain the mineralised area is combined with mineralogical, geochemical and stable isotope characteristics of individual mineral grains separated from the stream sediments. A statistical approach is applied in order discriminate pathfinder indicator elements of the Cu mineralisation hosted by the Alta-Kvænangen Tectonic Window.

1.3 Mining history

The following summary of the mining activities in Kåfjord is based on Moberg (1968).

After hearing rumours about copper in the mountains in Kåfjord, the English businessmen John Rice Crowe and Henry Woodfall assigned a young miner named Joseph Mitchell to further examine the potential copper deposits in 1825. The location was ideal with the ocean nearby. Large ships could dock just 100 meters from the potential facility. There also were streams running down from the mountain which could be used to crush and separate the ore. When Mitchell came back with positive news regarding the copper in the mountain, Crowe and Woodfall secured financial support from London and in 1826 The Alten Copper Works was established.

1827 was an important year for the future of the mining activities in Kåfjord. Men from Sweden, England and Røros in Norway were hired, and the mining could finally start. At the end of the year, the first ship was loaded with 32 tons of ore, probably containing around 5 wt.% copper, and sent to England. Despite having sold their first batch, the operation was not profitable yet. The following years Crowe and Woodfall expanded the operation, hiring more men and building them houses. Henry Woodfall preferred to build a lasting mining society in Kåfjord over hiring labour from England. Beyond the 1830s, families from southern Norway and northern Finland and Sweden relocated to Kåfjord. In 1837, the Kåfjord Church was built and by 1840 Kåfjord was by far the largest settlement in Finnmark with around 1000 inhabitants, most of whom were associated with the mining activities.

Both the production in Kåfjord and the price of copper decreased during the 1850s and 1860s, and with the high administration fees to London, the operation incurred a deficit. Even though expenses were reduced and new sites trialled, it was clear that the mining activities were coming to an end. The Alten Copper Works ran until 1878. Since 1843 around 62 000 tons ore had been extracted from the Kåfjord Field. A number of mines had been in operation, the largest and by far the most yielding mine being Storgruven (The big mine), also called Gamle gruven (The old mine). Other, smaller mines are often named after people involved in the company, such as Woodfalls, Mitchells and Wilsons mine.

In 1895, the mining activity in Kåfjord started up again under Nils Persson, a Swedish consul and owner of the mining company Sultitjelma Gruber. This period was characterized by continued mining in the old mines and with few new occurrences being discovered. In 1908, the mining activity ended again because of the ever-decreasing profitability and the small known ore reserve.

It is estimated that in the early years of mining in Kåfjord, ore with around 5 wt.% copper was extracted, probably even lower towards the end. Based on the deficient data, somewhere between 5 and 6 000 tons of copper has in total been extracted from the Kåfjord Field.

1.4 Description of the study area

1.4.1 Geological setting

1.4.1.1 The Fennoscandian Shield

The Fennoscandian Shield, also known as the Baltic Shield, is the north-western crustal segment of the East European craton and is composed of several major crustal segments (Figure 2). The continental crust of the Fennoscandian Shield was formed progressively over more than 2 billion years and shows a zonation in age with the oldest remnants situated in the north-east, and getting younger towards the south-west.

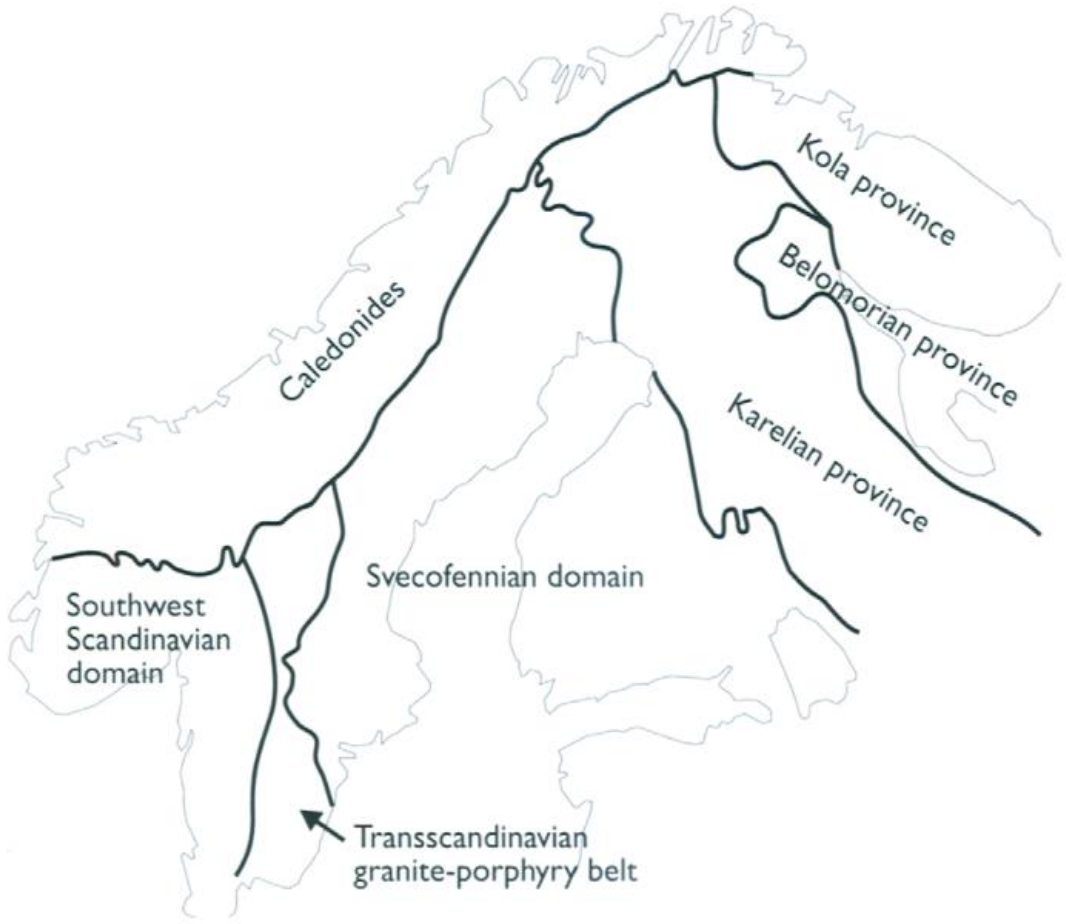

Figure 2: Crustal segments of the Fennoscandian Shield (from Lahtinen et al., 2005)

The earliest recognizable event of the Fennoscandian Shield is the Saamian Orogeny (≥3.1-2.9 Ga). During this event predominately tonalitic-trondhjemitic granitoids were formed. The late Archean Lopian cycle (2.9-2.7 Ga) created, deformed and altered the Lopian greenstone belts within the Karelian Province in eastern Finland and Russia (Gaál & Gorbatschev, 1987; Sorjonen-Ward & Luukkonen, 2005). Paleoproterozoic rifting of the Archean crust (2.505-2.1 Ga) resulted in the formation of numerous NW-SE-trending rift basins. The opening of the Kola Ocean and Svecofennian Sea (c. 2.1 Ga) followed by seafloor spreading and submarine eruptions of MORB-like pillow basalt (Melezhik, 2006; Lahtinen et al., 2008). During the collisional Lapland-Kola Orogen (1.94-1.86 Ga) in the north, the Kola Ocean and rift basins closed. The composite, partly overlapping, Svecofennian Orogen (1.92-1.79 Ga) forms a large unit of new Paleoproterozoic continental crust in the central part of the Fennoscandian Shield (Gorbatschev & Bogdanova, 1993; Lahtinen et al., 2005, 2008). The Transscandinavian Igneous Belt (1.81-1.67 Ga) separates the rocks formed during the Svecofennian Orogeny from the younger Mesoproterozoic rocks in southern Norway and Sweden. The Fennoscandian Shield grew along the active southwestern margin during the accretionary

Gothian Orogen (1.64-1.52 Ga) and the Sveconorwegian Orogen (1.14-0.9 Ga) (Bingen et al., 2008).

1.4.1.2 The Alta-Kvænangen Tectonic Window

The Alta-Kvænangen Tectonic Window (AKTW) is a northwestern continuation of the Kautokeino Greenstone Belt and can be traced underneath the Caledonian nappes on aeromagnetic anomaly maps (Figure 1) (Nasuti et al., 2015). The volcanic and sedimentary rocks of the AKTW constitute the Raipas Supergroup, base of which is unknown. They are tectonically deformed and metamorphosed at low greenschist facies. The Raipas Supergroup is unconformably overlain by the Bossekop and Borras Groups, comprised of dolostone and siltstone followed by sandstone, siltstone, conglomerate and tillite, respectively (Zwaan & Gautier, 1980).

1.4.1.3 Lithostratigraphy of the Raipas Supergroup in Kåfjord

Zwaan & Gautier (1980) divided the Raipas Supergroup into four formations: the Kvenvik formation, the Storviknes formation, the Skoađđovárri formation and the Luovosvárri formation. Only the three lower formations are present in Kåfjord (Figure 3).

The Cu mineralisation in the area is typically related to quartz-carbonate veins and can be divided into two distinct types: mafic rock-hosted and sediment-hosted. Sulphides hosted by the mafic rocks of the Kvenvik formation is mostly pyrite and chalcopyrite. Cu mineralisation found in Storviknes formation is more complex and appears in quartz-carbonate veins and in brecciated dolostone (Simonsen, 2021).

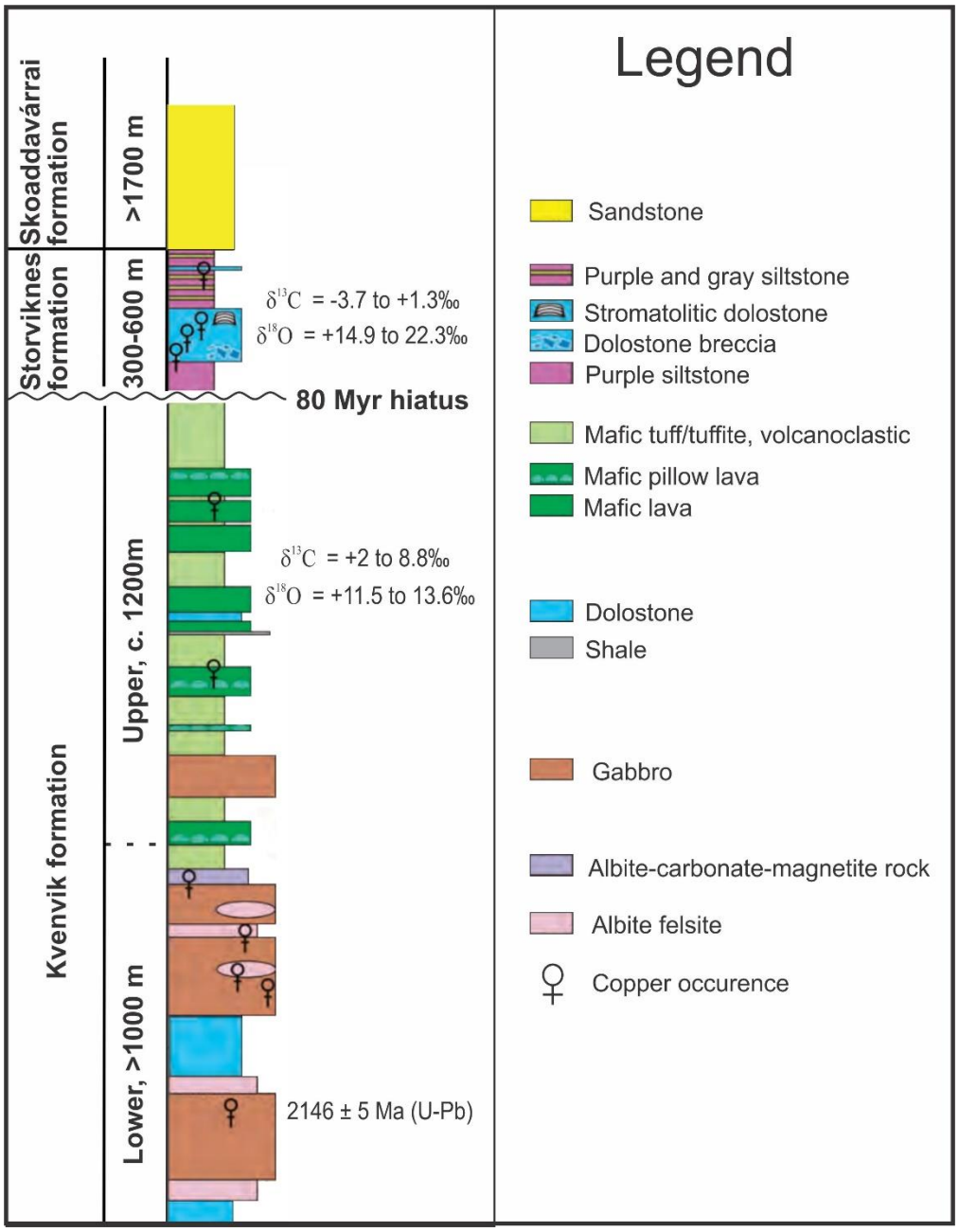

Figure 3: Simplified lithostratigraphic column of the Kvenvik, Storviknes and Skoaddovárri formations. Gabbro dated by Melezhik et al. (2015)*. Stable isotope compositions of carbonates from* Simonsen (2021)*, $\delta^{13}C$ and $\delta^{18}O$ values reported in VPDB and VSMOW, respectively. Entire figure modified from* Melezhik et al. (2015)*.*

The Kvenvik formation

The Kvenvik formation is the lowermost formation of the Raipas Supergroup. It has an unknown base and a thickness of >2200 m. The Kvenvik formation is a sequence of MORB-type, tholeiitic metabasaltic lavas and volcanoclastic rocks deposited cyclically in a shallow-water to terrestrial environment (Bergh & Torske, 1988). Vik (1985) divided the Kvenvik formation into a lower (>1000 m) and upper (c. 1200 m) unit based on lithological composition. The lower unit is comprised of dolomites and volcanoclastic sediments, intruded

by gabbroic sills, whereas the upper part is mainly composed of basaltic lavas and volcanoclastic sediments (Vik, 1985).

The mineralisation hosted by the mafic rocks of the Kvenvik formation is epigenetic and found in close relation to quartz-carbonate veins. Main ore minerals are pyrite [FeS_2] and chalcopyrite [$CuFeS_2$] with sphalerite [(Zn,Fe)S] occurring locally as an accessory mineral (Simonsen, 2021). Work by Melezhik et al. (2015) dates the deposition of the Kvenvik formation to between <2220 and 2146 ± 5 Ma, and suggests a hiatus of over 80 Ma, separating the depositional history of the Kvenvik formation from overlying the Storviknes formation.

The Storviknes formation

The 300-600m thick sedimentary Storviknes formation overlies the Kvenvik formation and is composed of partly brecciated and stromatolitic dolomites and shales (Bergh & Torske, 1988). Melezhik et al. (2015) suggested a minimum age of 2060 Ma for the formation. The formation hosts several Cu mineralisations, including the historic Anna and Lundstrøm mines. These mineralisations occur in relation to quartz-carbonate veins with chalcopyrite [$CuFeS_2$], bornite [Cu_5FeS_4] and digenite [Cu_9S_5] as main ore minerals. Molybdenite [MoS_2], tennantite [$(Cu,Fe)_{12}As_4S_{13}$], wulfenite [$PbMoO_4$], covellite [CuS] and wittichenite [Cu_3BiS_3] occur as accessory minerals (Simonsen, 2021).

The Skoađđovárri formation

The Storviknes formation is overlain by the sedimentary Skoađđovárri formation, at least 1700 m thick, mainly composed of sandstone, conglomerate and pebbly sandstone and shale. The formation is interpreted to be deposited in a subsiding marine basin as deltaic deposits by Bergh & Torske (1986). The Skoađđovárri formation appears in the centre of a southwards-trending syncline in the study area (Figure 4).

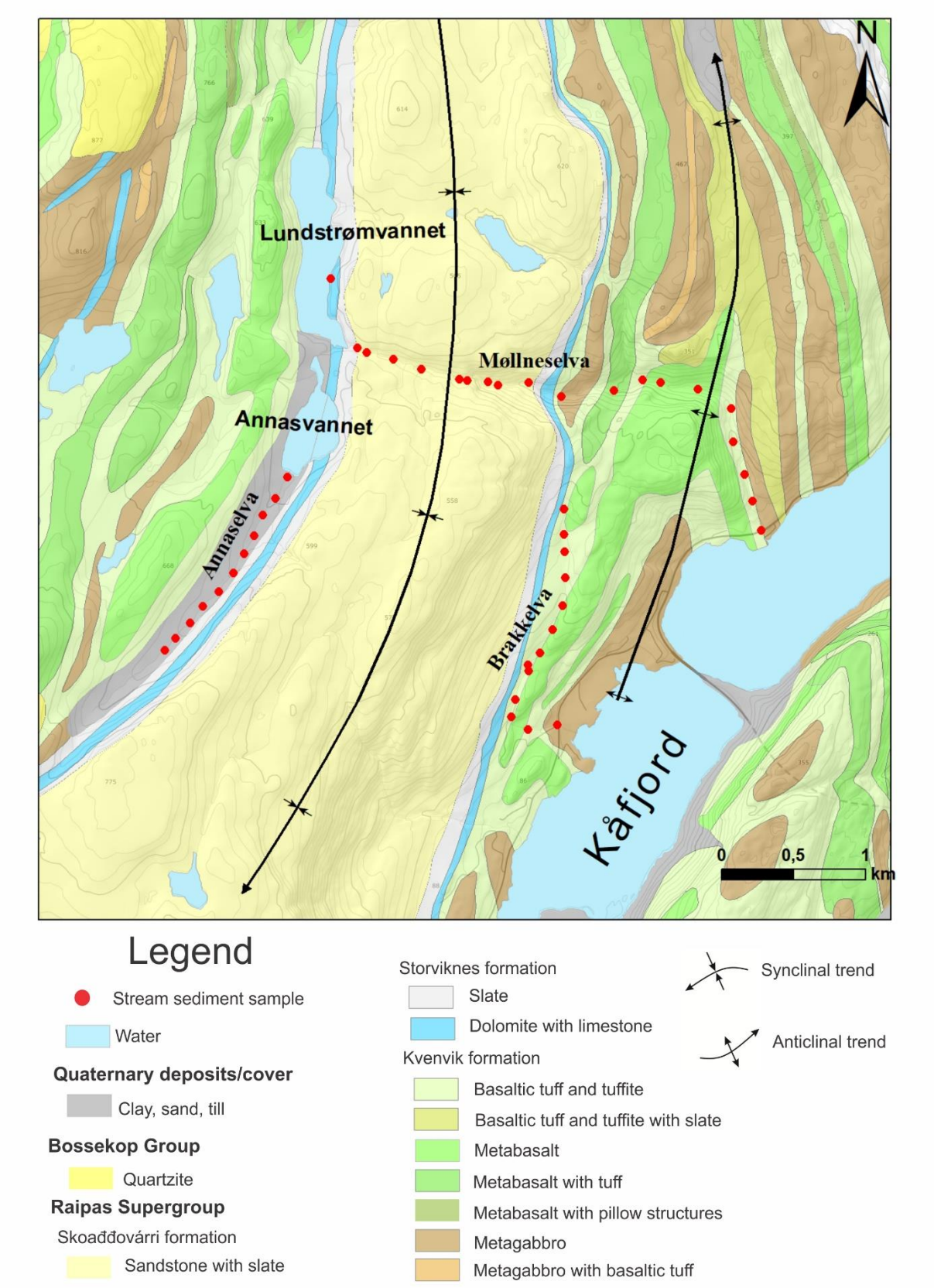

*Figure 4: Geological map of the bedrock in the study area. Base map m*odified after The Geological Survery of Norway (2021a) *with structures from* Bergh & Torske (1988)*. Sampling locations of stream sediments are marked. Sample numbers are indicated on Figure 10.*

1.4.2 Quaternary geology

The study area stretches from sea level and up to around 700 meters of elevation. Outcrops are rare in valleys, on concave slopes, and within low-lying and more densely vegetated areas, whereas north-south trending ridges at higher elevations show an abundance of outcrops. The most noticeable Quaternary deposits in the area are the avalanche deposits in the steep valley of the Møllneselva stream and the glacifluvial sediments between Annasvannet and Lundstrømvannet (Figure 5). Other Quaternary deposits in the area are till of varying thickness.

Several periods of glaciation affected the area throughout the Quaternary period (Mangerud et al., 2011). The last ice age (Weichselian, c. 115 000-11 600 before present) eroded the older glacial sediments, therefore most of the Quaternary deposits are from the last period of glaciation (Mangerud et al., 2011; Stroeven et al., 2016). The ice flow dynamics during Last Glacial Maximum are well documented. In northern Norway, and around Alta, the ice sheet came from the south and propagated north-westwards out into the sea and the Bjørnøya fan (Mangerud et al., 2011).

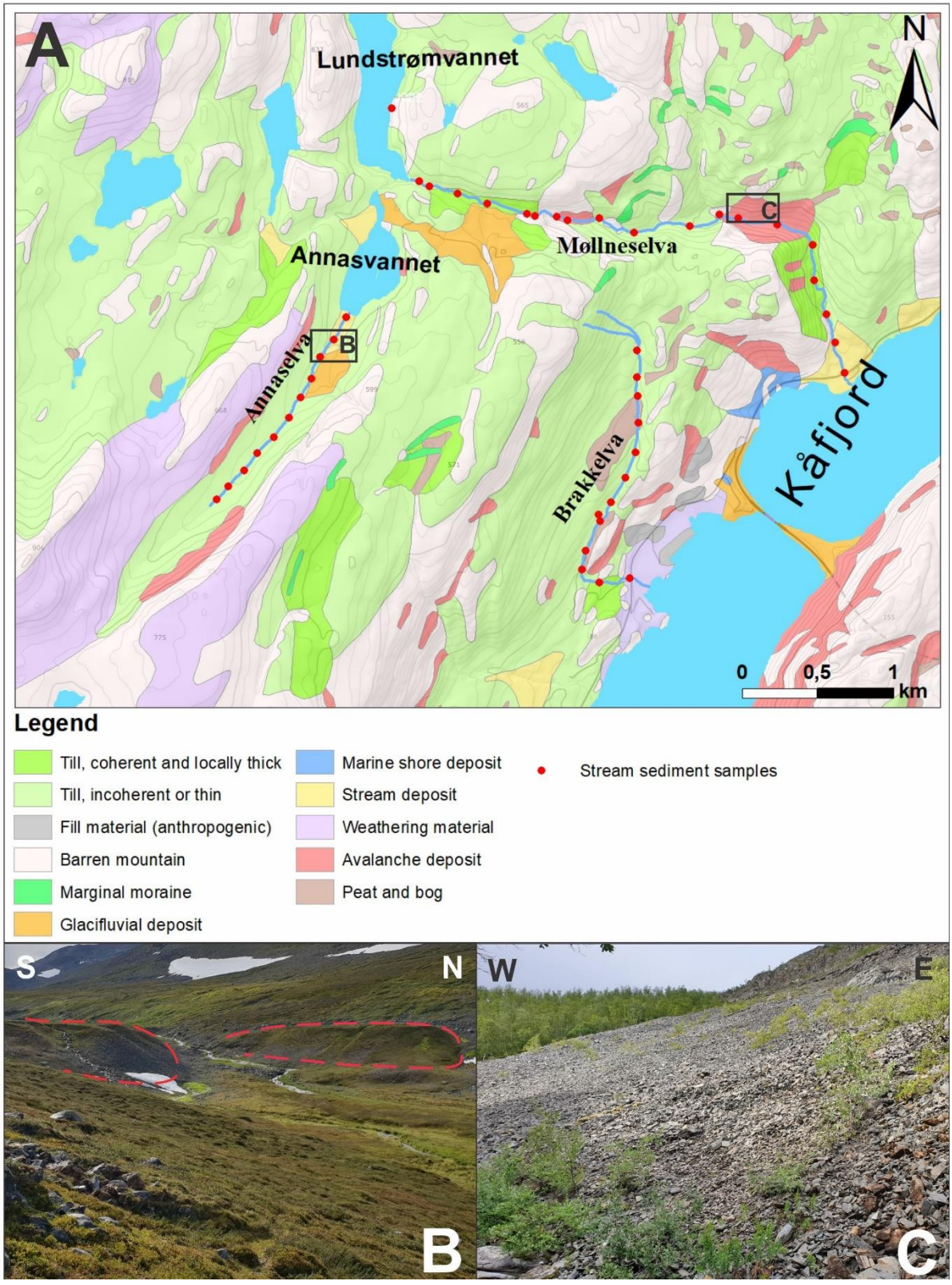

Figure 5: Overview of the Quaternary geology in the study area. A: Quaternary geologic map of the study area with black frames highlighting the location of Figures 5B and 5C. B: Photograph of Quaternary sediments (red outline) mapped as glacifluvial deposits and the Annaselva stream. C: Photograph of avalanche deposits in the steep valley of Møllneselva. Base map: (The Geological Survery of Norway, 2021b).

1.5 Climate and surface hydrology

Because of the mountainous character of the study area, there is a significant variation in vegetation and climate along the three streams that sediments are sampled from. According to data from The Norwegian Water Resources and Energy Directorate (NVE) and The Norwegian Meteorological Institute, mean annual precipitation during the years 1971-2000 in the study area ranged from 500-750 mm and up to 1000-1500 mm in the highest elevated areas. The mean annual temperature during the same time period was between -2 and +2 °C (senorge.no, 2021).

A basic overview of the drainage basins and some of the main characteristics of each of the streams are generated and presented using NVEs NEVINA mapping service, nevina.nve.no. NVE describes NEVINA as a mapping tool which calculates the drainage basin and various field parameters for a chosen point in a watercourse. The calculation is based on natural relationships in the area and does not consider active regulations which may be in place (Norges vassdrags- og energidirektorat, 2019).

The point for the calculation for each of the three streams was selected as the location furthest downstream where a sample was taken. By doing this, a large drainage basin constituting all of the upstream sampling locations is generated (Figure 6). Additionally, a few of the main catchment characteristics are generated with the NEVINA-computation (Appendix A), are summarized in the description of the streams.

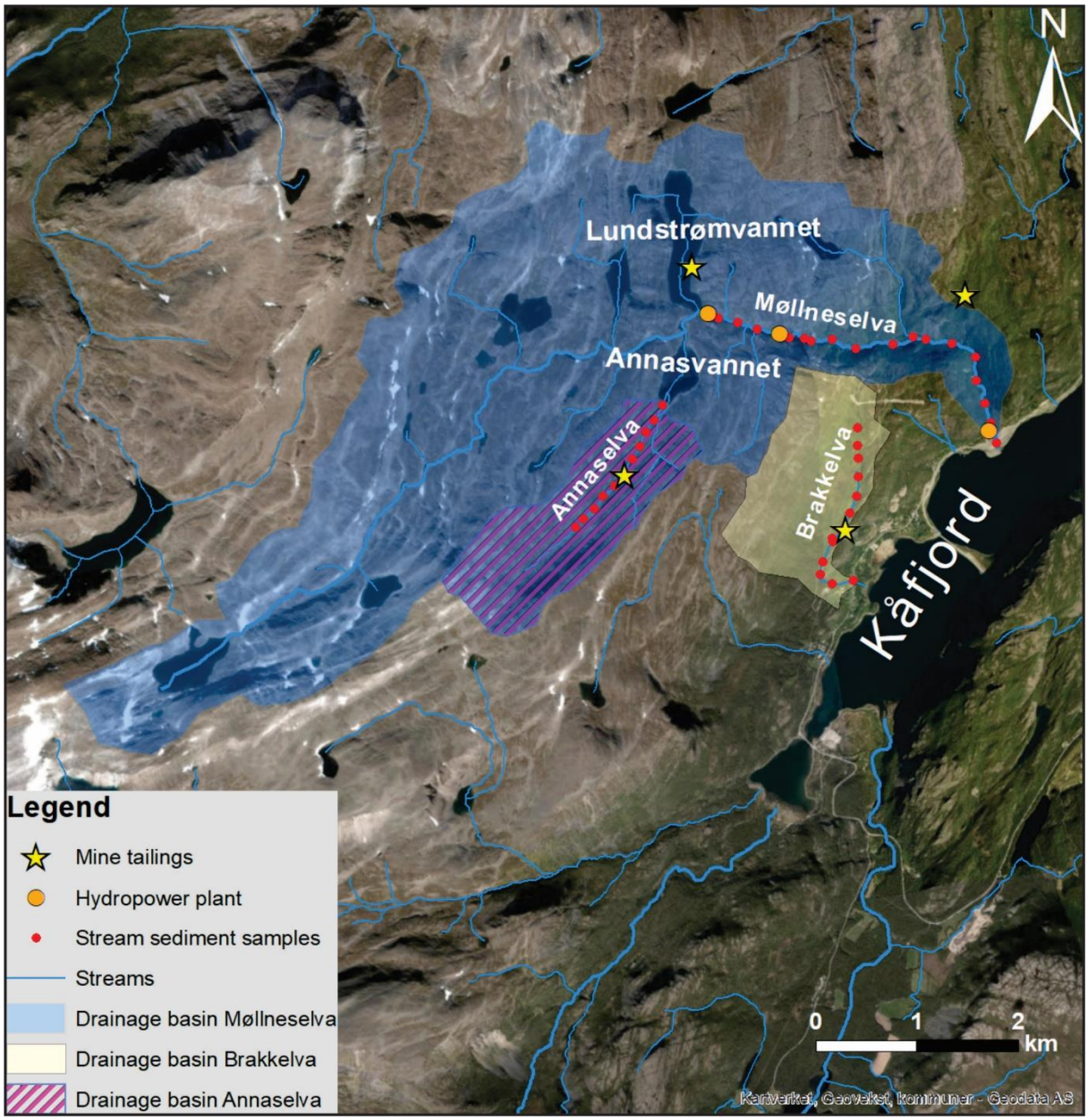

Figure 6: Overview of the streams in the study area and a projection of drainage basins computed using NVEs NEVINA mapping service. Main streams and tributaries are from NVEs ELVIS elvenett map (Norges vassdrags- og energidirektorat, 2020, 2021a).

Annasvannet and Lundstrømvannet are connected with a narrow channel, and the drainage basins for the Annaselva and Møllneselva streams are therefore overlapping. Within and in close vicinity of the generated drainage basins are several tailings from the mining activity in the area (marked with yellow stars in Figure 6). These tailings are composed of material with a large erosional surface and anomalous metal concentrations relative to the surrounding geology. Their location and distance from the streams may be an important factor for the mineralogy and bulk chemistry of the stream sediment samples.

Møllneselva

The Møllneselva stream is part of a longer branched river system and receives input from a number of tributaries. Multiple streams and small lakes, to the west and south-west in Figure 6, are part of the computed drainage basin of Møllneselva, but are outside the study area and were not considered during field work. The part of Møllneselva which was sampled for stream sediments runs through all of the main geological formations that are present in the study area.

In Møllneselva there are three constructions, part of the Mølleelva hydropower facility (marked as orange circles in Figure 6). A concession for the hydropower plant was given in 2010 and it has been operating since 2018. Farthest upstream there is a dam which regulates the amount of water in Lundstrømvannet. Downstream is a second dam where some of the water is taken out of the river and forced into an underground pipe, leading down to the third construction. At the third and furthest downstream hydropower plant construction the water from the pipe joins back with the main stream of Møllneselva (Norges vassdrags- og energidirektorat, 2021b). Consequently, the discharge between the second and third hydropower construction must be lower than what the NEVINA-computation indicates with a run-off of 31.8 l/s*km^2. It should also be noted that there are considerable encroachments along the river course of Møllneselva with excavation work and cementation of the dams (Figure 7).

The drainage basin of Møllneselva is quite large, covering 22.9 km^2, with most of the area comprised of barren mountain (86.6%), forest (6.6%) and lakes (6.3%) (Appendix A).

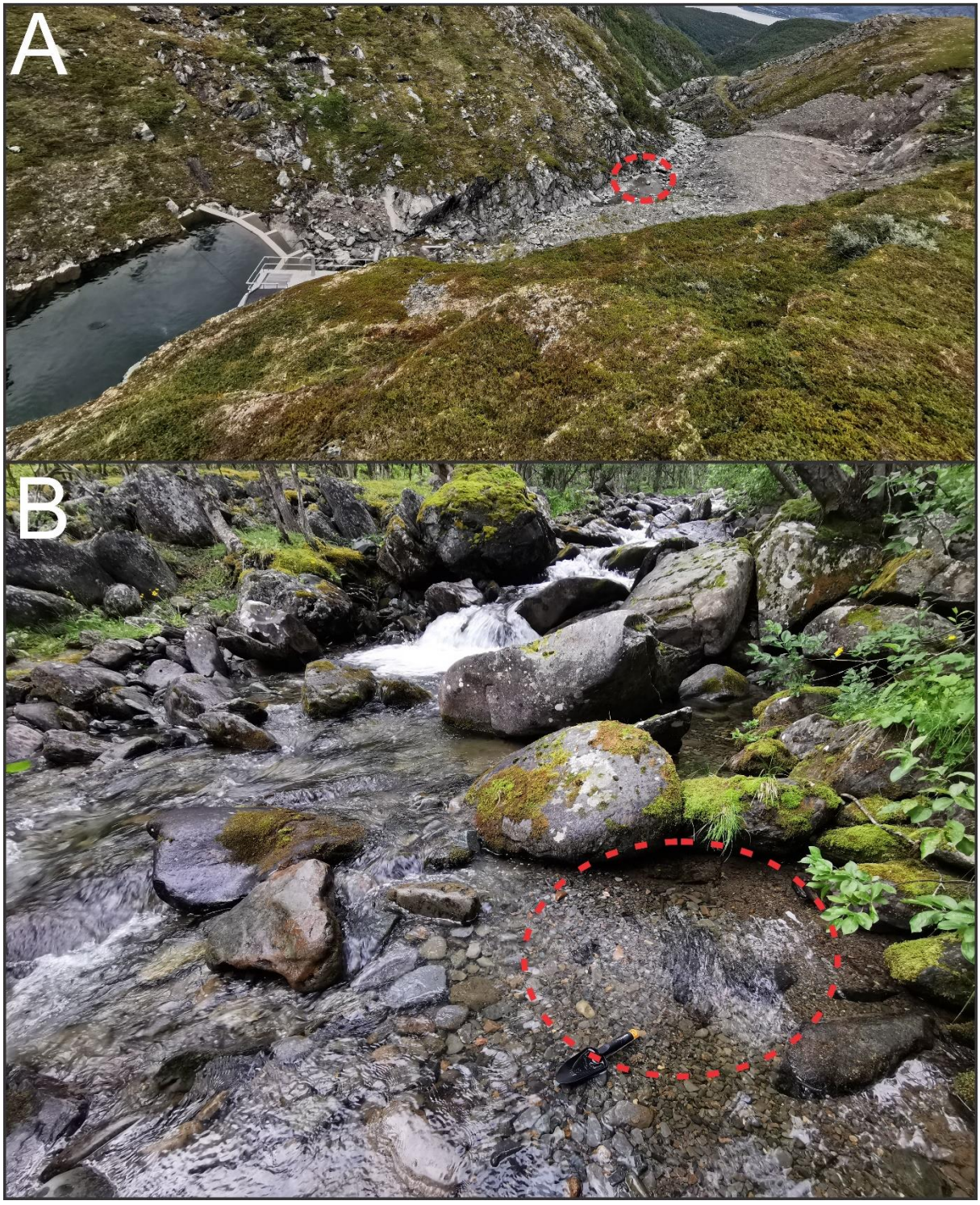

Figure 7: Photographs of the Møllneselva stream. A: Photo of the second dam and the excavation. Approximate sample location of J018 is marked. B: Downstream of the second dam where the sides of the stream are more vegetated. Red circle marks a typical sampling site for stream sediments in Møllneselva with little vegetation in the stream channel and coarse sediments, sampling location J032.

Annaselva

Annaselva is a small stream running into Annasvannet. It flows parallel to the sediment-hosted Cu mineralised carbonate and shale lithologies of the Storviknes formation. The drainage basin is quite small and has no additional streams joining the main stream. However, there is a smaller stream running parallel, just east of Annaselva, which is within the drainage basin (Figure 6). The tailings of Anna mine lie just a few meters from the stream and sample location J007 (Figure 8A). The stream channel of Annaselva is wide and packed with boulders further upstream. It is more vegetated once it flows through the glacifluvial deposits where the sides of the stream display growth of turf (Figure 8B). In general, the stream flows at a steady, quiet pace and there are only sparse amounts of sediments to be sampled.

The run-off is around 32.2 l/s*km^2 which is similar to the drainage basin of Møllneselva, and almost all of the 2.5 km^2 area is classified as barren mountain (99.9%) (Appendix A). However, it is evident that there are Quaternary deposits within the drainage basin of Annaselva and there is often a thin cover of vegetation (Figure 8).

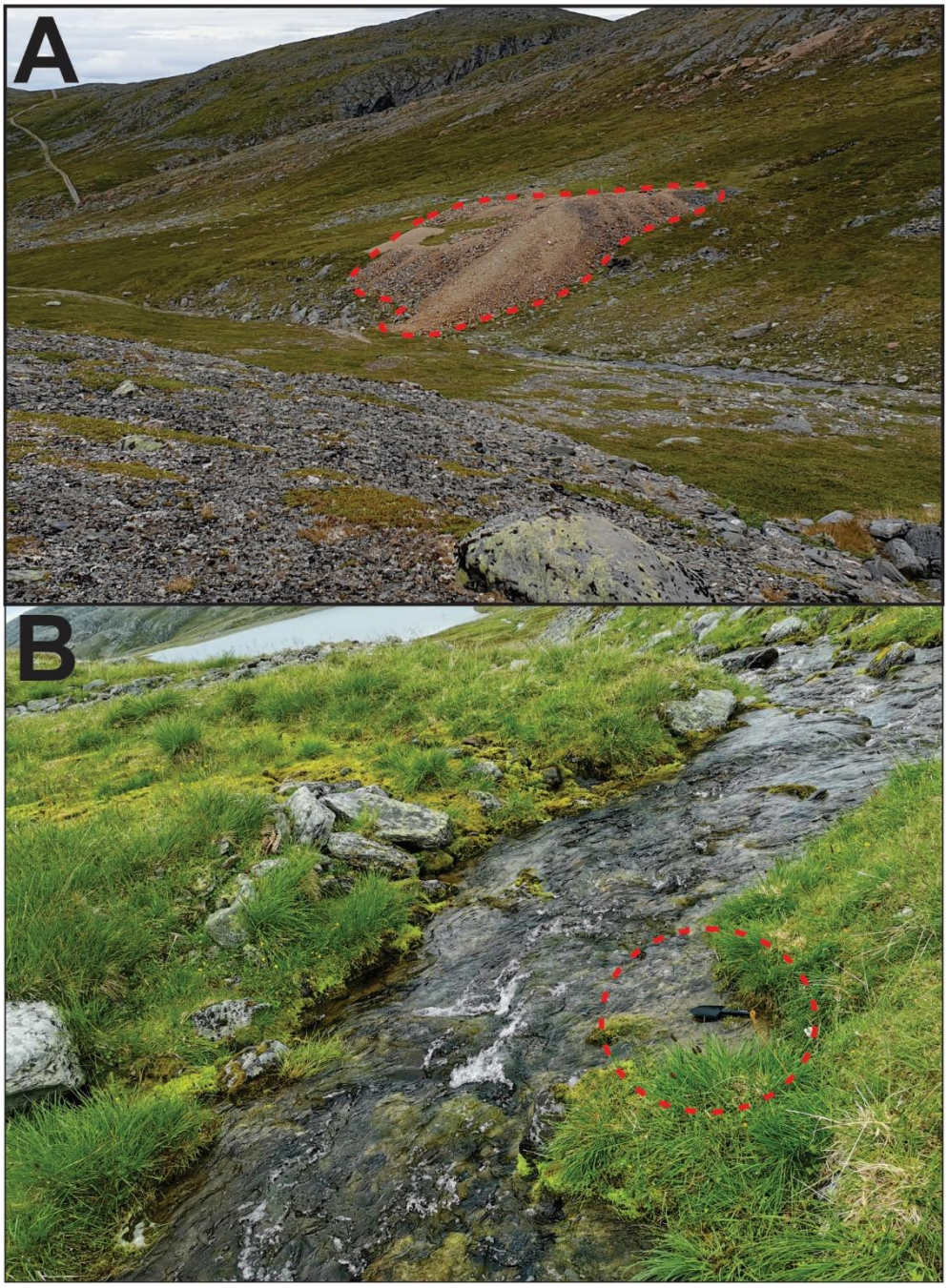

Figure 8: Photographs of Annaselva. A: Section where the stream channel is filled with boulders. The tailing of Anna mine is outlined. B: A few metres upstream from where the stream runs through the Quaternary glacifluvial deposits and where the surrounding vegetation is characterized by turf. The red circle marks a typical sample location where some sediments accumulate, sample location J010.

Brakkelva

Brakkelva primarily runs through and along lithologies of the Kvenvik formation in an area with mafic rock-hosted Cu mineralisations. The tailing of Mitchells mine is partly inside the drainage basin and is close to sample location J039. The surface area within the drainage basin is densely vegetated with 55.5% of it classified as forest and 3% bog. The mean annual

precipitation is less within this low lying drainage basin than the other two, as reflected in the computed run-off (14.5 l/s*km^2) (Appendix A).

Brakkelva receives input from a few small streams, all of which are originating from within the drainage basin and joining the main stream from west. Sample J016 is from such a tributary, emerging from a carbonate unit of the Storviknes formation and feeds into an area of bog where the main stream channel of Brakkelva runs (Figure 9A).

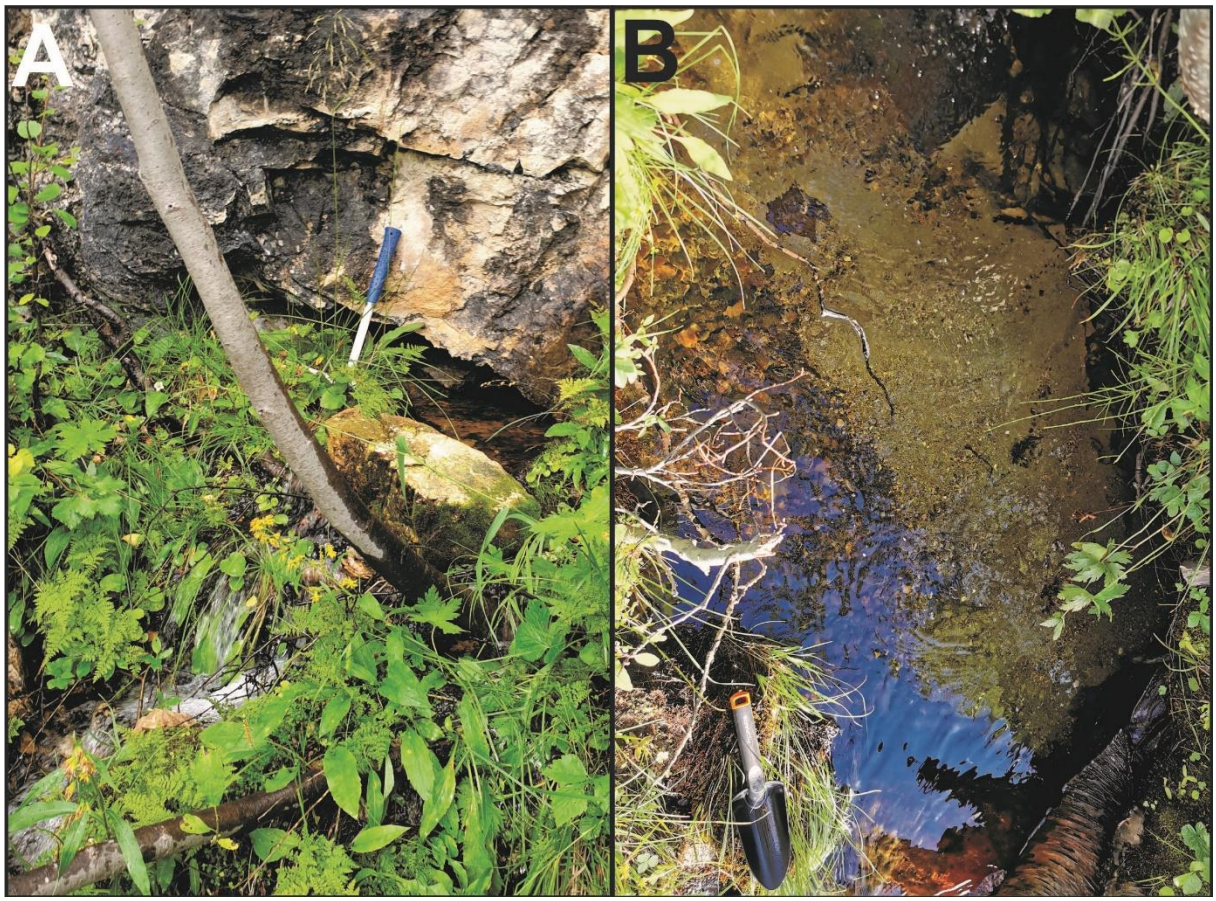

Figure 9: Photographs of Brakkelva. A: Tributary emerging from a barren carbonate unit of the Storviknes formation. Sample J016 was collected from this tributary. B: Sample location J040. Typical sampling site for stream sediments in Brakkelva, characterized by fine-grained material with vegetation and organic material within the stream channel.

1.6 Methods

1.6.1 Sampling

Field work took place on the western side of Kåfjorden, Alta, from the 10th to the 20th of August 2020. The goal was to collect representative lithological samples of the Cu mineralisation (see Simonsen, 2021) and stream sediment samples from streams that drain the sediment- and mafic rock-hosted Cu mineralisation (this work).

When sampling the stream sediments, the uppermost 1-2 centimetres of sediments were removed where there was an abundant amount of material available. This was done to minimize uncertainty related to frequent variations of the streamflow. Generally, fine-grained sediments were targeted when sampling stream sediments to ensure sufficient amounts of the fine fractions was collected. Areas of the streams where the current was weak was favoured, such as backwaters, behind large boulders or stream pools that occur after small waterfalls. Additional samples (B- and C-samples) were taken at most of the localities to ensure adequate amounts of material of different grain-sizes. However, only the A-samples have been used in this project, and B- and C-samples have been archived. A plastic soil trowel was used to scoop sediments into plastic bags which were sealed with a zip-lock. In total, stream sediment samples were taken at 44 locations mainly along three different streams: 1) Møllneselva; 2) Annaselva and 3) Brakkelva (Figure 10). The sampling spacing ranged from 150 to 250 m and GPS coordinates were taken at each sampling location with a Garmin GPSMAP 64st (Table 1).

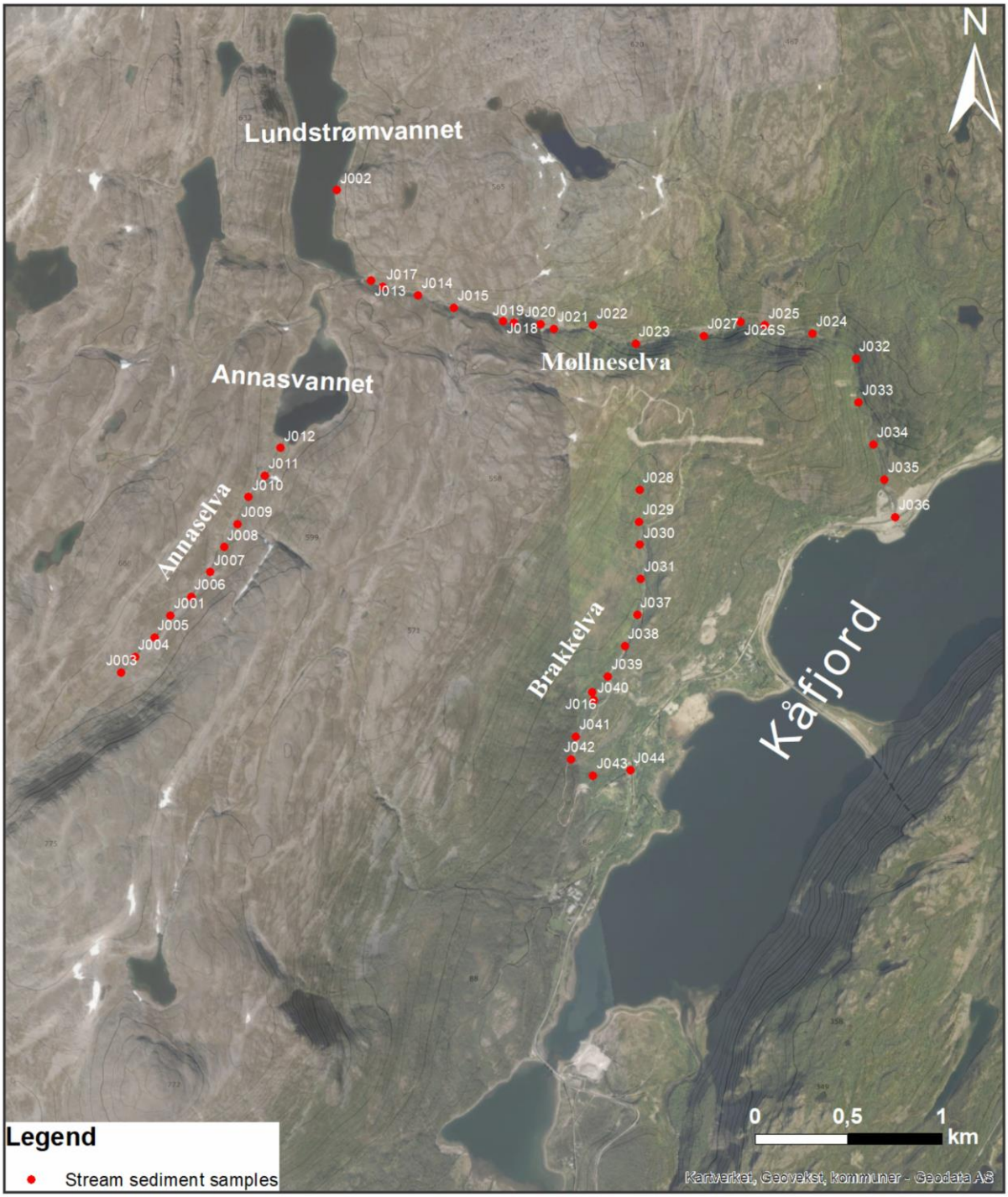

Figure 10: Overview of the study area with the targeted streams and sampling locations.

Table 1: List of samples including field observations of the water depth before sediments were removed, thickness of sediment cover which was removed, the colour of sampled sediments and general field notes of some sampling sites.

Sample	Water depth (cm)	Sediments removed (cm)	Colour of sediments	Field notes
J001	10	0	Brown	
J002	5	4	Dark brown	At the partly underwater tailing of Lundstrøm mine
J003	15	10 (boulders/gravel)	Brown	Weak current, 10 m wide stream filled with boulders
J004	3	4 (gravel)	Brown	
J005	15	0	Light brown	Stronger current, 5 m wide and some boulders. Some humus.
J006	10	0.5	Light brown	Stronger current, 2 m wide.
J007	5	1	Brown	Right below tailing of Anna mine.
J008	7	4	Brown	150-200m downstream from tailing of Anna mine
J009	10	2.5	Brown	
J010	3	3	Brown	
J011	5	3 (gravel)	Brown - grey	Influx of sediments from quaternary deposits?
J012	5	3 (gravel)	Brown - grey	Influx of sediments from quaternary deposits?
J013	10	2	Brown	Downstream from first newly built dam.
J014	20	3	Dark grey	
J015	15	0.5	Dark brown	
J016	5	2	Dark-black	Small tributary emerging from a barren carbonate unit.
J017	20	1	Brown - dark brown	
J018	2	3	Dark brown	Downstream from the second, newly built dam where water is taken out of the stream.
J019	3	2	Brown - grey	
J020	1	7	Brown	
J021	3	5	Brown - grey	
J022	5	2	Brown - grey	
J023	4	2	Grey	

Table 1: (Continued).

Sample	Water depth (cm)	Sediments removed (cm)	Colour of sediments	Field notes
J024	6	2 (gravel)	Dark brown	Some vegetation in the stream, humus, roots.
J025	5	1.5	Brown - grey	Downstream from J026 where a tributary joins main stream. Large scree/rock fall deposit north side of stream.
J026	5	1	Dark grey	Sample from a tributary joining Møllneselva from north, steep gradient.
J027	3	2	Brown	Sampled at the side of the stream. Stagnant water?
J028	4	2	Grey	
J029	3	5	Brown - grey	
J030	8	0.5	Dark brown	Vegetated area, humus-rich. Low stream gradient and right before bog area farthest upstream.
J031	4	1	Dark brown - red	Right after bog area farthest upstream.
J032	4	3	Grey	Backwater, behind large boulders. Weak current
J033	6	0.2	Grey	
J034	10	0.5	Grey	Centre of the stream, behind a large boulder.
J035	3.5	2 (gravel)	Dark grey	Downstream from a mineralised shear zone close the stream.
J036	4	1	Grey	Downstream from third hydropower construction. Water re-joins main stream. Approx. 10m upstream from main road, E6.
J037	3	1	Brown	A lot of muscovite? Ms-rich boulders close by the stream.
J038	3.5	1	Dark brown	
J039	3	2	Dark grey	Upstream of the second and largest bog area
J040	15	2	Grey	Downstream from the second bog area. Narrow, deep, meandering stream.
J041	8	1	Dark brown	
J042	6	1	Brown - grey	
J043	3	2	Brown - grey	Downstream from a waterfall and steeper part of the stream
J044	4	1	Dark grey	Approx. 10 m upstream from old main road. Some houses close by.

1.6.2 Sieving preparation

Samples were sieved with the principal goal of collecting sufficient amounts of material for further preparation and mineralogical and geochemical analyses of different fractions, as listed in Table 2. The study of fluid inclusions is out of scope for this thesis, but may be published at a later stage.

Table 2: Sieved fractions, additional preparation steps and analyses that are performed.

Fraction (µm)	Additional preparation	Method
<63		Bulk chemistry
63-125		
125-250	Magnetic separation Picking of minerals	Bulk chemistry Stable isotopes of carbonates SEM-EDS LA-ICP-MS
250-1000		
>1000		Fluid inclusions

An attempt was made to only wet sieve the samples. For the first processed sample (J006), the finest fraction (<63 µm) was collected together with the water in two 2000 ml beakers when wet sieving. Most of the material was in suspension and the beakers were put in a heating cabinet set to 40 °C until all the water had evaporated. The rest of the samples were first dry sieved to extract the <63 µm and >1 mm fractions before wet sieving to save time.

Samples were freeze dried before dry sieving to remove all water. Based on a very rough estimate of the grain-size distribution in each sample, the samples were resampled into new representable portions of various mass. The resampled material was left in the freezer for minimum 24 hours before it was put in the freeze dryer for 24-72 hours depending on the mass and grain-size distribution of the sample.

Two sets of sieves were used in order to keep sieves dry for the dry sieving and avoid clogging.

1.6.2.1 Dry sieving

Mesh sizes 63 µm, 125 µm, 250 µm and 1 mm were used together with a sieving pan to collect grains smaller than 63 µm. Each sample was dry sieved for 12-15 minutes with an amplitude of 70 using a Retsch AS 200 basic vibratory sieve shaker. The <63µm and >1 mm fractions were weighed and sampled in plastic bags with zip-locks.

1.6.2.2 Wet sieving

Material was transferred from the sieves used in the dry sieving with mesh sizes of 63 µm, 125 µm and 250 µm to a new set of sieves of corresponding mesh sizes. After wet sieving, each fraction was collected in separate glass bowls and left to desiccate in a drying cabinet set to 40 °C. These dried fractions were weighed and stored in plastic bags with zip-locks.

1.6.3 Bulk chemical analysis

1-2 g aliquots of the <63 µm and 125-250 µm fractions were sent to Bureau Veritas Mineral Laboratories, Vancouver, Canada, and analysed by combining the Aqua Regia Digestion and Ultratrace ICP-MS methods (AQ250) in order to obtain concentrations of 37 elements in the stream sediments (Appendix C). On request from Bureau Veritas Mineral Laboratories and to cut down on processing time, the 125-250 µm fraction was pulverized at UiT using an agate mortar prior to sending the samples.

1.6.4 Physicochemical characteristics

Physicochemical properties (pH and redox potential) of the pore water in sediments was measured using a HACH HQ440D Laboratory Dual Input multimeter equipped with an automatic temperature compensation probe. The measurements was performed in May 2021, several months after the initial field work, on eight of the sealed sediment samples. The multimeter was left in sediments for 10 minutes in order to stabilize in the environment before the measured physicochemical properties were read.

1.6.5 Mineral separation

Individual grains of sulphides, Fe-oxides, Fe-oxy-hydroxides and carbonates were separated from the 125-250 µm fraction by magnetic separation and hand-picking under a binocular microscope.

1.6.5.1 Magnetic separation

The process of magnetic mineral separation has been based on procedure described in the USGS Open-File Report *Magnetic Susceptibilities of Minerals* (Sam Rosenblum and Isabelie K. Brownfield, 2000). The Frantz Isodynamic Magnetic Separator, Model L-1, at the Geological laboratory of the Department of Geosciences, UiT-The Arctic University of Norway, was used.

Material weighing upwards of 10 g was placed in a funnel with an adjustable opening on top of the magnetic separator. As the machine is turned on, it vibrates and material drops down

from the funnel and into a chute at a steady pace. The magnetic separation of mineral grains takes place as grains move down the chute and through a magnetic field where a divider in the chute keeps the magnetic and non-magnetic fractions separate. The two fractions are collected in two cups hanging at the end of the chute.

The chute is tilted in two directions: forward and sideways. The forward slope is the tilt of the chute in the direction which grains slide or tumble over each other down the chute. This was fixed at 25° and regulates the travel speed of mineral grains together with the funnel opening and vibratory intensity. The side slope is the tilt of the chute towards the magnetic barrier and is directly related to the amperages of which the different minerals are separated at. The side slope was fixed at 15°.

44 samples of the 125-250 µm fraction was magnetically separated into 6 new fractions. First, a handheld magnet covered with a piece of paper was used to separate magnetite and pyrrhotite. The remaining material, free of magnetite and pyrrhotite, was processed through the magnetic separator at 0.3 A. The magnetic material was extracted, while the non-magnetic fraction was processed through the magnetic separator again, at 0.5 A. Each sample was processed through the magnetic separator four times, at each of the following amperages: 0.3, 0.5, 1.4 and 1.7 A (Figure 11).

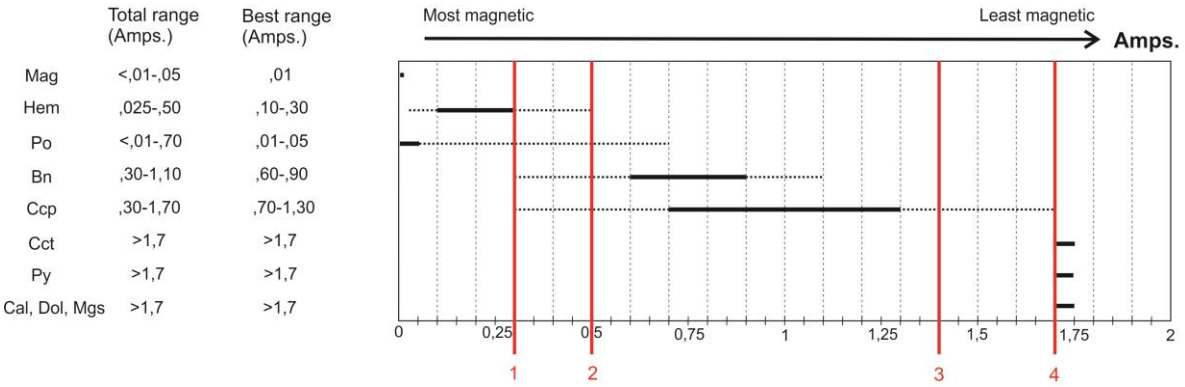

Figure 11: Magnetic susceptibilities of minerals targeted for separation. Modified after Rosenblum & Brownfield (2000)*. A total and best range for extraction is given for each of the minerals. Carbonates targeted are the least magnetic minerals (calcite, dolomite and magnesite). Vertical red lines denoted with numbers 1-4 illustrate at which amperages the magnetic separation was done and which of the targeted minerals would be expected in the magnetic and non-magnetic fractions. Mineral abbreviations are listed in Appendix B.*

1.6.5.2 Picking of minerals

The targeted minerals were hand-picked from the magnetically separated fractions using a Leica MZ12 stereomicroscope together with a needle and a single-hair brush. Mineral mounts were prepared by placing grains of sulphides, Fe-oxy-hydroxides and Fe-oxides inside 22 mm

diameter circles drawn on two-sided adhesive tape fixed on plexiglass. The grains were grouped by sampling localities and organized in easy recognizable patterns. The picked sulphides, Fe-oxy-hydroxides and Fe-oxides was delivered to the Geologic laboratory of the Department of Geosciences, UiT-The Arctic University of Norway, to be cast together in an epoxy puck and polished to get a cross-section through the grains (Figure 12). Carbonates were picked from five samples and placed in glass vials to be analysed for their stable isotope compositions.

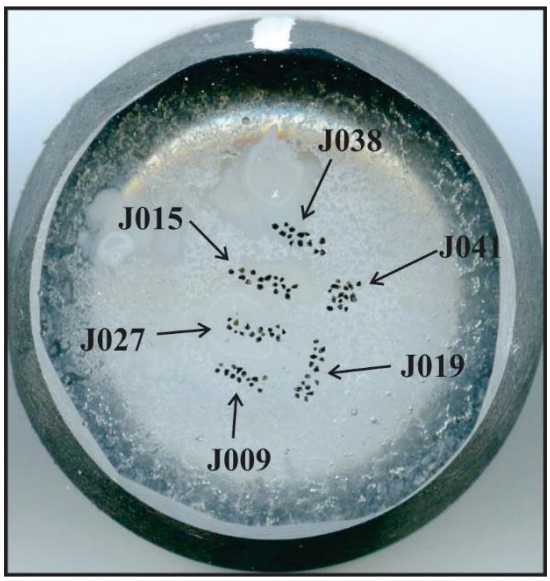

Figure 12: An example of one of the mineral mounts with groupings of magnetite grains separated from different samples (J015, J027, J009, J019, J041 and J038).

1.6.6 SEM-EDS analyses

The scanning electron microscope (SEM) technique was used on all mineral mounts, except for those with magnetite, to confirm mineralogy of mineral phases and determination of concentrations of heavy elements in mineral grains.

The polished mineral mounts were carbon coated with a thickness of approximately 15 nm using a Quorum 150R ES Plus coater. SEM-EDS was performed at the Advance Microscope Core Facility, UiT – The Arctic University of Norway using a Zeiss Merlin Compact VP field emission scanning electron microscope equipped with an AsB (Angle selective Backscatter) detector for detailed crystalline surface structure imaging. An X-max EDS (energy dispersive spectrometry) detector from Oxford Instruments was utilized for determination of element compositions, by producing EDS-maps and performing spot analyses. A working distance (WD) of 8.5 mm, aperture size of 60 µm and EHT of 20 kV (extra-high tension acceleration voltage) was used. EDS-data was acquired and processed utilizing the AZtecTEM software.

Because Fe is a major element in every mineral analysed by the FE-SEM-EDS method, it was chosen as the internal standard to be used in the following LA-ICP-MS analyses. The processing of the data included interpretation of X-ray peak interferences and compilation of laser ablation targets based on Fe concentration (Appendix D).

1.6.7 Minor and trace element analyses by LA-ICP-MS

The mineral mounts were polished to remove the carbon coating before all mounts were sent to The Geological Survey of Finland (Geologian Tutkimuskeskus; GTK) together with processed EDS-data maps showing spot targets for LA-ICP-MS analysis.

Laser ablation single collector ICP-MS analyses of sulphide minerals were performed using a Nu AttoM SC-ICPMS (Nu Instruments Ltd., Wrexham, UK) and an Analyte 193 ArF laser-ablation system (Photon Machines, San Diego, USA). The laser was run at a pulse frequency of 10 Hz and a pulse energy of 5 mJ at 30% attenuation to produce an energy flux of 2.5 J/cm^2 on the sample surface with a 40 µm spot size. This spot size was chosen to provide the best compromise between resolution and limit of detection (LOD). This allowed for adequate spot analysis of compositional zones determined by SEM imaging set at high contrast, while keeping limits of detection (LOD) as low as possible. Each analysis was initiated with a 20 second baseline measurement followed by switching on the laser for 40 seconds for signal acquisition. Analyses were perfomed using time-resolved analysis (TRA) with continuous acquisition of data for each set of points (generally following the scheme of primary standard, quality control standard, 15 unknowns). Analyses of sulphides determined concentrations of 39 isotopes (^{29}Si, ^{34}S, ^{48}Ti, ^{49}Ti, ^{51}V, ^{53}Cr, ^{55}Mn, ^{57}Fe, ^{59}Co, ^{60}Ni, ^{65}Cu, ^{67}Zn, ^{71}Ga, ^{73}Ge, ^{75}As, ^{77}Se, ^{93}Nb, ^{95}Mo, ^{99}Ru, ^{101}Ru, ^{103}Rh, ^{106}Pd, ^{109}Ag, ^{111}Cd, ^{115}In, ^{120}Sn, ^{123}Sb, ^{126}Te, ^{137}Ba, ^{183}W, ^{187}Re, ^{190}Os, ^{193}Ir, ^{195}Pt, ^{197}Au, ^{202}Hg, ^{203}Tl, ^{208}Pb and ^{238}U), covering 37 elements.

For the LA-ICP-MS analyses of oxides, GSE glass was used as the primary external standard, with GSD glass BHVO-2G and BCR-2G as reference materials for quality control. The isotope ^{57}Fe was used as an internal standard. Concentrations of 35 isotopes (^{24}Mg, ^{27}Al, ^{29}Si, ^{31}P, ^{34}S, ^{44}Ca, ^{45}Sc, ^{49}Ti, ^{51}V, ^{53}Cr, ^{55}Mn, ^{57}Fe, ^{59}Co, ^{60}Ni, ^{63}Cu, ^{66}Zn, ^{71}Ga, ^{73}Ge, ^{75}As, ^{77}Se, ^{89}Y, ^{90}Zr, ^{93}Nb, ^{95}Mo, ^{107}Ag, ^{118}Sn, ^{121}Sb, ^{139}La, ^{147}Sm, ^{172}Yb, ^{178}Hf, ^{181}Ta, ^{182}W, ^{197}Au and ^{208}Pb) covering 35 elements were determined. Measurements were performed at low resolution ($\Delta M/M = 300$) using the fast scanning mode.

Data reduction was handled using the software GLITTER ™ (Van Actherbergh et al., 2001) which allows for baseline subtraction, the integration of the signal over a selected time resolve area and the quantification using known concentrations of the external and internal standards.

Data are presented in chapter 3.4 where minerals are categorized by the mineral separation as described in section 1.6.5 and compositions from SEM-EDS analyses. Additionally, a few Fe-oxide grains with a recorded concentration of 5-25 wt.% or >40 wt.% Ti by LA-ICP-MS analysis are not included in the presentation of data. These grains have an elemental composition different from the heavy minerals in focus. Heavy minerals separated from samples collected at tailings or tributaries (i.e. samples J002, J016 and J026) may have formed in and/or been subjected to different geochemical environments and are also excluded from the presentation of data.

1.6.8 Carbonate stable isotopes

To analyse the stable isotope composition of carbonates ($\delta^{13}C$, $\delta^{18}O$) approximately 0.05 mg of carbonate grains, except for grains from one of the five samples, was pulverized in an agate mortar. Samples were analysed at The Stable Isotope Laboratory at CAGE – Centre for Arctic Gas Hydrate, Environment and Climate (http://site.uit.no/sil/). Carbonate from sample J023 was not pulverized because of the very limited number of grains and the inevitable loss of material which follows the process of pulverization. An additional B-analysis was performed on two of the five samples that provided large amounts of material.

Carbonate samples were placed in 4.5 mL glass vials which were flushed with He, and 4 drops of water-free H_3PO_4 was added manually with a syringe. After equilibration >2h at T = 50 °C, the samples were analysed on Gasbench II and Thermo Scientific MAT253 IRMS. Normalisation to VPDB was done by 2-3 in-house standards with a wide range of $\delta^{13}C$ and $\delta^{18}O$ values. The in-house standards have been normalised by several international standards. The instrument uncertainty for $\delta^{13}C$ and $\delta^{18}O$ was a standard deviation of $\leq 0.1‰$ (Thermo Scientific). Uncertainty in $\delta^{13}C$ and $\delta^{18}O$ may be larger for heterogeneous or small samples, i.e. sample J023.

2 Theoretical background

Exploration geochemistry investigates the enrichment or depletion of elements in the vicinity of mineral deposits and is based on systematic measurements of one or more chemical parameters. The results from the investigation may show an abnormal distribution of elements, commonly referred to as a geochemical anomaly, for the studied area. By identifying and interpreting the geochemical anomalies, economically viable near-surface or deep-seated ore deposits may be identified (Haldar, 2018).

Stream sediment sampling is a widely used approach in geochemical surveys and has proven to be a robust method for identifying areas of high mineral potential (Fletcher, 1997). Material derived from weathering of rocks within the upstream catchment can be transported by groundwater, surface waters or other media and into the stream. Consequently, the concentration of heavy metals in stream sediments is high close to mineralised rocks, but gradually decrease downstream due to the dilution of sediments.

2.1 Geochemical dispersion

The process in which particles are redistributed to new locations and geochemical environments is called geochemical dispersion. Dispersion may be primary or secondary and the terminology is related to the timing of the process. Primary dispersion is the emplacement of particles during the formation of an ore deposit, whereas secondary dispersion is the redistribution of primary patterns at a later stage and usually occurs in the surface environment (Rose et al., 1979).

Figure 13 shows a simplified model illustrating the dispersion of base metals from an ore body and the genesis of a geochemical anomaly. A residual anomaly may be present in the overburden soil from an ore body as a result of weathering of the bedrock. Major and trace elements from the products of weathering can be incorporated in the groundwater solution and dispersed further away from the ore deposit, typically following the bedrock topography. Precipitation of elements related to the ore body may happen as the solution enters a new environment, for example a stream where the Eh-pH conditions can differ from groundwater (Rose et al., 1979).

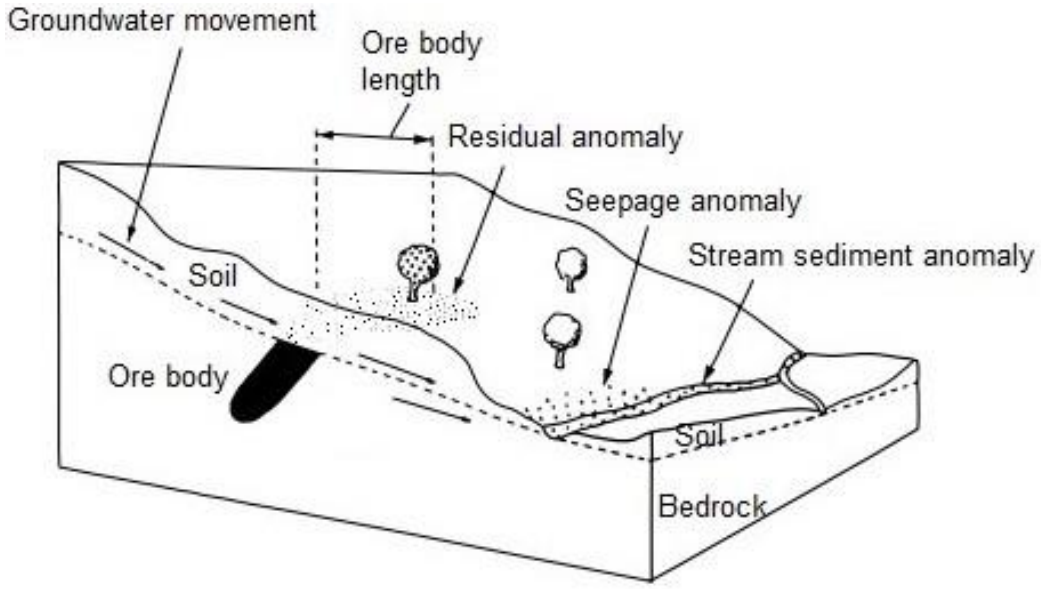

Figure 13: Simplified illustration of the dispersion of base metals from an ore body through hydromorphic pathways and the resulting geochemical anomalies in an imaginary environment (from Jaacks et al., 2011*).*

Dispersion in the surficial environment is controlled by the mobility of the dispersed material, including mechanical and chemical properties. The mechanical properties controlling the dispersion in a stream environment are the size, density and shape of grains. Small grains with a low density are dispersed more easily than large and dense particles. The chemical properties controlling the mobility of elements in the surficial environment is more complex. Because various minerals dissolve at different rates, the mobility of elements in the surficial environment is largely controlled by their solubility in water (Rose et al., 1979).

An additional contributory chemical quality which may control the redistribution of elements in a geochemical environment is surface reactions with the most dominant mechanism being adsorption. Dissolved elements may accumulate on surfaces through adsorption because of electrical charges on the surface of particles. Materials with a large surface area are good absorbers and have the potential to scavenge greater amounts of dissolved elements than material with a smaller surface area. For a given mass of sediment, small grain sizes generally have larger surface areas than more coarse-grained material (Figure 14). Consequently, sediments with small grain sizes are often the main sites for transport and collection of trace elements (Horowitz, 1991).

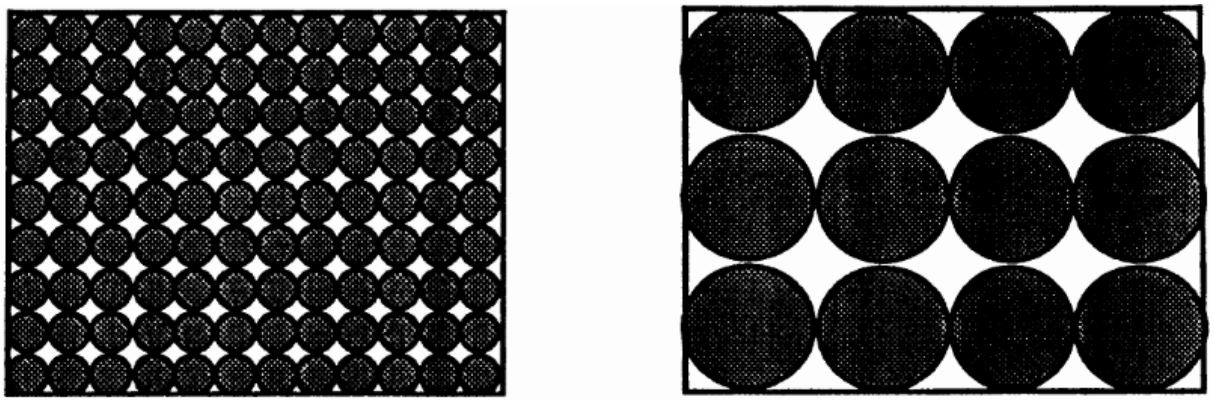

Figure 14: Schematic illustrating how surface area of a given mass of sediments changes with grain size. The surface area of small grains is greater than for larger grain sizes (from Horowitz, 1991).

2.2 Pathfinder elements

The valuable component which is pursued in a geochemical survey may be difficult to single out. It can be immobile in the surficial environment, difficult to analyse, or yield inconsistent data that is hard to interpret. Some elements have similar relative mobility through a set of geological processes. This means that their ratio remains relatively constant through these processes. Pathfinder elements are elements which are associated with the valuable component of an ore body. Thus, the spatial distribution of the pathfinder element can be used as an indicator for the source of the valuable component which is sought after. Additionally, the pathfinder element may have some advantageous properties, for example, a higher mobility in the surficial environment or can be detected by simpler analytical methods (Rose et al., 1979).

2.3 Oxidation of base-metal sulphides

Oxidation of sulphide minerals has the potential to cause serious harm to the environment and living organisms by acidifying natural waters. When exposed to water and an oxidant (e.g. dissolved oxygen or Fe^{3+}), sulphides can oxidize. The oxidation of sulphides is complex and can proceed through a number of pathways depending on the mineralogy, temperature, pH, Eh, presence of certain microorganisms and the type of oxidant (Blowes et al., 2013; Nordstrom et al., 2015).

2.3.1 Eh-pH relationships

The relationship between the oxidation potential, Eh, and the concentration of hydrogen ions, pH, is an important factor that has an effect on the solubility of sulphides and other minerals in water. Water in the streams targeted in this study is derived from the precipitation of rain and snow within the drainage basins. Precipitation contains small amounts of various

dissolved gases and is normally acidic. Additionally, natural waters change their composition as they interact with the environment and other parts of Earth's climate system through the water cycle. When encountering clastic material, major and trace elements are incorporated in the water by dissolving minerals (Garrels & MacKenzie, 1967). As illustrated by Figure 15, natural waters can be placed in a large field in Eh-pH diagrams depending on the geochemical environment. However, most natural waters have a pH value between 4 (acidic) to 9 (alkaline) and an Eh between -0.5 V (reducing) and 0.6 V (oxidizing) (Rose et al., 1979).

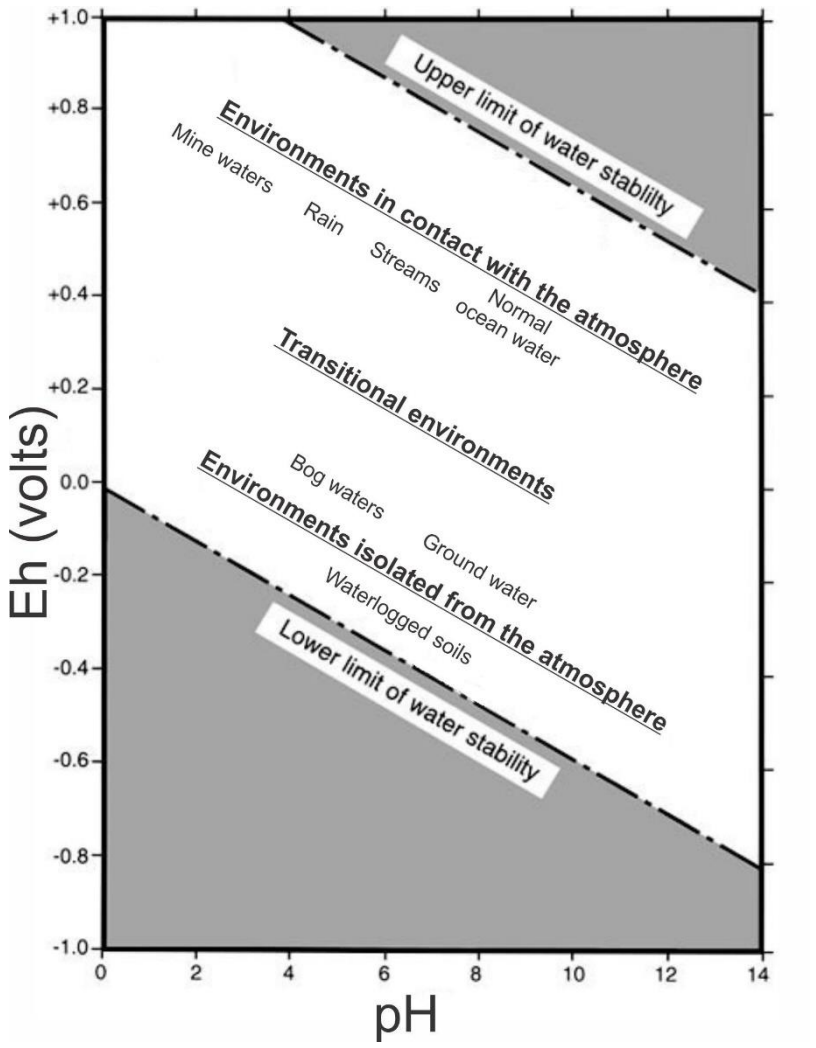

Figure 15: Approximation of range of Eh-pH conditions in natural environments. Modified after Patterson (1999).

Streams generally have a steady input of oxygen due to the turbulence of the water and its interaction with the atmosphere. However, there may be considerable variations in sediment redox potential along a stream, from the upper fast flowing part to the lower slowly flowing stretches with more abundant microbial activity. This is evident when soils become waterlogged, e.g. wetlands and swamps, where oxygen typically is depleted and redox potential reduced (Søndergaard, 2009).

Pyrite and other sulphide minerals generally have a low solubility in water, but they may oxidize in contact with water and an oxidant. Considering oxidation of pyrite, the type of oxidant and the products of the oxidation is dependent on pH. According to Singer & Stumm (1970) and Blowes et al. (2013), the main oxidant in a system at circumneutral pH-conditions is dissolved oxygen and the main oxidation product is an Fe(III)oxy-hydroxide. Thus, the oxidation of pyrite at circumneutral pH conditions may be summarized as

$$4\,FeS_2(s) + 15\,O_2(g) + 14\,H_2O(l) \Rightarrow 4\,Fe(OH)_3(s) + 8SO_4^{2-}(aq) + 16\,H^+(aq) \qquad (E.1)$$

where the dissociation of H_2SO_4 and increased concentration of H^+-ions is included (Misra, 2012, pp. 186-187). Both iron and sulphur is oxidized from Fe^{2+} and S^- in FeS_2 to Fe^{3+} and S^{6+} in $Fe(OH)_3$ and SO_4^{2-}. Additionally, the oxidation of pyrite leaves the system more acidic than before, as seen by the increase in concentration of H^+-ions. The solid product of the oxidation, $Fe(OH)_3$, is often referred to as limonite or an Fe-oxy-hydroxide ($FeO(OH)\cdot nH_2O$) and has a variable composition.

Carbonates are some of the most soluble minerals and dissolve in slightly acidic atmospheric aqueous solutions (Bauer & Velde, 2014). In contrast to the oxidation of sulphide minerals, which leaves the system more acidic, dissolution of carbonates promotes alkaline surface waters, as seen by reaction E.2 with calcite as an example.

$$CaCO_3(s) + H_2O(l) \Rightarrow Ca^{2+}(aq) + HCO_3^-(aq) + OH^-(aq) \qquad (E.2)$$

Because of the rapid dissolution of carbonates, the pH can remain neutral at sites where dissolution of carbonates and oxidation of sulphides occur simultaneously (Blowes et al., 2013).

2.3.2 Galvanic effects

Sulphide ores may be complex, composing of a mixture of various sulphide minerals with different features. Galvanic interactions can occur when free particles of different sulphide minerals are in contact in a solution. The effect of this interaction may change the reactivity and oxidation of the sulphide minerals, but has not been thoroughly studied in the context of acidification of natural waters or generation of acid mine drainage (Chopard et al., 2017).

The phenomenon stems from a difference in rest potential of the semi-conductive sulphides. In a solution where two sulphide minerals with a difference in rest potentials are in contact with each other, the mineral with the highest rest potential may act as a cathode, whereas the

mineral with the lower rest potential acts as an anode. The cathode will be reduced and galvanically protected while the anode oxidizes and its dissolution is favoured (Chopard et al., 2017; Yang et al., 2021). Consequently, galvanic interaction between minerals can take place in systems with complex sulphide assemblages immersed in a solution and result in accelerated oxidation of low rest potential sulphides.

2.4 Statistical analysis

Geochemical data are generally complex with many variables and with a wide range of factors, both natural and anthropogenic, which influence the data set. A data set commonly contains an abundance of small values along with a few very large values, so-called outliers. Because of this, geochemical data is rarely normal or even lognormal distributed, but is often positively skewed. Acknowledging this is important when performing a statistical analysis on geochemical data as many of the traditional statistical methods assume a normal or lognormal distribution of data (Reimann & Filzmoser, 2000).

Values below or above the detection limit, often referred to as censored values, should be recognized and dealt with in one way or another. A value reported at the detection limit is likely to be a wrong estimate of the true value, resulting in biased estimates of statistical indexes such as mean and standard deviation (Grunsky & Smee, 1999). Multiple approaches have been discussed in order to deal with censored values (e.g. Helsel & Cohn, 1988; Sanford et al., 1993) and the favourable method is dependent on various factors such as the number of replacements. Censored values in the geochemical data sets presented are treated with simple substitution factors similar to those proposed by Sanford et al. (1993) and Carranza (2011). Values below the detection limit are multiplied by ½ and values above the detection limit are multiplied by 2.

Various statistical methods have been applied to the geochemical data sets. Descriptive statistics summarize the data by listing indexes such as the arithmetic mean, median, standard deviation, skewness and minimum and maximum values. Correlation matrices list the Pearson's correlation coefficient (r) between elements. The correlation coefficient is a number between and including -1 to 1, and is a measure of the strength of the linear relationship between two variables. If r = - 1 for two variables, there is a perfect negative correlation between them, and opposite if r = 1. However, if the correlation coefficient is equal to zero, there is no linear relationship between the two variables. (Davis, 2002, pp. 43-45). It should

be noted that correlation analyses assumes a normal or lognormal distribution and is not recommended to be used with original, untransformed data by Reimann & Filzmoser (2000).

Hypothesis testing is a method which can be used to test if there is a statistical inference in the data set. It can be performed to determine the significance of the correlation coefficients and to decide whether the linear relationships between elements are reliable. Expressing a null and alternate hypothesis defined by the population correlation coefficient (ρ) is the first step.

H_0: $\rho = 0$ There is not a significant linear relationship between the two variables in the population.

H_a: $\rho \neq 0$. There is a significant linear relationship between the two variables in the population.

The significance of the correlation coefficients is not only dependant on the value of r, but also the number of samples (n) and a chosen level of significance (α). Using a table for the critical values of the Pearson correlation coefficient to find the intersection of the chosen level of significance, say $\alpha = 0.05$, and degrees of freedom ($df = n - 2$), for example $df = 9$, the critical value is 0.602. A chosen level of significance of $\alpha = 0.05$ means it is accepted that the statistical test is in error five out of 100 times. Finally, the value of the Pearson correlation coefficient in the correlation matrices may be compared to the critical value to assess if the relationship between two variables is statistically significant at the chosen level of significance. An element which shows a significant positive correlation with the valuable component of an ore is interesting because it may be used as a pathfinder element for the ore deposit.

2.5 Element analyses of heavy minerals

Internal standards are often used together with the LA-ICP-MS technique to improve accuracy and precision by correcting measured variations. This means that the concentration of at least one element has to be determined by another analysis using an alternative method, e.g. SEM, or obtained from the known elemental stoichiometry (Longerich et al., 1996).

2.5.1 Scanning electron microscopy

The fundamental operating principle of a scanning electron microscope is that a beam of electrons is focused onto the surface of a sample and that various signals are emitted back (Figure 16). The microscope can be equipped with different accessories (detectors) that can

read these signals to provide information on local chemistry and crystallography (Scheu & Kaplan, 2012). Signal detectors commonly used are those for backscattered electrons (high energy), secondary electrons (low energy) and excited (characteristic) X-rays (Brandon & Kaplan, 2008).

A fraction of the incident high energy electrons will be backscattered and is dependent on the atomic number of the specimen. Thus, the backscattered electron signal is used to produce images of the atomic number contrast (surface crystallography) and when combined with the excited X-ray signals, maps of the element distribution (Brandon & Kaplan, 2008). Secondary electron emissions are commonly used to reveal information of the surface topography of the specimen, but is often obscured due to a conductive layer of C or Au, applied to prevent electron charging on the sample surface (Lloyd, 1987; Scheu & Kaplan, 2012).

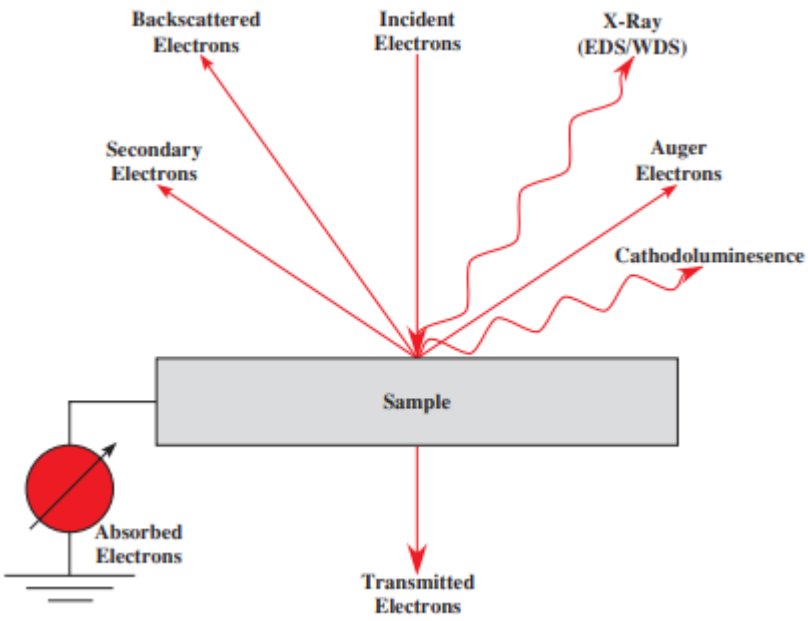

Figure 16: Schematic drawing of signals generated when an incident electron beam interacts with a solid sample (from Brandon & Kaplan, 2008*).*

The excited X-ray signals are analysed to determine the chemical composition of the region of interest using either energy-dispersive (EDS) or wavelength-dispersive (WDS) detectors. In WDS spectroscopy the energy of the excited X-rays is collected as a function of their wavelength, whereas EDS detectors collect the energy of emitted X-rays and converts it to an electrical charge proportional to the energy of the X-ray (Brandon & Kaplan, 2008).

2.5.2 Laser ablation ICP-MS

Laser ablation inductively coupled plasma mass spectrometry (LA-ICP-MS) is one of the most versatile compositional analysis methods of solid materials due to its sensitivity and the minor sample preparation required (Koch & Günther, 2016). The LA-ICP-MS method utilizes a pulsed laser beam which is focused onto the sample. The sample is ablated and material is gasified before it is transported by a carrier gas (He and/or Ar) into the ICP where the particles are converted into ions (Figure 17) (Liu et al., 2013).

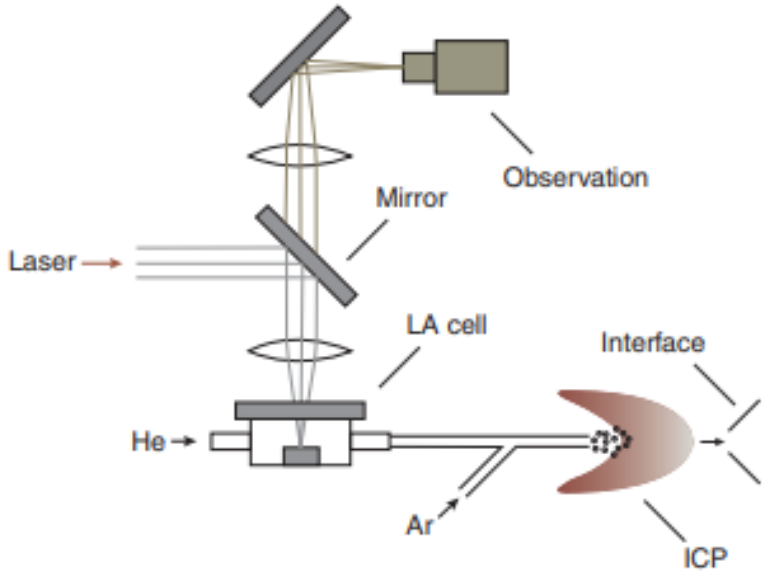

Figure 17: Schematic of the components of a LA-ICP-MS system (the mass spectrometry system is not shown) (from Koch & Günther, 2010).

Moving from the ion source, the ions are passed towards the mass spectrometer. Ions move through a magnetic field which separates them by their mass-to-charge ratio. The ions with a high mass-to-charge ratio will be deflected less than the highly charged, low ionic mass species. At the end of the mass spectrometer is a detector which reads the location where the incoming signals are hitting. The detector then sends out electrical signals that are amplified and read by a signal processor (Figure 18).

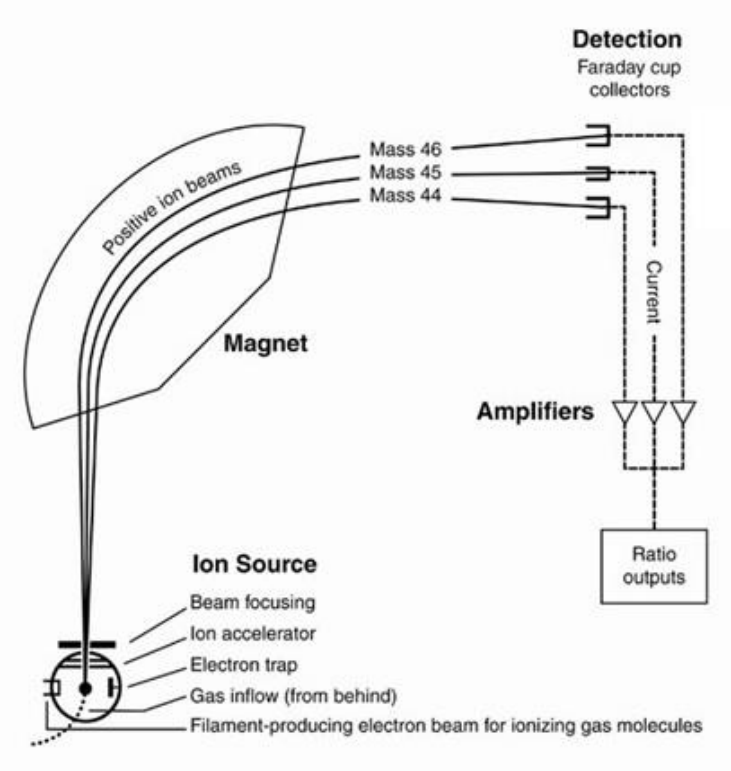

Figure 18: Schematic of the mass spectrometer part of the LA-ICP-MS system (from Coplen et al., 2012).

2.5.3 Element analyses of hydrous minerals

$Fe(OH)_3$ is often referred to as limonite or an Fe-oxy-hydroxide and may be expressed as $FeO(OH)\cdot nH_2O$ where it has a variable hydrous phase (Rose et al., 1979, p. 144). The SEM-EDS method, which was used to determine mineralogy of mineral grains prior to LA-ICP-MS, has some limitations. The EDS detector uses the energy of X-rays emitted from the sample to identify and quantify elements present on the sample surface (Newbury & Ritchie, 2013). The lightest elements with the lowest atomic number emit low-energy X-rays and are difficult to measure. Hydrogen for instance, is not detectable at all (Wolfgong, 2016). Additionally, the content of oxygen in the sample is calculated by means of assumed stoichiometry based on measured cations present (Nash, 1992; Newbury & Ritchie, 2013). Consequently, oxygen attached to hydrogen in H_2O-bearing minerals is not detected by the SEM-EDS method.

2.6 Stable isotopes

Isotopes are atoms with the same number of protons but different number of neutrons in their nuclei and can be divided into two distinct groups: unstable (radiogenic) and stable isotopes. The unstable isotopes spontaneously decay emitting radioactive energy, whereas stable isotopes do not decay into new elements. However, the abundance of the stable isotopes also

varies and is caused by isotope fractionation. Isotope fractionation is a processes promoted by small chemical and physical differences between the isotopes of an element. The small mass difference between two isotopes of the same element causes isotopes to partition during biological and geological processes (Hoefs, 2018).

To compare isotope data from different laboratories, a set of standards are used in the calculation and presentation of isotope ratios. The unit of isotope ratio measurements is "delta", δ, and may be expressed as

$$\delta_{\text{sample}(‰)} = \frac{(\text{R}_{\text{sample}} - R_{standard})}{\text{R}_{\text{standard}}} * 1000 \qquad \text{(E.3)}$$

for a sample, where R is the heavy to light isotope ratio in the sample or the standard being used. For instance, the standards for oxygen ($\delta^{18}O$) are the VSMOW (Vienna Standard Mean Ocean Water) and VPDB (Vienna Pee Dee Belemnite) standards. The VPDB standard is also a standard for the carbon isotope composition ($\delta^{13}C$) (Hoefs, 2018). It should be noted that the δ-value can be positive or negative and that a negative value display a depletion of the heavier isotope in the sample relative to the standard.

2.6.1 Stable isotope composition of carbonates

In geology, the term "carbonate minerals" refers to minerals containing the carbonate ion, CO_3^{2-}. Because both carbon and oxygen are elements with two or more stable isotopes, the isotopic composition of carbonates is commonly used to estimate the conditions at which they are formed (Hoefs, 2018).

Carbonates may be formed in various geological environments, e.g. in hydrothermal systems associated with mafic magmatism or in marine systems deposited as sedimentary sequences (Veizer & Hoefs, 1976; Stakes & O'Neil, 1982). The isotopic composition of carbon and oxygen in the hydrothermal fluid and the proportions of dissolved carbon species in the system, such as CO_2 and HCO_3^-, will impact the stable isotope composition of hydrothermal carbonates. Sedimentary carbonates display variations in their isotopic composition due to fractionation processes related to the climate and temperatures of the oceans (Hoefs, 2018). Based on the system and conditions they are formed in, different fractionation processes affect the isotopic composition and may result in carbonates with a characteristic isotopic fingerprint.

3 Results

3.1 Bulk chemistry of stream sediments

Two fractions, <63 and 125-250 µm, of 44 stream sediment samples have been analysed for 37 elements by combining the Aqua Regia digestion and the Ultratrace ICP-MS method. The obtained results are listed in Appendix C.

The concentrations of selected elements from the analysed stream sediment samples are summarized as box plots in Figure 19. Outliers are labelled by sample names. Samples J002 from the tailing area of Lundstrøm mine and J026 from a tributary joining the Møllneselva stream are defined as high, positive outliers for multiple elements (e.g. Cu, Sc, Ag, Mg).

The great majority of metals shows enrichment in the <63 µm fraction comparing to the fraction 125-250 µm. Sediments from the Annaselva stream have lower concentrations of Cu, V, Sc, Co, Fe, Ti, Mn, Mg and Ca relative to the two streams draining the Kvenvik formation. However, Au, Se, Bi, Pb, Hg and As are enriched in sediments from the Annaselva stream comparing to the Møllneselva and Brakkelva streams.

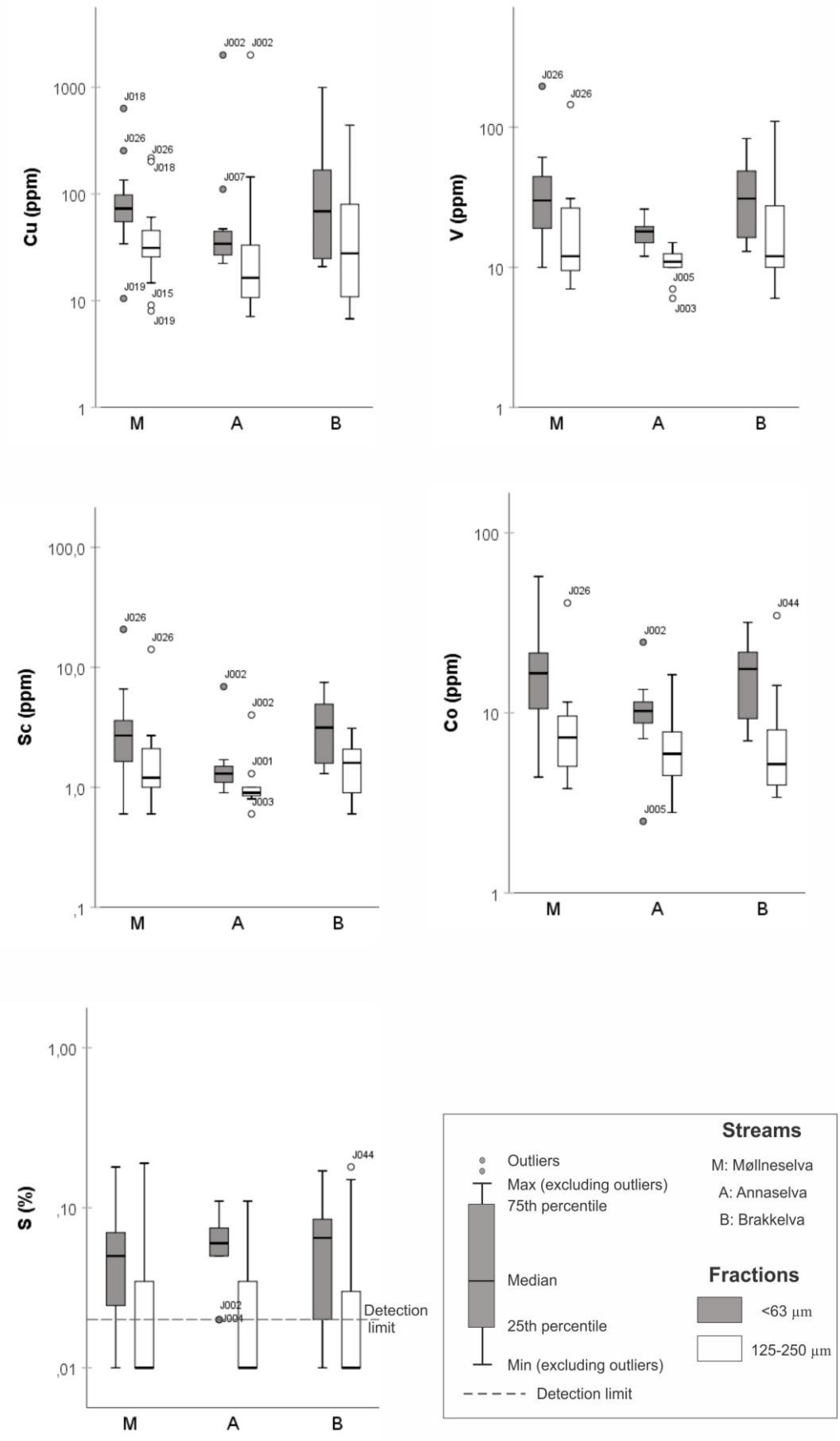

Figure 19: Log-scale boxplots of a selection of elements from the bulk chemistry data set. Detection limits are shown when there are measured concentrations below the detection limit.

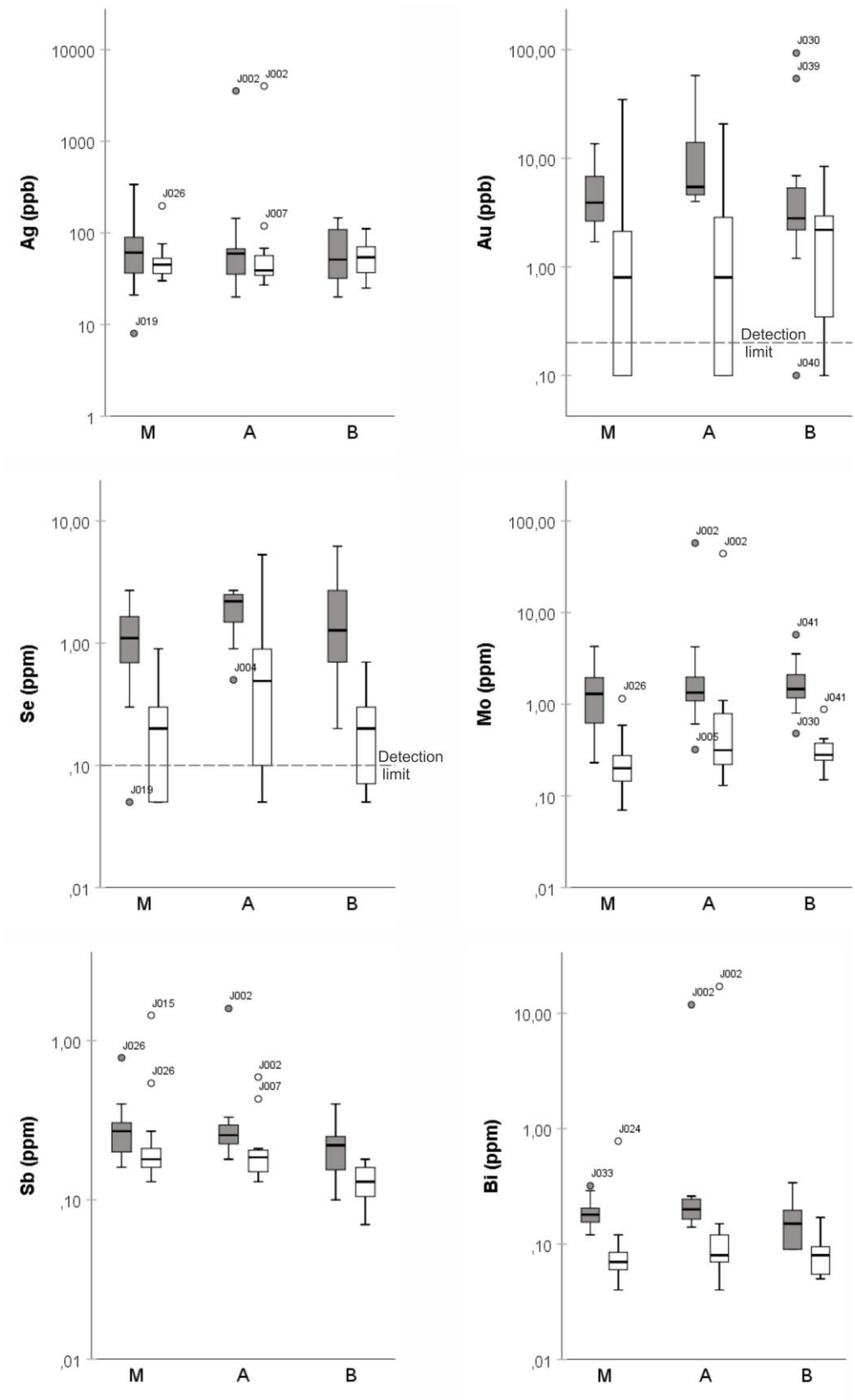

Figure 19: (Continued).

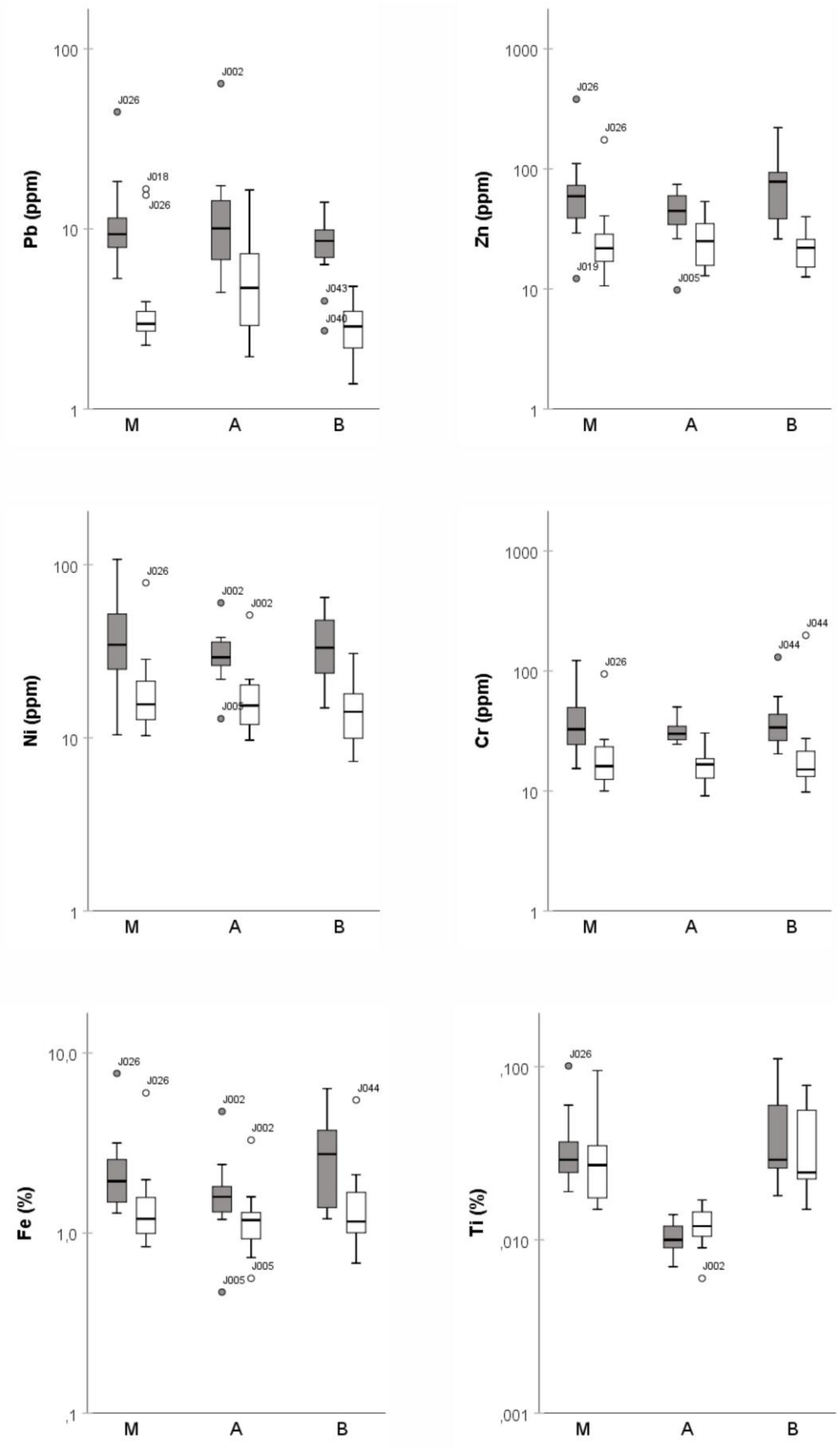

Figure 19: (Continued).

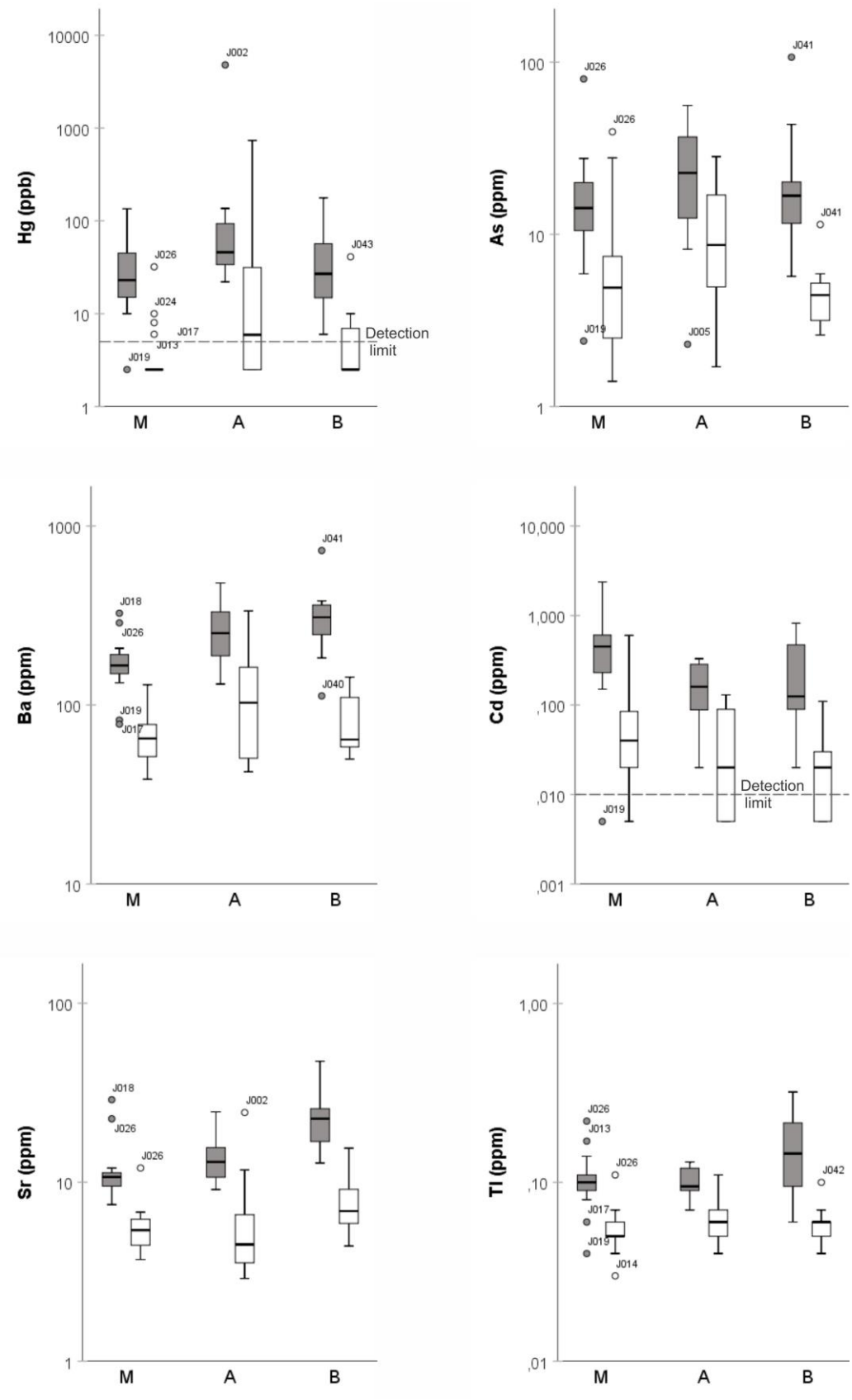

Figure 19: (Continued).

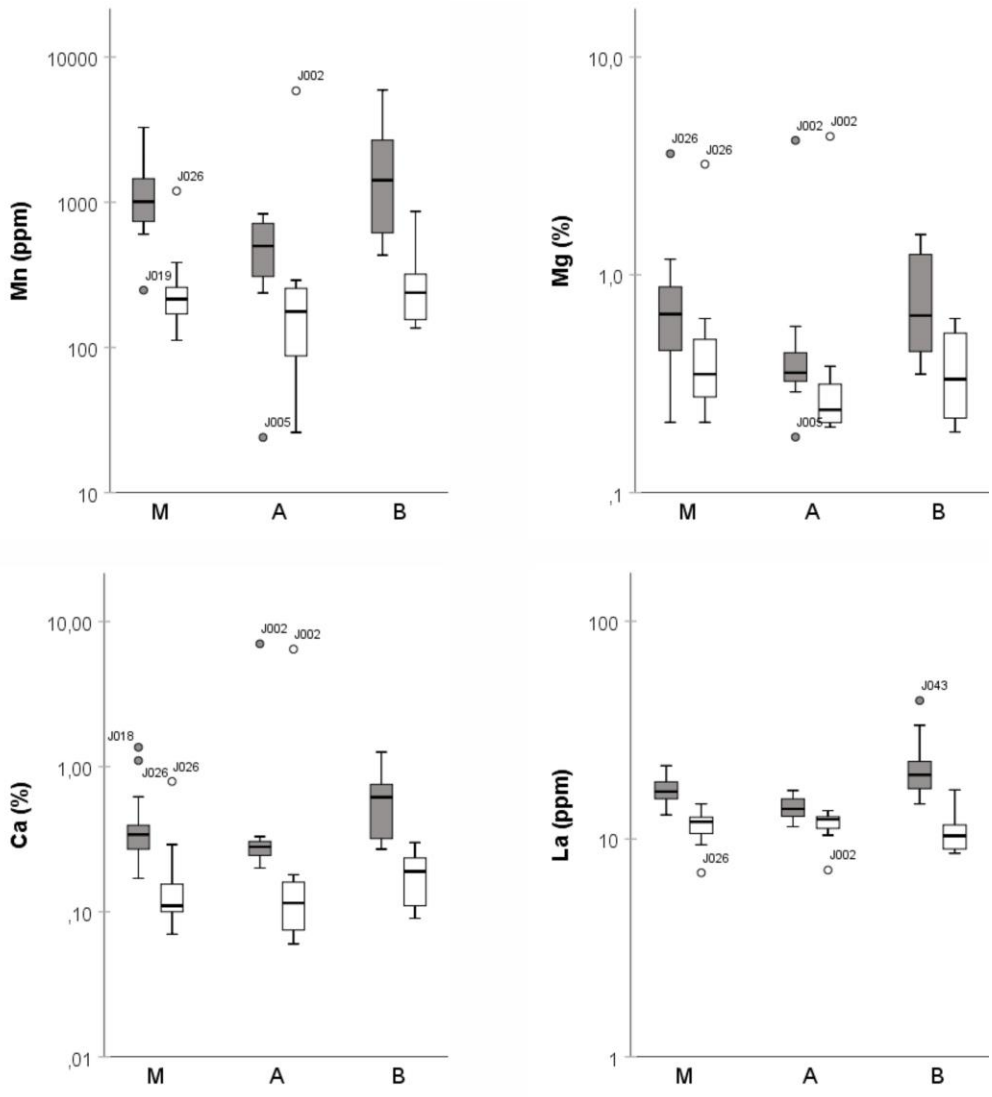

Figure 19: (Continued).

3.1.1 Statistical analysis

Samples J002, J016 and J026S are from tributaries or underwater tailings and not part of any of the streams. They are therefore not included in the following statistical analysis. Boron (B) and tungsten (W) are excluded from the statistical analysis because most of the values are below the detection limits.

Descriptive statistics for all three studied streams and for the fractions <63 µm (Table 3) and 125-250 µm (Table 4) are listed below. Comparison of mean and median concentrations between the two fractions reveal that the <63 µm fraction is enriched in all analysed elements except for Th and Na which is slightly more enriched in fraction 125-250 µm.

The content of Cu in stream sediment samples shows large variations, as seen by high values of standard deviation and the minimum and maximum. Additionally, the value of skewness is

positive and in the range of 2.52 to 3.86 for both fractions and all three streams, meaning there are outlying samples with high contents of Cu.

Results from Lilliefors corrected Kolomogorov-Smirnov test (K-S test) for normality show that only a few of the elements follows a normal distribution (Appendix E). In the <63 µm fraction ten elements (Pb, Ni, Th, Sb, Bi, P, Al, S, Se and Ga) show normal distribution, whereas only four elements (Zn, La, Al, Ga) pass the test for the 125-250 µm fraction.

Table 3: Descriptive statistics of the bulk chemistry of fraction <63 µm from stream sediment samples. DL = detection limit, Mean = arithmetic mean, SD = standard deviation, Min = minimum, Max = maximum, M = Møllneselva stream (n = 18 samples), A = Annaselva stream (n=11 samples), B = Brakkelva stream (n = 12 samples).

Fraction <63 µm			Mean			Median			SD			Skewness			Min			Max		
Element	Unit	DL	M	A	B	M	A	B	M	A	B	M	A	B	M	A	B	M	A	B
Mo	PPM	0.01	1.35	1.52	1.93	1.25	1.21	1.47	0.96	1.04	1.43	1.68	1.91	2.00	0.23	0.32	0.48	4.27	4.23	5.74
Cu	PPM	0.01	102.20	39.71	182.23	70.51	34.02	68.79	135.90	24.67	285.96	3.86	2.80	2.52	10.47	22.31	20.82	631.51	110.70	995.42
Pb	PPM	0.01	9.81	10.03	8.31	9.22	9.44	8.59	3.31	4.33	3.08	1.22	0.57	-0.11	5.31	4.44	2.72	18.33	17.37	14.07
Zn	PPM	0.1	57.35	42.20	85.27	57.15	44.60	78.15	25.14	16.04	58.35	0.42	-0.53	1.46	12.20	9.80	26.10	110.70	63.40	220.70
Ag	PPB	2	61.61	57.36	68.83	61.00	58.00	51.50	33.29	33.66	46.41	0.38	1.73	0.74	8.00	20.00	20.00	133.00	144.00	146.00
Ni	PPM	0.1	36.64	28.67	36.43	32.85	29.10	33.25	14.84	7.27	16.61	0.17	-0.80	0.51	10.40	12.90	14.90	62.70	38.00	64.70
Co	PPM	0.1	15.52	9.55	17.33	15.55	10.00	17.55	6.24	2.89	8.58	0.02	-1.46	0.60	4.40	2.50	7.00	24.90	13.50	31.80
Mn	PPM	1	1104.50	504.45	1875.75	1003.50	499.00	1423.00	509.17	262.50	1659.07	0.69	-0.45	1.52	248.00	24.00	432.00	2330.00	832.00	5927.00
Fe	%	0.01	1.98	1.51	2.87	1.84	1.57	2.75	0.61	0.48	1.54	0.63	-0.48	0.93	1.29	0.47	1.20	3.16	2.40	6.34
As	PPM	0.1	14.46	23.90	24.59	14.05	22.40	16.75	6.59	15.49	27.62	0.01	0.68	2.83	2.40	2.30	5.70	27.60	56.00	106.90
U	PPM	0.1	3.98	8.81	5.28	4.00	10.30	2.85	1.63	3.47	6.43	0.90	-0.49	2.68	1.50	3.70	1.60	8.30	12.90	24.00
Au	PPB	0.2	5.13	7.60	14.60	3.95	5.20	2.80	3.43	4.72	28.82	1.21	1.22	2.40	1.70	4.00	0.10	13.60	16.50	93.00
Th	PPM	0.1	3.09	0.75	3.60	2.90	0.60	3.55	1.39	0.27	0.95	1.21	0.45	-0.60	1.10	0.40	1.60	7.00	1.20	4.90
Sr	PPM	0.5	11.20	13.01	22.80	10.35	12.10	22.65	4.58	3.21	9.18	3.76	0.79	1.77	7.50	9.10	12.80	28.90	19.80	47.40
Cd	PPM	0.01	0.43	0.17	0.28	0.42	0.16	0.13	0.25	0.10	0.27	0.43	0.09	0.96	0.01	0.02	0.02	0.99	0.33	0.82
Sb	PPM	0.02	0.26	0.25	0.22	0.26	0.25	0.22	0.07	0.05	0.08	0.56	-0.01	0.66	0.16	0.18	0.10	0.40	0.33	0.40
Bi	PPM	0.02	0.18	0.20	0.16	0.18	0.19	0.15	0.05	0.04	0.08	1.29	0.06	1.24	0.12	0.14	0.09	0.32	0.26	0.34
V	PPM	1	30.89	17.73	36.33	27.50	18.00	31.00	15.17	3.88	23.46	0.51	0.67	1.00	10.00	12.00	13.00	61.00	26.00	83.00
Ca	%	0.01	0.39	0.27	0.62	0.33	0.27	0.62	0.26	0.04	0.31	3.34	-0.47	0.74	0.17	0.20	0.27	1.36	0.33	1.26
P	%	0.001	0.07	0.09	0.08	0.07	0.09	0.08	0.01	0.02	0.02	0.24	-0.42	1.09	0.06	0.06	0.06	0.09	0.11	0.12
La	PPM	0.5	16.88	13.83	21.99	16.50	13.50	19.70	2.15	1.64	8.30	0.30	0.73	1.90	12.90	11.40	14.50	21.70	16.70	43.20
Cr	PPM	0.5	35.66	30.95	42.51	31.60	29.60	33.90	14.13	7.42	29.79	0.43	2.04	2.70	15.40	24.50	20.40	60.70	50.20	130.30
Mg	%	0.01	0.66	0.36	0.82	0.61	0.35	0.65	0.27	0.11	0.45	0.33	0.72	0.67	0.21	0.18	0.35	1.18	0.58	1.53
Ba	PPM	0.5	168.72	257.03	321.69	165.95	244.50	309.90	52.46	103.73	151.16	1.16	0.85	1.75	78.10	130.90	112.40	325.70	480.90	729.70
Ti	%	0.001	0.03	0.01	0.05	0.03	0.01	0.03	0.01	0.00	0.03	1.38	-0.17	1.29	0.02	0.01	0.02	0.06	0.01	0.11
Al	%	0.01	0.95	0.93	1.20	0.94	0.96	1.22	0.28	0.11	0.36	0.01	0.02	0.03	0.36	0.76	0.64	1.51	1.11	1.84
Na	%	0.001	0.00	0.00	0.01	0.00	0.00	0.01	0.00	0.00	0.00	1.06	-0.23	0.25	0.00	0.00	0.01	0.01	0.00	0.01
K	%	0.01	0.13	0.14	0.16	0.13	0.14	0.14	0.02	0.02	0.07	-0.20	-1.31	0.97	0.08	0.08	0.08	0.16	0.17	0.31
Sc	PPM	0.1	2.67	1.27	3.45	2.30	1.30	3.15	1.49	0.25	1.95	1.08	0.29	0.76	0.60	0.90	1.30	6.60	1.70	7.50
Tl	PPM	0.02	0.10	0.10	0.16	0.10	0.10	0.15	0.03	0.02	0.07	0.29	-0.14	0.79	0.04	0.07	0.06	0.17	0.13	0.32
S	%	0.02	0.05	0.06	0.07	0.05	0.06	0.07	0.03	0.02	0.05	1.00	0.07	0.90	0.01	0.02	0.01	0.13	0.11	0.17
Hg	PPB	5	27.97	57.91	48.33	22.50	42.00	27.00	17.43	37.81	53.50	0.62	1.35	1.79	2.50	22.00	6.00	63.00	136.00	177.00
Se	PPM	0.1	1.12	1.87	1.87	1.10	2.20	1.35	0.63	0.71	1.68	-0.03	-0.86	1.65	0.05	0.50	0.20	2.20	2.70	6.20
Te	PPM	0.02	0.05	0.02	0.04	0.04	0.02	0.03	0.04	0.01	0.03	1.26	0.76	0.77	0.01	0.01	0.01	0.16	0.05	0.09
Ga	PPM	0.1	2.72	2.84	3.36	2.55	2.80	3.10	0.90	0.39	1.40	0.25	0.28	0.94	1.00	2.20	1.90	4.40	3.50	6.30

Elements in red: follows normal distribution (Lilliefors corrected K-S test, n = 41, significance level $\alpha = 0.05$).

Table 4: Descriptive statistics of the bulk chemistry of fraction 125-250 µm from stream sediment samples. DL = detection limit, Mean = arithmetic mean, SD = standard deviation, Min = minimum, Max = maximum, M = Møllneselva stream (n = 18 samples), A = Annaselva stream (n=11 samples), B = Brakkelva stream (n = 12 samples).

Fraction 125-250 µm			Mean			Median			SD			Skewness			Min			Max		
Element	Unit	DL	M	A	B	M	A	B	M	A	B	M	A	B	M	A	B	M	A	B
Mo	PPM	0.01	0.22	0.43	0.33	0.20	0.31	0.28	0.13	0.33	0.19	1.63	1.40	2.49	0.07	0.13	0.15	0.59	1.10	0.88
Cu	PPM	0.01	41.55	28.75	77.86	29.55	14.66	27.77	45.87	39.48	123.86	3.63	2.98	2.67	8.01	7.09	6.77	216.99	144.11	440.47
Pb	PPM	0.01	3.76	4.77	2.93	2.96	4.17	2.88	3.25	2.39	0.98	4.10	0.69	0.49	2.26	1.95	1.38	16.66	9.20	4.80
Zn	PPM	0.1	22.70	24.41	22.58	20.70	23.80	22.05	7.65	10.12	9.24	0.67	0.55	0.98	10.60	12.90	12.60	40.60	43.00	40.00
Ag	PPB	2	46.50	47.09	55.67	44.50	39.00	54.50	13.39	26.33	24.41	1.03	2.41	0.79	30.00	27.00	25.00	76.00	119.00	111.00
Ni	PPM	0.1	17.04	15.38	15.35	15.10	14.50	14.15	5.33	4.08	6.86	0.70	0.41	1.14	10.30	9.70	7.30	28.40	21.80	30.70
Co	PPM	0.1	7.21	5.60	8.55	6.60	5.50	5.20	2.53	1.94	8.77	0.14	-0.07	2.82	3.80	2.80	3.40	11.50	8.20	34.70
Mn	PPM	1	217.00	157.09	293.92	214.50	152.00	239.00	71.68	91.31	200.12	0.72	0.03	2.38	112.00	26.00	136.00	385.00	290.00	864.00
Fe	%	0.01	1.26	1.09	1.62	1.17	1.14	1.16	0.35	0.29	1.29	0.58	-0.22	2.85	0.84	0.56	0.68	1.98	1.59	5.48
As	PPM	0.1	5.94	10.94	4.75	4.85	6.90	4.45	5.87	8.24	2.37	3.30	1.02	2.17	1.40	1.70	2.60	27.80	28.30	11.40
U	PPM	0.1	1.17	2.66	1.37	1.00	2.40	0.80	0.44	1.74	1.70	1.19	0.80	3.34	0.70	0.80	0.70	2.10	6.20	6.70
Au	PPB	0.2	3.04	1.49	2.33	0.50	0.80	2.20	8.04	2.13	2.27	4.01	1.78	1.80	0.10	0.10	0.10	34.70	6.40	8.40
Th	PPM	0.1	3.64	1.88	3.85	3.65	1.50	3.65	0.58	1.03	2.17	-0.35	0.68	2.86	2.50	0.80	1.70	4.50	3.70	10.40
Sr	PPM	0.5	5.21	5.12	8.08	5.20	4.20	6.90	0.94	2.51	3.44	0.13	2.06	1.30	3.70	2.90	4.40	6.80	11.70	15.50
Cd	PPM	0.01	0.05	0.04	0.03	0.04	0.02	0.02	0.04	0.04	0.03	1.09	1.24	2.54	0.01	0.01	0.01	0.16	0.13	0.11
Sb	PPM	0.02	0.25	0.19	0.13	0.18	0.18	0.13	0.30	0.08	0.03	4.13	2.67	-0.08	0.13	0.13	0.07	1.44	0.43	0.18
Bi	PPM	0.02	0.11	0.09	0.09	0.07	0.08	0.08	0.17	0.03	0.04	4.10	0.64	1.36	0.04	0.04	0.05	0.78	0.15	0.17
V	PPM	1	16.33	10.73	24.75	12.00	10.00	12.00	8.69	2.69	28.67	0.58	-0.25	2.77	7.00	6.00	6.00	31.00	15.00	110.00
Ca	%	0.01	0.13	0.11	0.18	0.11	0.11	0.19	0.05	0.04	0.07	1.86	0.24	0.21	0.07	0.06	0.09	0.29	0.18	0.30
P	%	0.001	0.03	0.03	0.02	0.03	0.03	0.02	0.00	0.02	0.01	0.15	1.57	2.23	0.02	0.02	0.02	0.03	0.07	0.04
La	PPM	0.5	12.00	12.19	10.88	12.05	12.40	10.35	1.45	0.98	2.39	0.20	-0.50	1.51	9.40	10.40	8.60	14.50	13.50	16.80
Cr	PPM	0.5	17.34	16.07	31.48	15.95	15.40	15.10	5.59	4.63	52.79	0.44	0.80	3.41	10.00	9.10	9.80	26.90	26.30	198.30
Mg	%	0.01	0.38	0.26	0.37	0.33	0.24	0.34	0.14	0.06	0.16	0.59	1.01	0.34	0.21	0.20	0.19	0.63	0.38	0.63
Ba	PPM	0.5	64.71	114.38	81.42	62.70	91.60	64.15	17.34	88.72	32.07	0.20	1.80	0.94	38.50	42.40	49.90	97.60	335.30	143.20
Ti	%	0.001	0.03	0.01	0.04	0.03	0.01	0.02	0.01	0.00	0.02	0.46	0.33	1.00	0.02	0.01	0.02	0.04	0.02	0.08
Al	%	0.01	0.49	0.51	0.49	0.45	0.48	0.48	0.12	0.12	0.15	0.33	-0.19	-0.02	0.31	0.30	0.26	0.70	0.70	0.70
Na	%	0.001	0.01	0.00	0.01	0.01	0.00	0.01	0.00	0.00	0.01	0.13	0.98	1.63	0.00	0.00	0.01	0.01	0.01	0.03
K	%	0.01	0.12	0.12	0.11	0.12	0.12	0.11	0.02	0.02	0.03	-0.31	-0.88	0.14	0.08	0.08	0.07	0.16	0.15	0.16
Sc	PPM	0.1	1.43	0.91	1.58	1.15	0.90	1.60	0.65	0.17	0.79	0.62	0.72	0.58	0.60	0.60	0.60	2.70	1.30	3.10
Tl	PPM	0.02	0.05	0.06	0.06	0.05	0.06	0.06	0.01	0.02	0.02	-0.06	1.46	1.53	0.03	0.04	0.04	0.07	0.11	0.10
S	%	0.02	0.03	0.02	0.04	0.01	0.01	0.01	0.03	0.01	0.06	3.23	1.12	2.04	0.01	0.01	0.01	0.15	0.05	0.18
Hg	PPB	5	3.42	14.55	7.08	2.50	2.50	2.50	2.22	17.76	10.99	2.35	1.42	3.14	2.50	2.50	2.50	10.00	49.00	41.00
Se	PPM	0.1	0.21	0.47	0.23	0.15	0.40	0.20	0.22	0.38	0.20	2.10	0.23	1.42	0.05	0.05	0.05	0.90	1.00	0.70
Te	PPM	0.02	0.02	0.01	0.02	0.01	0.01	0.02	0.01	0.00	0.01	1.83	1.17	0.64	0.01	0.01	0.01	0.05	0.01	0.04
Ga	PPM	0.1	1.41	1.57	1.55	1.25	1.60	1.45	0.46	0.39	0.70	0.49	0.44	0.79	0.80	0.90	0.70	2.20	2.40	3.00

Elements in red: follows normal distribution (Lilliefors corrected K-S test, n = 41, significance level $\alpha = 0.05$).

Pearson's correlation coefficient (r) of untransformed data between elements are shown in correlation matrices for both fractions sampled from each of the three streams in tables below. The level of significance is set to $\alpha = 0.05$ and elements which shows a statistically significant correlation with Cu is emphasised.

Sediments collected from the Møllneselva stream shows that in the <63 µm fraction, Cu has a positive correlation with Mo, Pb, Ag, Fe, Sr, Ca, Cr, Mg, Ba, Ti, Na, Sc, S and Te (Table 5). In the 125-250 µm fraction, Cu only shows a positive correlation with Pb and Ca (Table 6).

Stream sediments from Annaselva, the stream that drains the sediment-hosted Cu mineralised Anna deposit and runs parallel to the sedimentary Storviknes formation, shows that in the fraction <63 µm Cu has a positive correlation with Pb, Zn, Ag, Sr, Sb, Bi, Ba and Hg (Table 7). In fraction 125-250 µm, Cu correlates positively with Pb, Zn, Ag, Ni, Au, Sr, Cd, Sb, Bi, Ba and Hg (Table 8).

Stream sediments from Brakkelva, the stream primarily draining Cu mineralised mafic lithologies of the Kvenvik formation and runs just besides the tailing of Mitchells mine shows that in fraction <63 µm, Cu correlates positively with Zn, Ag, Ni, Co, Bi, V, Al and S (Table 9). In sediments of the 125-250 µm fraction, Cu has a positive correlation with Zn, Ni, Au, Al, S and Te (Table 10).

Table 5: Pearson correlation analysis between elements in stream sediments (<63 µm fraction) from Møllneselva (n=18). Elements which correlates significantly with Cu are highlighted with red text.

	Mo	Cu	Pb	Zn	Ag	Ni	Co	Mn	Fe	As	U	Au	Th	Sr	Cd	Sb	Bi	V	Ca	P	La	Cr	Mg	Ba	Ti	Al	Na	K	Sc	Tl	S	Hg	Se	Te	Ga
Mo	1.00																																	
Cu	0.81*	1.00																																
Pb	0.64*	0.52*	1.00																															
Zn	0.58*	0.36	0.66*	1.00																														
Ag	0.7*	0.63*	0.77*	0.65*	1.00																													
Ni	0.64*	0.41	0.54*	0.88*	0.68*	1.00																												
Co	0.63*	0.43	0.58*	0.89*	0.71*	0.96*	1.00																											
Mn	0.75*	0.40	0.74*	0.65*	0.65*	0.63*	0.71*	1.00																										
Fe	0.67*	0.53*	0.58*	0.9*	0.66*	0.93*	0.94*	0.62*	1.00																									
As	0.59*	0.23	0.56*	0.75*	0.54*	0.63*	0.64*	0.73*	0.59*	1.00																								
U	0.30	0.12	0.79*	0.46	0.61*	0.34	0.35	0.59*	0.31	0.61*	1.00																							
Au	-0.24	-0.01	-0.01	-0.04	0.05	-0.11	-0.05	-0.27	-0.13	-0.02	-0.03	1.00																						
Th	0.15	0.20	-0.35	-0.20	-0.25	-0.07	-0.07	-0.18	0.10	-0.34	-0.65*	-0.25	1.00																					
Sr	0.81*	0.96*	0.53*	0.25	0.65*	0.31	0.33	0.40	0.39	0.23	0.17	-0.02	0.15	1.00																				
Cd	0.35	0.09	0.72*	0.83*	0.61*	0.74*	0.79*	0.69*	0.67*	0.64*	0.62*	0.01	-0.41	0.05	1.00																			
Sb	0.45	0.35	0.42	0.56*	0.71*	0.74*	0.77*	0.40	0.63*	0.33	0.21	0.06	-0.01	0.36	0.59*	1.00																		
Bi	0.24	0.15	0.39	0.49*	0.46	0.66*	0.72*	0.42	0.59*	0.31	0.30	-0.04	-0.08	0.10	0.57*	0.72*	1.00																	
V	0.37	0.19	0.46	0.91*	0.55*	0.91*	0.92*	0.49*	0.89*	0.56*	0.30	-0.01	-0.12	0.05	0.81*	0.71*	0.67*	1.00																
Ca	0.81*	0.96*	0.49*	0.39	0.67*	0.51*	0.48*	0.39	0.55*	0.28	0.12	-0.04	0.16	0.94*	0.16	0.43	0.16	0.24	1.00															
P	0.43	0.24	0.78*	0.57*	0.69*	0.42	0.45	0.62*	0.42	0.77*	0.91*	0.07	-0.51*	0.31	0.62*	0.32	0.36	0.38	0.25	1.00														
La	-0.11	-0.06	-0.05	-0.54*	-0.29	-0.62*	-0.58*	-0.23	-0.48*	-0.42	-0.11	0.01	0.41	0.05	-0.45	-0.32	-0.32	-0.64*	-0.20	-0.11	1.00													
Cr	0.7*	0.53*	0.6*	0.91*	0.72*	0.96*	0.94*	0.59*	0.97*	0.62*	0.34	-0.12	0.00	0.42	0.69*	0.72*	0.59*	0.9*	0.58*	0.44	-0.53*	1.00												
Mg	0.66*	0.57*	0.56*	0.91*	0.74*	0.93*	0.94*	0.55*	0.94*	0.58*	0.26	0.00	-0.03	0.46	0.68*	0.76*	0.59*	0.9*	0.61*	0.40	-0.58*	0.97*	1.00											
Ba	0.76*	0.83*	0.62*	0.45	0.7*	0.41	0.45	0.49*	0.46	0.27	0.22	-0.06	-0.06	0.84*	0.23	0.44	0.21	0.24	0.77*	0.33	-0.07	0.53*	0.59*	1.00										
Ti	0.62*	0.58*	0.19	0.65*	0.39	0.75*	0.74*	0.34	0.86*	0.33	-0.16	-0.20	0.5*	0.43	0.28	0.51*	0.43	0.69*	0.59*	0.03	-0.37	0.82*	0.81*	0.41	1.00									
Al	0.58*	0.40	0.75*	0.96*	0.76*	0.91*	0.91*	0.65*	0.9*	0.7*	0.59*	-0.01	-0.32	0.31	0.84*	0.65*	0.59*	0.9*	0.44	0.64*	-0.55*	0.93*	0.91*	0.5*	0.58*	1.00								
Na	0.78*	0.65*	0.51*	0.56*	0.73*	0.75*	0.72*	0.52*	0.72*	0.49*	0.24	0.00	0.13	0.66*	0.36	0.74*	0.49*	0.54*	0.71*	0.41	-0.23	0.77*	0.75*	0.62*	0.66*	0.64*	1.00							
K	0.39	0.28	0.64*	0.52*	0.73*	0.58*	0.57*	0.38	0.48*	0.37	0.57*	0.11	-0.41	0.33	0.53*	0.74*	0.56*	0.53*	0.30	0.58*	-0.19	0.6*	0.59*	0.56*	0.19	0.7*	0.68*	1.00						
Sc	0.79*	0.8*	0.62*	0.79*	0.78*	0.83*	0.85*	0.56*	0.89*	0.52*	0.25	0.06	0.07	0.7*	0.54*	0.69*	0.48*	0.73*	0.8*	0.40	-0.41	0.91*	0.94*	0.72*	0.81*	0.82*	0.81*	0.54*	1.00					
Tl	0.46	0.22	0.85*	0.76*	0.66*	0.7*	0.71*	0.71*	0.6*	0.59*	0.72*	-0.11	-0.51*	0.21	0.89*	0.57*	0.58*	0.67*	0.26	0.66*	-0.33	0.67*	0.63*	0.46	0.19	0.83*	0.44	0.71*	0.53*	1.00				
S	0.63*	0.62*	0.51*	0.64*	0.72*	0.84*	0.83*	0.47*	0.8*	0.46	0.32	-0.02	-0.03	0.57*	0.5*	0.79*	0.69*	0.71*	0.69*	0.41	-0.51*	0.84*	0.84*	0.51*	0.69*	0.75*	0.85*	0.64*	0.86*	0.53*	1.00			
Hg	0.49*	0.41	0.85*	0.69*	0.71*	0.61*	0.68*	0.64*	0.6*	0.63*	0.74*	0.04	-0.42	0.42	0.81*	0.63*	0.57*	0.61*	0.41	0.76*	-0.25	0.63*	0.63*	0.46	0.23	0.78*	0.48*	0.66*	0.63*	0.85*	0.65*	1.00		
Se	0.46	0.36	0.66*	0.64*	0.85*	0.73*	0.77*	0.57*	0.64*	0.55*	0.63*	0.06	-0.40	0.39	0.72*	0.83*	0.7*	0.69*	0.43	0.69*	-0.47*	0.71*	0.72*	0.45	0.32	0.79*	0.7*	0.82*	0.67*	0.73*	0.83*	0.81*	1.00	
Te	0.46	0.52*	0.22	0.51*	0.52*	0.75*	0.7*	0.23	0.7*	0.22	-0.07	0.01	0.22	0.44	0.38	0.68*	0.48*	0.63*	0.68*	0.05	-0.55*	0.71*	0.74*	0.33	0.73*	0.55*	0.69*	0.32	0.73*	0.30	0.8*	0.35	0.54*	1.00
Ga	0.51*	0.32	0.65*	0.96*	0.66*	0.93*	0.92*	0.59*	0.91*	0.65*	0.48*	0.02	-0.24	0.21	0.83*	0.66*	0.61*	0.95*	0.36	0.53*	-0.57*	0.94*	0.92*	0.41	0.64*	0.98*	0.63*	0.66*	0.8*	0.79*	0.74*	0.71*	0.73*	0.57*

* *Correlation is significant at the significance level* α = 0.05 (2-tailed).

Table 6: Pearson correlation analysis between elements in stream sediments (125-250 µm fraction) from Møllneselva (n=18). Elements which correlates significantly with Cu are highlighted with red text.

	Mo	*Cu*	*Pb*	*Zn*	*Ag*	*Ni*	*Co*	*Mn*	*Fe*	*As*	*U*	*Au*	*Th*	*Sr*	*Cd*	*Sb*	*Bi*	*V*	*Ca*	*P*	*La*	*Cr*	*Mg*	*Ba*	*Ti*	*Al*	*Na*	*K*	*Sc*	*Tl*	*S*	*Hg*	*Se*	*Te*	*Ga*
Mo	1.00																																	
Cu	0.30	1.00																																
Pb	0.26	0.97*	1.00																															
Zn	0.78*	0.11	-0.01	1.00																														
Ag	0.57*	0.13	0.02	0.65*	1.00																													
Ni	0.52*	0.09	-0.03	0.85*	0.67*	1.00																												
Co	0.44	0.42	0.31	0.76*	0.42	0.86*	1.00																											
Mn	0.77*	0.23	0.24	0.62*	0.37	0.5*	0.48*	1.00																										
Fe	0.29	0.04	-0.09	0.72*	0.44	0.82*	0.82*	0.24	1.00																									
As	0.84*	0.10	0.02	0.78*	0.54*	0.5*	0.39	0.44	0.36	1.00																								
U	0.75*	-0.05	-0.04	0.67*	0.46	0.33	0.18	0.57*	0.16	0.7*	1.00																							
Au	0.72*	0.16	0.05	0.63*	0.54*	0.41	0.32	0.25	0.32	0.93*	0.46	1.00																						
Th	-0.21	-0.23	-0.28	-0.17	-0.12	-0.24	-0.26	-0.51*	0.16	0.07	-0.27	0.24	1.00																					
Sr	0.27	0.14	0.13	0.18	0.27	-0.06	-0.06	-0.04	0.18	0.32	0.34	0.32	0.52*	1.00																				
Cd	0.73*	-0.07	-0.08	0.65*	0.44	0.39	0.25	0.77*	0.07	0.53*	0.81*	0.31	-0.57*	-0.09	1.00																			
Sb	-0.12	-0.20	-0.11	-0.09	-0.13	-0.16	-0.25	-0.27	-0.08	0.09	-0.01	-0.02	0.15	0.21	-0.16	1.00																		
Bi	0.7*	0.08	-0.03	0.59*	0.51*	0.34	0.23	0.22	0.26	0.92*	0.46	0.99*	0.28	0.34	0.33	-0.01	1.00																	
V	0.32	0.01	-0.14	0.79*	0.5*	0.88*	0.84*	0.24	0.97*	0.43	0.20	0.38	0.08	0.07	0.16	-0.08	0.32	1.00																
Ca	0.56*	0.88*	0.83*	0.48*	0.46	0.48*	0.66*	0.41	0.36	0.41	0.20	0.40	-0.23	0.26	0.12	-0.08	0.31	0.36	1.00															
P	0.62*	0.08	0.08	0.54*	0.47	0.30	0.22	0.55*	0.27	0.47	0.71*	0.28	-0.23	0.52*	0.58*	0.09	0.29	0.22	0.31	1.00														
La	-0.22	-0.28	-0.19	-0.54*	-0.13	-0.62*	-0.72*	-0.34	-0.48*	-0.19	-0.02	-0.07	0.49*	0.46	-0.29	-0.07	-0.01	-0.58*	-0.41	-0.10	1.00													
Cr	0.43	-0.03	-0.17	0.83*	0.56*	0.87*	0.8*	0.30	0.97*	0.53*	0.30	0.48*	0.16	0.23	0.21	-0.11	0.44	0.97*	0.35	0.33	-0.43	1.00												
Mg	0.55*	0.19	0.03	0.91*	0.58*	0.87*	0.87*	0.40	0.85*	0.6*	0.38	0.52*	-0.06	0.07	0.39	-0.17	0.47	0.93*	0.51*	0.30	-0.65*	0.9*	1.00											
Ba	-0.01	0.09	-0.01	0.12	0.27	0.11	0.12	-0.21	0.31	0.02	-0.02	0.13	0.53*	0.61*	-0.26	-0.24	0.13	0.27	0.13	-0.08	0.38	0.35	0.23	1.00										
Ti	0.16	-0.05	-0.21	0.62*	0.46	0.8*	0.73*	0.03	0.94*	0.33	-0.02	0.36	0.28	0.15	-0.09	-0.05	0.32	0.94*	0.28	0.10	-0.42	0.93*	0.79*	0.39	1.00									
Al	0.52*	0.01	-0.14	0.91*	0.65*	0.92*	0.8*	0.38	0.86*	0.59*	0.45	0.49*	-0.06	0.11	0.42	-0.14	0.45	0.93*	0.39	0.30	-0.52*	0.93*	0.95*	0.32	0.82*	1.00								
Na	0.13	-0.11	-0.23	0.37	0.61*	0.49*	0.37	-0.08	0.54*	0.23	0.07	0.32	0.27	0.35	0.01	-0.08	0.31	0.56*	0.13	0.03	0.09	0.61*	0.47*	0.69*	0.66*	0.61*	1.00							
K	-0.07	-0.37	-0.42	0.14	0.43	0.32	0.04	-0.31	0.34	0.18	0.01	0.29	0.44	0.32	-0.23	0.04	0.29	0.34	-0.11	-0.19	0.35	0.42	0.17	0.62*	0.51*	0.40	0.76*	1.00						
Sc	0.52*	0.23	0.08	0.88*	0.6*	0.89*	0.87*	0.31	0.86*	0.63*	0.35	0.58*	-0.01	0.13	0.27	-0.15	0.51*	0.92*	0.57*	0.25	-0.59*	0.91*	0.96*	0.27	0.83*	0.95*	0.5*	0.32	1.00					
Tl	0.25	-0.12	-0.21	0.54*	0.59*	0.59*	0.49*	0.10	0.6*	0.43	0.31	0.46	0.04	0.30	0.17	-0.19	0.43	0.6*	0.17	0.22	-0.01	0.68*	0.52*	0.45	0.63*	0.68*	0.75*	0.7*	0.62*	1.00				
S	0.03	0.21	0.17	0.32	0.00	0.55*	0.7*	0.19	0.68*	0.10	-0.16	0.10	-0.08	-0.16	-0.21	-0.06	0.01	0.61*	0.36	-0.07	-0.48*	0.56*	0.44	-0.05	0.59*	0.43	0.08	0.15	0.54*	0.40	1.00			
Hg	0.73*	-0.01	-0.03	0.53*	0.40	0.26	0.08	0.41	-0.03	0.81*	0.82*	0.7*	-0.20	0.17	0.66*	-0.08	0.7*	0.05	0.18	0.45	0.06	0.17	0.25	-0.08	-0.07	0.32	0.05	0.11	0.28	0.33	-0.17	1.00		
Se	0.32	0.37	0.37	0.49*	0.16	0.6*	0.71*	0.37	0.62*	0.32	0.14	0.24	-0.18	0.05	0.00	0.06	0.14	0.56*	0.6*	0.22	-0.5*	0.54*	0.49*	-0.12	0.48*	0.47*	-0.02	0.05	0.61*	0.36	0.89*	0.05	1.00	
Te	0.25	0.17	0.10	0.51*	0.41	0.74*	0.75*	0.24	0.73*	0.39	0.00	0.44	-0.01	-0.05	-0.07	-0.05	0.34	0.71*	0.46	0.00	-0.38	0.71*	0.59*	0.09	0.72*	0.63*	0.43	0.42	0.7*	0.63*	0.84*	0.09	0.76*	1.00
Ga	0.5*	0.03	-0.13	0.9*	0.57*	0.89*	0.81*	0.33	0.84*	0.59*	0.40	0.5*	-0.05	0.04	0.40	-0.13	0.46	0.93*	0.38	0.27	-0.61*	0.91*	0.97*	0.25	0.83*	0.98*	0.54*	0.29	0.95*	0.57*	0.40	0.29	0.43	0.58*

* *Correlation is significant at the significance level* α = 0.05 (2-tailed).

Table 7: Pearson correlation analysis between elements in stream sediments (<63 µm fraction) from Annaselva (n=11). Elements which correlates significantly with Cu are highlighted with red text.

	Mo	Cu	Pb	Zn	Ag	Ni	Co	Mn	Fe	As	U	Au	Th	Sr	Cd	Sb	Bi	V	Ca	P	La	Cr	Mg	Ba	Ti	Al	Na	K	Sc	Tl	S	Hg	Se	Te	Ga
Mo	1.00																																		
Cu	0.00	1.00																																	
Pb	0.00	0.73*	1.00																																
Zn	0.03	0.64*	0.91*	1.00																															
Ag	-0.09	0.93*	0.81*	0.79*	1.00																														
Ni	0.28	0.41	0.75*	0.87*	0.62*	1.00																													
Co	0.42	0.34	0.69*	0.82*	0.53	0.93*	1.00																												
Mn	0.09	0.33	0.75*	0.79*	0.58	0.9*	0.89*	1.00																											
Fe	0.86*	0.12	0.21	0.39	0.14	0.56	0.7*	0.34	1.00																										
As	0.83*	0.22	0.14	0.23	0.09	0.26	0.40	-0.01	0.86*	1.00																									
U	-0.12	0.43	0.42	0.52	0.49	0.45	0.34	0.29	0.08	0.19	1.00																								
Au	0.59	-0.08	0.01	0.14	-0.05	0.21	0.34	0.00	0.64*	0.62*	0.16	1.00																							
Th	0.64*	-0.22	-0.47	-0.27	-0.24	0.07	0.06	-0.18	0.59	0.53	0.01	0.34	1.00																						
Sr	0.00	0.86*	0.86*	0.85*	0.9*	0.66*	0.59	0.56	0.24	0.30	0.72*	0.09	-0.21	1.00																					
Cd	-0.24	0.38	0.81*	0.74*	0.57	0.68*	0.59	0.85*	-0.03	-0.24	0.18	-0.34	-0.49	0.55	1.00																				
Sb	0.13	0.74*	0.65*	0.77*	0.75*	0.64*	0.51	0.36	0.40	0.46	0.72*	0.17	0.09	0.85*	0.31	1.00																			
Bi	0.30	0.67*	0.73*	0.72*	0.63*	0.61*	0.62*	0.45	0.46	0.59	0.74*	0.18	-0.03	0.87*	0.37	0.81*	1.00																		
V	0.83*	-0.11	-0.02	0.09	-0.10	0.29	0.52	0.20	0.88*	0.7*	-0.27	0.64*	0.52	-0.06	-0.17	-0.04	0.13	1.00																	
Ca	-0.13	0.39	0.58	0.74*	0.65*	0.85*	0.7*	0.8*	0.21	-0.10	0.60	-0.01	0.04	0.63*	0.62*	0.58	0.43	-0.04	1.00																
P	0.38	0.22	0.41	0.63*	0.31	0.66*	0.72*	0.45	0.67*	0.64*	0.72*	0.49	0.27	0.59	0.17	0.66*	0.78*	0.39	0.53	1.00															
La	0.63*	-0.31	-0.35	-0.25	-0.31	0.02	0.17	-0.11	0.57	0.38	-0.27	0.71*	0.52	-0.32	-0.53	-0.28	-0.22	0.78*	-0.13	0.13	1.00														
Cr	0.37	-0.03	0.14	0.25	0.18	0.58	0.59	0.55	0.46	0.09	0.18	0.50	0.35	0.16	0.12	0.03	0.07	0.51	0.59	0.35	0.64*	1.00													
Mg	0.31	0.00	0.25	0.42	0.26	0.71*	0.76*	0.74*	0.53	0.03	-0.03	0.30	0.24	0.12	0.36	0.06	0.02	0.56	0.65*	0.32	0.49	0.84*	1.00												
Ba	-0.04	0.78*	0.41	0.29	0.6*	0.00	-0.05	-0.14	-0.03	0.34	0.58	0.06	-0.13	0.73*	-0.01	0.62*	0.64*	-0.23	0.05	0.25	-0.30	-0.23	-0.47	1.00											
Ti	0.56	-0.24	-0.05	0.14	-0.11	0.48	0.57	0.41	0.69*	0.26	-0.36	0.32	0.47	-0.21	0.05	-0.09	-0.13	0.77*	0.27	0.22	0.66*	0.61*	0.83*	-0.64*	1.00										
Al	0.13	0.26	0.36	0.39	0.36	0.40	0.39	0.33	0.25	0.26	0.63*	0.55	0.08	0.57	0.11	0.33	0.47	0.20	0.47	0.57	0.27	0.63*	0.27	0.45	-0.07	1.00									
Na	-0.17	-0.07	0.20	0.43	0.20	0.51	0.59	0.63*	0.20	-0.10	0.34	0.00	-0.01	0.25	0.41	0.10	0.20	0.19	0.66*	0.55	0.04	0.47	0.63*	-0.25	0.37	0.35	1.00								
K	0.41	0.18	0.50	0.68*	0.29	0.69*	0.84*	0.62*	0.72*	0.61*	0.42	0.35	0.13	0.52	0.38	0.49	0.7*	0.55	0.46	0.89*	0.10	0.30	0.44	0.06	0.39	0.38	0.64*	1.00							
Sc	0.7*	0.02	-0.28	-0.17	-0.13	-0.01	0.07	-0.28	0.62*	0.79*	0.26	0.49	0.79*	0.07	-0.59	0.24	0.36	0.55	-0.12	0.50	0.52	0.22	-0.03	0.32	0.18	0.34	-0.07	0.31	1.00						
Tl	-0.15	0.44	0.38	0.26	0.36	-0.01	-0.06	-0.05	-0.14	0.23	0.61*	0.12	-0.21	0.61*	0.14	0.43	0.55	-0.30	0.05	0.30	-0.41	-0.20	-0.50	0.82*	-0.74*	0.60	-0.12	0.13	0.17	1.00					
S	-0.67*	0.28	0.25	0.03	0.27	-0.18	-0.33	-0.04	-0.72*	-0.52	0.39	-0.35	-0.56	0.34	0.25	0.02	0.09	-0.71*	0.13	-0.21	-0.51	-0.13	-0.42	0.51	-0.77*	0.40	-0.06	-0.35	-0.34	0.66*	1.00				
Hg	-0.08	0.82*	0.92*	0.75*	0.83*	0.60	0.46	0.58	0.00	0.02	0.43	-0.18	-0.46	0.84*	0.72*	0.64*	0.67*	-0.24	0.50	0.20	-0.46	0.04	0.06	0.55	-0.24	0.28	-0.04	0.22	-0.27	0.43	0.42	1.00			
Se	-0.35	0.28	0.73*	0.67*	0.50	0.60	0.56	0.83*	-0.15	-0.32	0.35	-0.29	-0.57	0.54	0.92*	0.21	0.39	-0.24	0.63*	0.26	-0.51	0.19	0.33	0.01	-0.08	0.28	0.57	0.42	-0.56	0.24	0.40	0.63*	1.00		
Te	-0.05	0.44	0.62*	0.57	0.56	0.62*	0.52	0.73*	0.11	-0.07	0.13	-0.39	-0.08	0.53	0.81*	0.30	0.36	0.03	0.62*	0.17	-0.34	0.26	0.39	0.11	0.17	0.22	0.40	0.36	-0.20	0.15	0.23	0.61*	0.69*	1.00	
Ga	0.55	0.04	-0.04	0.03	-0.04	0.05	0.12	-0.21	0.55	0.69*	0.22	0.86*	0.41	0.18	-0.45	0.21	0.27	0.55	-0.11	0.45	0.63*	0.36	0.01	0.36	0.10	0.66*	-0.15	0.26	0.69*	0.39	-0.10	-0.13	-0.42	-0.28	1.00

* *Correlation is significant at the significance level* α = 0.05 (2-tailed).

Table 8: Pearson correlation analysis between elements in stream sediments (125-250 µm fraction) from Annaselva (n=11). Elements which correlates significantly with Cu are highlighted with red text.

	Mo	Cu	Pb	Zn	Ag	Ni	Co	Mn	Fe	As	U	Au	Th	Sr	Cd	Sb	Bi	V	Ca	P	La	Cr	Mg	Ba	Ti	Al	Na	K	Sc	Tl	S	Hg	Se	Te	Ga
Mo	1.00																																		
Cu	0.21	1.00																																	
Pb	0.25	0.75*	1.00																																
Zn	0.24	0.73*	0.99*	1.00																															
Ag	0.34	0.94*	0.71*	0.69*	1.00																														
Ni	0.20	0.69*	0.88*	0.86*	0.64*	1.00																													
Co	0.42	0.55	0.82*	0.86*	0.52	0.85*	1.00																												
Mn	0.27	0.54	0.89*	0.91*	0.47	0.89*	0.94*	1.00																											
Fe	0.51	0.26	0.47	0.53	0.16	0.53	0.79*	0.73*	1.00																										
As	0.92*	0.35	0.52	0.52	0.50	0.37	0.59	0.46	0.52	1.00																									
U	0.38	0.54	0.79*	0.76*	0.67*	0.79*	0.65*	0.68*	0.28	0.63*	1.00																								
Au	0.57	0.69*	0.27	0.24	0.67*	0.14	0.16	0.06	0.18	0.50	0.11	1.00																							
Th	0.11	-0.43	-0.7*	-0.66*	-0.53	-0.53	-0.31	-0.43	0.22	-0.22	-0.75*	0.09	1.00																						
Sr	0.28	0.94*	0.86*	0.85*	0.94*	0.8*	0.69*	0.7*	0.37	0.49	0.76*	0.53	-0.57	1.00																					
Cd	0.04	0.63*	0.87*	0.82*	0.54	0.85*	0.61*	0.8*	0.27	0.23	0.66*	0.14	-0.66*	0.69*	1.00																				
Sb	0.35	0.97*	0.75*	0.72*	0.9*	0.68*	0.58	0.58	0.38	0.44	0.51	0.76*	-0.32	0.91*	0.64*	1.00																			
Bi	0.46	0.79*	0.83*	0.79*	0.8*	0.82*	0.65*	0.7*	0.44	0.62*	0.84*	0.50	-0.50	0.89*	0.75*	0.81*	1.00																		
V	0.55	0.23	0.52	0.56	0.19	0.58	0.79*	0.72*	0.95*	0.60	0.43	0.10	0.07	0.38	0.29	0.35	0.48	1.00																	
Ca	0.14	0.53	0.7*	0.65*	0.62*	0.82*	0.52	0.58	0.14	0.35	0.93*	0.01	-0.73*	0.71*	0.67*	0.46	0.78*	0.30	1.00																
P	0.54	0.46	0.73*	0.71*	0.63*	0.74*	0.69*	0.67*	0.37	0.75*	0.97*	0.14	-0.62*	0.7*	0.57	0.46	0.81*	0.50	0.85*	1.00															
La	0.53	0.07	0.21	0.26	0.09	0.34	0.64*	0.55	0.83*	0.46	0.18	0.07	0.33	0.20	0.06	0.22	0.24	0.78*	0.02	0.34	1.00														
Cr	0.08	0.25	0.40	0.46	0.13	0.65*	0.69*	0.66*	0.79*	0.13	0.35	-0.12	0.10	0.37	0.29	0.27	0.38	0.78*	0.40	0.34	0.61*	1.00													
Mg	-0.20	0.26	0.27	0.36	0.07	0.52	0.59	0.55	0.67*	-0.17	0.06	-0.15	0.21	0.29	0.21	0.24	0.17	0.57	0.15	0.04	0.52	0.9*	1.00												
Ba	0.35	0.9*	0.83*	0.81*	0.95*	0.73*	0.62*	0.59	0.26	0.58	0.81*	0.55	-0.64*	0.96*	0.6*	0.85*	0.86*	0.32	0.74*	0.74*	0.08	0.26	0.12	1.00											
Ti	0.05	-0.33	-0.34	-0.29	-0.50	-0.24	0.04	0.01	0.53	-0.18	-0.63*	-0.05	0.82*	-0.42	-0.31	-0.18	-0.39	0.38	-0.65*	-0.53	0.57	0.34	0.48	-0.56	1.00										
Al	0.21	0.49	0.72*	0.73*	0.51	0.85*	0.76*	0.73*	0.52	0.42	0.84*	-0.04	-0.50	0.67*	0.54	0.44	0.69*	0.65*	0.86*	0.79*	0.31	0.75*	0.51	0.69*	-0.32	1.00									
Na	0.74*	0.16	0.33	0.37	0.36	0.15	0.43	0.31	0.41	0.87*	0.49	0.29	-0.17	0.35	0.01	0.21	0.44	0.45	0.19	0.64*	0.46	0.00	-0.19	0.40	-0.17	0.25	1.00								
K	0.52	0.16	0.51	0.57	0.13	0.48	0.78*	0.75*	0.92*	0.61*	0.36	0.05	0.05	0.33	0.31	0.28	0.44	0.9*	0.15	0.48	0.82*	0.6*	0.48	0.23	0.41	0.45	0.62*	1.00							
Sc	0.61*	0.30	0.60	0.58	0.46	0.62*	0.66*	0.59	0.45	0.74*	0.83*	0.08	-0.46	0.52	0.37	0.35	0.59	0.64*	0.7*	0.86*	0.43	0.43	0.07	0.61*	-0.32	0.78*	0.51	0.46	1.00						
Tl	0.48	0.43	0.66*	0.65*	0.61*	0.71*	0.65*	0.59	0.33	0.68*	0.95*	0.08	-0.61*	0.66*	0.44	0.40	0.72*	0.51	0.87*	0.96*	0.27	0.41	0.09	0.75*	-0.56	0.87*	0.55	0.38	0.91*	1.00					
S	0.06	0.58	0.42	0.35	0.65*	0.58	0.19	0.18	-0.18	0.16	0.66*	0.25	-0.54	0.59	0.44	0.45	0.63*	-0.05	0.83*	0.57	-0.31	0.14	-0.01	0.67*	-0.72*	0.60	-0.04	-0.27	0.40	0.63*	1.00				
Hg	0.15	0.78*	0.86*	0.82*	0.73*	0.88*	0.64*	0.73*	0.23	0.33	0.73*	0.31	-0.66*	0.81*	0.92*	0.73*	0.85*	0.26	0.76*	0.66*	0.02	0.27	0.19	0.76*	-0.45	0.61*	0.13	0.25	0.39	0.56	0.67*	1.00			
Se	0.21	0.49	0.8*	0.75*	0.54	0.86*	0.61*	0.74*	0.25	0.42	0.93*	-0.02	-0.75*	0.68*	0.82*	0.48	0.8*	0.39	0.93*	0.86*	0.14	0.40	0.13	0.68*	-0.53	0.8*	0.22	0.30	0.74*	0.82*	0.64*	0.8*	1.00		
Te	0.00	0.00	0.00	0.00	0.00	0.00	0.00	0.00	0.00	0.00	0.00	0.00	0.00	0.00	0.00	0.00	0.00	0.00	0.00	0.00	0.00	0.00	0.00	0.00	0.00	0.00	0.00	0.00	0.00	0.00	0.00	0.00	0.00	1.00	
Ga	0.36	0.34	0.67*	0.68*	0.45	0.73*	0.73*	0.68*	0.50	0.57	0.87*	-0.09	-0.53	0.58	0.43	0.32	0.62*	0.67*	0.81*	0.85*	0.38	0.64*	0.33	0.64*	-0.34	0.95*	0.43	0.50	0.91*	0.93*	0.47	0.46	0.79*	0.00	1.00

** Correlation is significant at the significance level* α = 0.05 (2-tailed).

Table 9: Pearson correlation analysis between elements in stream sediments (<63 µm fraction) from Brakkelva (n=12). Elements which correlates significantly with Cu are highlighted with red text.

	Mo	Cu	Pb	Zn	Ag	Ni	Co	Mn	Fe	As	U	Au	Th	Sr	Cd	Sb	Bi	V	Ca	P	La	Cr	Mg	Ba	Ti	Al	Na	K	Sc	Tl	S	Hg	Se	Te	Ga
Mo	1.00																																	
Cu	0.22	1.00																																
Pb	0.41	0.15	1.00																															
Zn	0.72*	0.75*	0.51	1.00																														
Ag	0.36	0.6*	0.13	0.59*	1.00																													
Ni	0.54	0.7*	0.26	0.85*	0.42	1.00																												
Co	0.46	0.68*	0.37	0.75*	0.36	0.88*	1.00																											
Mn	0.89*	0.25	0.56	0.76*	0.51	0.55	0.46	1.00																										
Fe	0.91*	0.46	0.40	0.85*	0.41	0.77*	0.75*	0.84*	1.00																									
As	0.96*	0.30	0.38	0.77*	0.52	0.53	0.38	0.89*	0.86*	1.00																								
U	0.13	0.06	-0.21	-0.02	0.69*	-0.22	-0.25	0.09	-0.02	0.27	1.00																							
Au	-0.35	0.31	-0.15	0.02	-0.01	-0.07	-0.04	-0.26	-0.23	-0.23	-0.19	1.00																						
Th	0.27	0.25	0.23	0.44	-0.15	0.7*	0.61*	0.27	0.49	0.13	-0.6*	-0.16	1.00																					
Sr	0.8*	0.27	0.47	0.68*	0.74*	0.47	0.37	0.82*	0.69*	0.87*	0.51	-0.35	0.01	1.00																				
Cd	0.76*	0.30	0.53	0.74*	0.51	0.52	0.47	0.96*	0.76*	0.77*	0.00	-0.12	0.25	0.68*	1.00																			
Sb	0.56	0.17	0.44	0.53	0.36	0.14	-0.03	0.68*	0.37	0.69*	0.12	0.12	-0.26	0.56	0.69*	1.00																		
Bi	0.21	0.74*	0.35	0.64*	0.34	0.45	0.39	0.34	0.31	0.29	-0.18	0.34	0.05	0.16	0.45	0.53	1.00																	
V	0.38	0.78*	0.29	0.72*	0.41	0.83*	0.97*	0.33	0.68*	0.32	-0.13	0.04	0.53	0.34	0.33	-0.11	0.40	1.00																
Ca	0.63*	0.39	0.38	0.65*	0.75*	0.61*	0.64*	0.64*	0.68*	0.67*	0.44	-0.27	0.11	0.88*	0.53	0.25	0.10	0.62*	1.00															
P	0.58*	0.20	0.08	0.46	0.8*	0.30	0.16	0.58*	0.50	0.69*	0.78*	-0.37	-0.11	0.85*	0.46	0.32	-0.07	0.18	0.75*	1.00														
La	0.26	0.00	-0.06	0.07	0.67*	-0.19	-0.29	0.23	0.05	0.41	0.96*	-0.25	-0.54	0.63*	0.12	0.26	-0.14	-0.20	0.45	0.83*	1.00													
Cr	0.11	0.32	0.04	0.24	0.12	0.55	0.75*	-0.02	0.36	0.02	-0.13	-0.11	0.34	0.14	-0.08	-0.43	-0.08	0.77*	0.55	0.02	-0.26	1.00												
Mg	-0.04	0.18	-0.16	0.19	0.03	0.63*	0.57	0.01	0.24	-0.12	-0.34	-0.24	0.75*	-0.05	0.03	-0.51	-0.17	0.51	0.24	0.01	-0.41	0.6*	1.00											
Ba	0.78*	0.23	0.64*	0.69*	0.43	0.43	0.28	0.86*	0.62*	0.84*	0.08	-0.16	0.05	0.8*	0.78*	0.84*	0.47	0.18	0.57	0.44	0.26	-0.10	-0.24	1.00										
Ti	-0.03	0.44	0.17	0.25	-0.04	0.52	0.72*	-0.14	0.27	-0.15	-0.33	0.07	0.6*	-0.08	-0.18	-0.58*	0.02	0.78*	0.27	-0.20	-0.41	0.8*	0.55	-0.23	1.00									
Al	0.58*	0.58*	0.32	0.79*	0.64*	0.88*	0.79*	0.61*	0.76*	0.59*	0.14	-0.29	0.58*	0.7*	0.52	0.06	0.21	0.77*	0.82*	0.63*	0.18	0.52	0.59*	0.42	0.47	1.00								
Na	0.09	0.32	0.22	0.33	0.12	0.58*	0.62*	-0.02	0.32	0.03	-0.08	-0.29	0.62*	0.20	-0.14	-0.50	-0.17	0.66*	0.46	0.19	-0.10	0.7*	0.67*	-0.12	0.81*	0.7*	1.00							
K	0.03	0.28	0.58*	0.25	-0.05	0.35	0.55	0.01	0.20	-0.08	-0.30	-0.04	0.51	0.08	-0.07	-0.36	0.09	0.58*	0.27	-0.18	-0.28	0.52	0.27	0.04	0.84*	0.40	0.72*	1.00						
Sc	0.34	0.56	0.15	0.59*	0.55	0.81*	0.87*	0.35	0.59*	0.32	0.08	-0.12	0.46	0.49	0.30	-0.17	0.12	0.86*	0.81*	0.40	0.00	0.83*	0.68*	0.19	0.66*	0.87*	0.71*	0.46	1.00					
Tl	0.27	0.33	0.67*	0.43	0.24	0.41	0.61*	0.28	0.42	0.19	-0.03	-0.15	0.48	0.38	0.20	-0.20	0.05	0.64*	0.52	0.19	0.01	0.46	0.23	0.19	0.72*	0.59*	0.72*	0.91*	0.55	1.00				
S	0.66*	0.67*	0.38	0.85*	0.9*	0.63*	0.59*	0.75*	0.73*	0.76*	0.45	-0.06	0.07	0.84*	0.74*	0.52	0.47	0.6*	0.82*	0.76*	0.48	0.19	0.05	0.64*	0.05	0.76*	0.20	0.06	0.61*	0.37	1.00			
Hg	0.33	0.18	0.00	0.25	0.84*	0.02	-0.06	0.37	0.20	0.49	0.94*	-0.21	-0.50	0.73*	0.29	0.35	0.00	0.01	0.64*	0.9*	0.94*	-0.08	-0.26	0.35	-0.35	0.35	-0.05	-0.29	0.24	0.03	0.68*	1.00		
Se	0.79*	0.32	0.50	0.74*	0.73*	0.43	0.34	0.9*	0.71*	0.89*	0.42	-0.18	-0.05	0.91*	0.85*	0.76*	0.35	0.28	0.74*	0.78*	0.53	-0.07	-0.17	0.83*	-0.28	0.57	-0.05	-0.12	0.33	0.21	0.89*	0.68*	1.00	
Te	0.63*	0.57	0.65*	0.87*	0.57	0.71*	0.62*	0.85*	0.7*	0.67*	-0.09	-0.03	0.36	0.66*	0.88*	0.64*	0.67*	0.52	0.58*	0.36	0.02	0.07	0.13	0.81*	0.05	0.65*	0.09	0.21	0.47	0.36	0.78*	0.22	0.77*	1.00
Ga	0.08	0.48	0.11	0.37	0.23	0.7*	0.82*	0.04	0.39	-0.01	-0.17	-0.10	0.65*	0.14	0.01	-0.53	0.00	0.84*	0.51	0.08	-0.26	0.85*	0.78*	-0.13	0.9*	0.72*	0.87*	0.69*	0.88*	0.67*	0.28	-0.11	-0.06	0.22

* *Correlation is significant at the significance level* α = 0.05 (2-tailed).

Table 10: Pearson correlation analysis between elements in stream sediments (125-250 µm fraction) from Brakkelva (n=12). Elements which correlates significantly with Cu are highlighted with red text.

	Mo	Cu	Pb	Zn	Ag	Ni	Co	Mn	Fe	As	U	Au	Th	Sr	Cd	Sb	Bi	V	Ca	P	La	Cr	Mg	Ba	Ti	Al	Na	K	Sc	Tl	S	Hg	Se	Te	Ga
Mo	1.00																																		
Cu	0.13	1.00																																	
Pb	-0.23	-0.04	1.00																																
Zn	0.55	0.78*	0.08	1.00																															
Ag	-0.21	0.22	0.49	0.12	1.00																														
Ni	0.20	0.65*	0.14	0.69*	0.31	1.00																													
Co	-0.07	0.40	0.19	0.32	0.29	0.88*	1.00																												
Mn	0.83*	0.35	0.05	0.69*	0.24	0.40	0.12	1.00																											
Fe	-0.03	0.33	0.23	0.31	0.27	0.85*	0.99*	0.16	1.00																										
As	0.89*	0.35	-0.14	0.64*	-0.01	0.42	0.24	0.91*	0.27	1.00																									
U	0.06	-0.05	-0.29	-0.27	0.18	-0.26	-0.16	0.01	-0.19	0.17	1.00																								
Au	-0.43	0.66*	0.06	0.22	0.27	0.08	0.05	-0.18	-0.01	-0.24	-0.05	1.00																							
Th	-0.22	-0.10	0.59*	0.01	0.71*	0.06	-0.02	0.14	0.00	-0.22	-0.35	0.09	1.00																						
Sr	0.05	0.15	0.57	0.19	0.26	0.52	0.61*	0.12	0.61*	0.24	0.18	-0.21	-0.07	1.00																					
Cd	0.82*	0.28	-0.21	0.52	-0.07	0.08	-0.17	0.88*	-0.13	0.84*	0.05	-0.08	-0.08	-0.19	1.00																				
Sb	-0.40	-0.19	0.03	-0.38	0.27	-0.44	-0.35	-0.21	-0.34	-0.46	-0.21	0.41	0.41	-0.63*	-0.04	1.00																			
Bi	-0.32	0.32	-0.12	0.15	-0.04	-0.08	-0.21	-0.11	-0.28	-0.29	-0.33	0.45	0.07	-0.53	0.05	0.43	1.00																		
V	-0.03	0.37	0.23	0.32	0.26	0.86*	0.99*	0.15	0.99*	0.28	-0.14	0.00	-0.05	0.66*	-0.14	-0.40	-0.27	1.00																	
Ca	0.16	0.41	0.34	0.40	0.50	0.63*	0.65*	0.38	0.63*	0.48	0.42	-0.03	-0.03	0.83*	0.06	-0.6*	-0.38	0.68*	1.00																
P	0.01	0.01	-0.12	-0.13	0.37	0.09	0.21	0.04	0.17	0.19	0.89*	-0.16	-0.24	0.46	-0.11	-0.40	-0.44	0.22	0.7*	1.00															
La	-0.21	-0.32	-0.01	-0.48	0.02	-0.51	-0.27	-0.34	-0.27	-0.18	0.78*	-0.02	-0.38	0.21	-0.29	-0.04	-0.34	-0.24	0.20	0.67*	1.00														
Cr	-0.10	0.18	0.13	0.11	0.23	0.76*	0.97*	0.04	0.97*	0.18	-0.12	-0.12	-0.04	0.57	-0.22	-0.30	-0.29	0.96*	0.56	0.23	-0.22	1.00													
Mg	0.17	0.50	0.17	0.6*	0.45	0.86*	0.64*	0.37	0.62*	0.28	-0.31	0.02	0.42	0.34	0.03	-0.36	-0.15	0.62*	0.47	0.02	-0.63*	0.54	1.00												
Ba	0.22	0.04	0.01	0.03	0.12	0.45	0.54	0.24	0.55	0.27	-0.12	-0.24	-0.15	0.32	0.13	0.08	-0.18	0.54	0.21	0.05	-0.15	0.61*	0.17	1.00											
Ti	0.05	0.57	0.53	0.58*	0.17	0.78*	0.73*	0.20	0.73*	0.27	-0.28	0.18	-0.02	0.79*	-0.07	-0.51	-0.16	0.76*	0.66*	0.01	-0.24	0.59*	0.56	0.28	1.00										
Al	0.25	0.65*	0.34	0.71*	0.48	0.88*	0.67*	0.45	0.64*	0.43	-0.06	0.08	0.20	0.68*	0.09	-0.54	-0.24	0.67*	0.77*	0.27	-0.32	0.52	0.86*	0.25	0.8*	1.00									
Na	0.01	0.21	0.62*	0.25	0.13	0.6*	0.69*	0.07	0.71*	0.18	-0.13	-0.12	-0.05	0.94*	-0.21	-0.57	-0.40	0.74*	0.68*	0.16	-0.02	0.64*	0.39	0.35	0.9*	0.65*	1.00								
K	-0.29	0.20	0.76*	0.11	0.38	0.36	0.38	-0.13	0.38	-0.24	-0.26	0.19	0.27	0.66*	-0.38	0.00	-0.13	0.39	0.35	-0.05	0.00	0.30	0.26	0.37	0.69*	0.50	0.72*	1.00							
Sc	0.05	0.56	0.46	0.53	0.52	0.84*	0.79*	0.32	0.77*	0.35	0.06	0.11	0.15	0.82*	-0.05	-0.53	-0.28	0.81*	0.9*	0.40	-0.13	0.67*	0.72*	0.26	0.86*	0.93*	0.79*	0.55	1.00						
Tl	0.19	0.28	0.58*	0.36	0.13	0.33	0.20	0.17	0.20	0.19	0.06	-0.05	-0.07	0.8*	-0.04	-0.51	-0.32	0.25	0.56	0.20	0.16	0.09	0.21	0.17	0.72*	0.62*	0.76*	0.76*	0.61*	1.00					
S	-0.23	0.69*	0.10	0.39	0.39	0.84*	0.88*	0.05	0.83*	0.12	-0.09	0.45	0.02	0.43	-0.16	-0.19	0.05	0.85*	0.58*	0.18	-0.30	0.78*	0.65*	0.34	0.69*	0.68*	0.51	0.35	0.77*	0.15	1.00				
Hg	0.07	-0.05	-0.30	-0.24	0.18	-0.28	-0.18	0.03	-0.21	0.18	0.99*	-0.03	-0.35	0.13	0.08	-0.17	-0.32	-0.16	0.40	0.88*	0.8*	-0.14	-0.33	-0.12	-0.31	-0.08	-0.18	-0.29	0.03	0.02	-0.12	1.00			
Se	0.07	0.17	-0.12	0.05	0.28	0.29	0.43	0.17	0.40	0.37	0.77*	-0.11	-0.35	0.51	0.01	-0.49	-0.32	0.45	0.8*	0.92*	0.52	0.43	0.08	0.13	0.19	0.33	0.28	-0.10	0.52	0.15	0.37	0.76*	1.00		
Te	0.13	0.69*	-0.25	0.61*	0.13	0.83*	0.65*	0.31	0.6*	0.32	-0.29	0.21	0.01	0.06	0.19	-0.22	0.18	0.6*	0.28	-0.08	-0.67*	0.55	0.77*	0.29	0.44	0.63*	0.16	0.01	0.51	-0.05	0.75*	-0.29	0.11	1.00	
Ga	0.14	0.54	0.42	0.61*	0.37	0.92*	0.84*	0.33	0.83*	0.37	-0.14	0.02	0.08	0.79*	-0.05	-0.59*	-0.27	0.86*	0.81*	0.24	-0.27	0.72*	0.77*	0.33	0.91*	0.93*	0.82*	0.55	0.96*	0.6*	0.75*	-0.16	0.39	0.58*	1.00

** Correlation is significant at the significance level* α = 0.05 (2-tailed)

3.1.2 Spatial distribution of elements

According to the correlation matrices above, there are several elements that correlates well with Cu and that may be used to trace Cu mineralisation in the sedimentary and mafic rocks in Kåfjord (e.g. Zn, Ag, Bi, Sb, Ni, Co, Sr). Figure 20 illustrate the spatial distribution pattern of some elements in fraction <63 µm and their relationship to the surrounding geology. Note that anomalies in the stream sediments may not be caused by natural relationships, but can be a result of anthropogenic activity in the area, e.g. mining or construction work.

Stream sediments from the Annaselva stream generally has low Cu concentrations compared to the Møllneselva and Brakkelva streams. Sediment samples from areas where the stream is draining the mafic rocks of the Kvenvik formation seem to have the highest concentrations of Cu. High content of Cu is also found in samples close to mine tailings and in sample J018 from the Møllneselva stream right below the second hydropower construction where there has been done excavation work. The sediment sample from the underwater tailing of Lundstrøm mine, J002, the content of Cu exceeds the detection limit of 1000 ppm.

Cobalt and Vanadium shows enrichment in sediments from streams draining the mafic rock-hosted Cu mineralised Kvenvik formation. Cobalt concentration ranges from 2.50 to 13.50 ppm with a median of 10.00 ppm in sediments from the Annaselva stream. In sediments from the Brakkelva stream the concentration of Co ranges from 7.00 to 31.80 ppm with a median of 17.55 ppm (Table 3). The same pattern can be seen for V, whereas the content of Ni in stream sediments is quite even, but increases close to and downstream from the historical Cu mines and their tailings.

Antimony is evenly distributed in the streams, but with one outlier being the sample from the tailing of Lundstrøm mine. The same sample is also a far outlier for Bi. Generally, there is a higher concentration of Bi in the Annaselva stream. Zinc on the other hand shows a pattern similar to Cu. Content of Zn in sediments is highest close to mine tailings and the lower part of the Brakkelva stream.

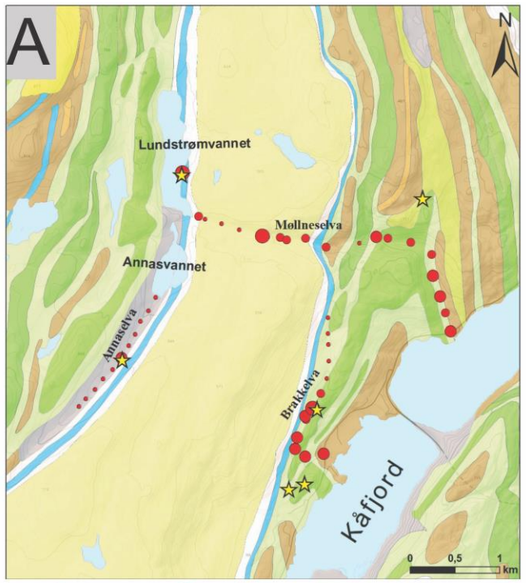

>500 ppm Cu 100-500 ppm Cu 50-100 ppm Cu 10-50 ppm Cu

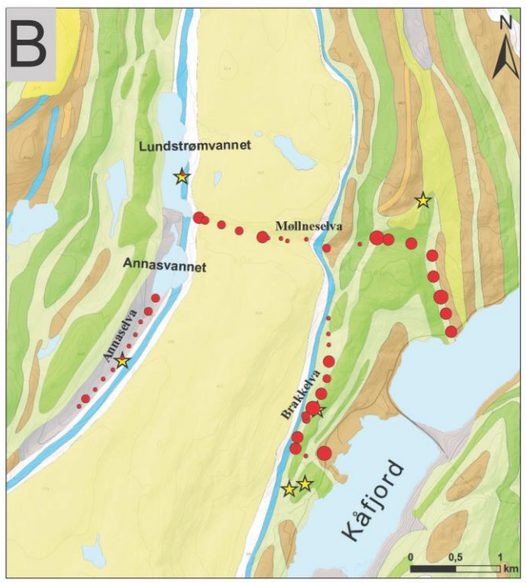

60-200 ppm V 30-60 ppm V 20-30 ppm V 10-20 ppm V

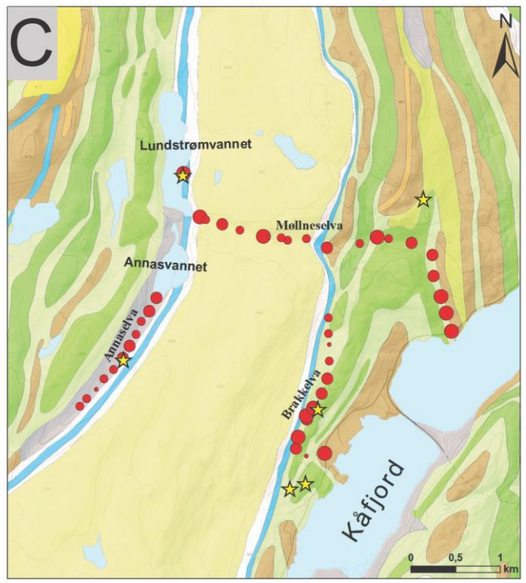

50-110 ppm Ni 30-50 ppm Ni 20-30 ppm Ni 10-20 ppm Ni

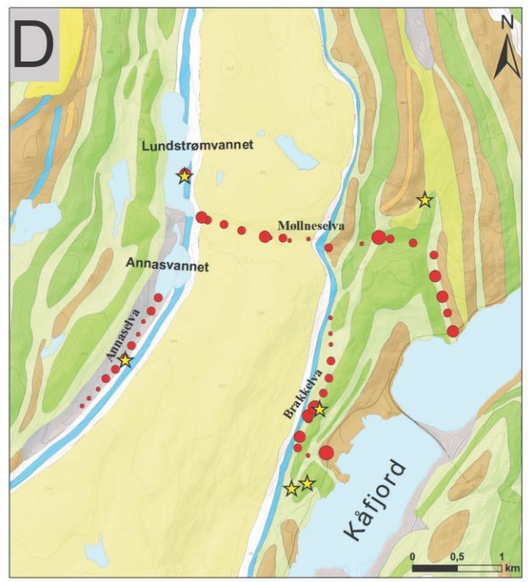

30-60 ppm Co 20-30 ppm Co 10-20 ppm Co 2.5-10 ppm Co

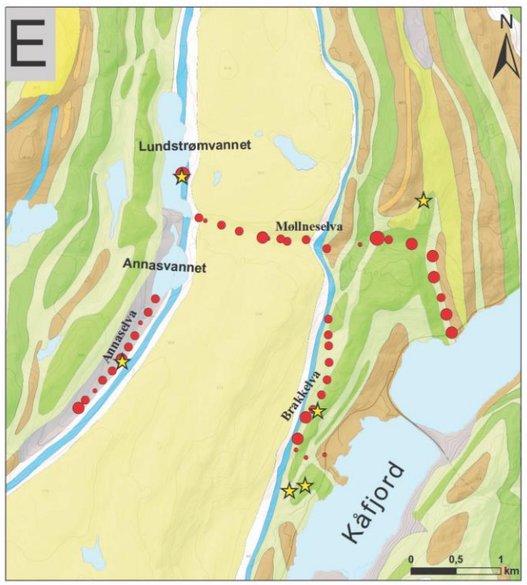

0.5-1.6 ppm Sb 0.3-0.5 ppm Sb 0.2-0.3 ppm Sb 0.1-0.2 ppm Sb

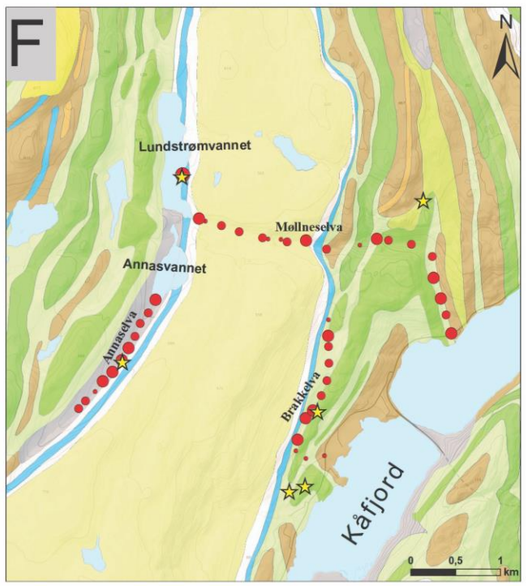

11.86 ppm Bi 0.20-0.35 ppm Bi 0.15-0.20 ppm Bi 0.09-0.15 ppm Bi

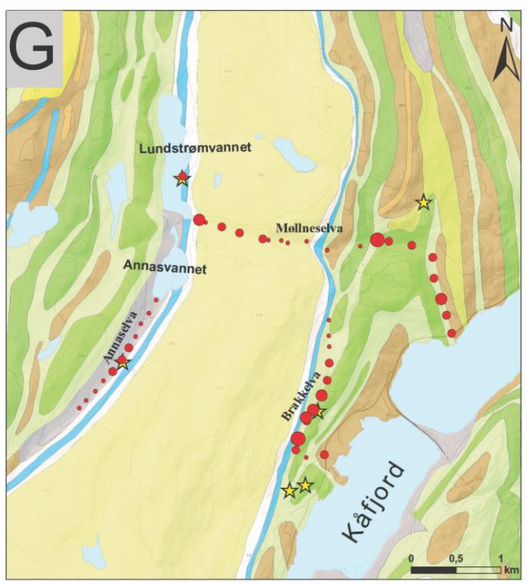

200-400 ppm Zn 100-200 ppm Zn 50-100 ppm Zn 9-50 ppm Zn

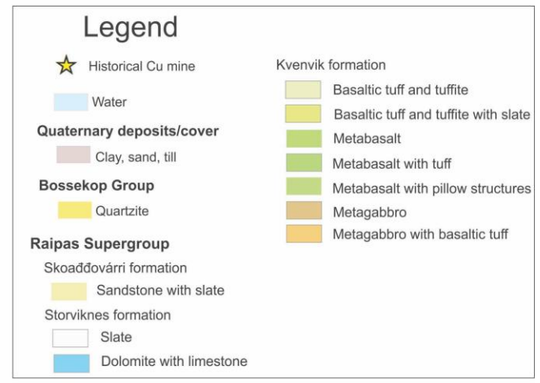

Figure 20: Spatial distribution of a few selected elements in the <63 µm fraction from stream sediment samples: A: Copper, B: Nickel, C: Vanadium, D: Cobalt, E: Antimony, F: Bismuth and G: Zinc. Historical Cu mines and their tailings marked with yellow stars. Geological base map of the bedrock modified from The Geological Survery of Norway (2021a).

3.2 Physicochemical characteristics of pore water in stream sediments

Redox potential (Eh) and pH values of pore water in eight stream sediment samples are presented in Figure 21. Pore water from stream sediments in the Møllneselva stream has the largest variation with Eh values in the range from 0.177 to 0.281 V and pH values between 5.52 and 6.55. Pore water from stream sediments in the Annaselva stream is generally the most oxidized and acidic with Eh and pH in the range of 0.216-0.285 V and 5.59-6.42, respectively. Pore water from the Brakkelva stream shows the most reducing and alkaline character with an Eh value of 0.177 and pH between 6.98 and 7.30.

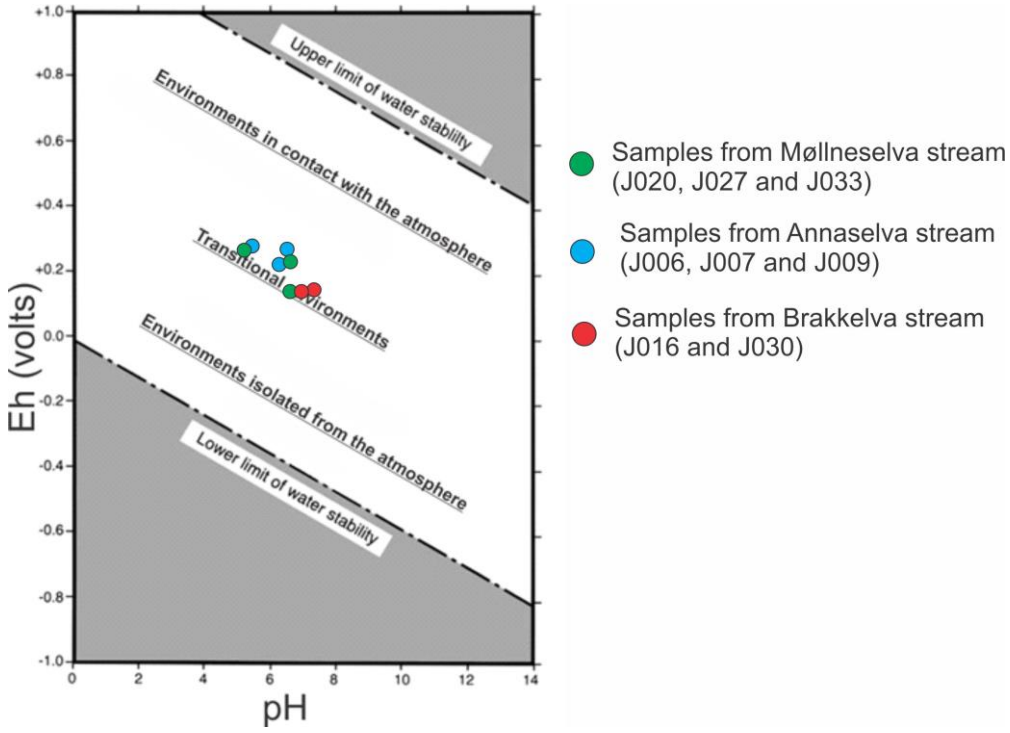

Figure 21: Plot of measured redox potential and pH in stream sediments in relation to geochemical environments.

3.3 Heavy mineral characterization

Fe-oxides were picked from all of 44 collected stream sediment samples (Table 11, Table 12 and Table 13). Almost all samples contain magnetite and a great majority of them also contain hematite. Fe-oxy-hydroxides were separated from 41 samples.

SEM-EDS analyses revealed that some of the grains initially identified as hematite have a significant content of titanium (~32 wt.%) and therefore these grains were classified as ilmenite. However, most of the Fe-oxides analysed by SEM-EDS had Ti content below the detection limit. Rare Fe-oxide grains have 3-15 wt.% Ti.

Grains of sulphides were confirmed by SEM-EDS in 15 stream sediment samples from the Møllneselva (Table 11) and Brakkelva (Table 13) streams which drain the Kvenvik formation. In particular, samples collected along the lower stretches of these streams often contained sulphides. On the contrary, none of the heavy mineral grains separated from samples collected in the Annaselva stream were in the scanning electron microscope identified as sulphides (Table 12). Bornite, chalcopyrite and pyrite were identified under the stereomicroscope as the most common sulphide minerals in the analysed stream sediment samples. However, SEM-EDS analyses showed that grains initially identified as bornite, were tarnished grains of chalcopyrite. From the separated sulphides, only grains of pyrite and chalcopyrite were confirmed in the SEM-EDS with the exception of pyrrhotite from sample J036.

In addition, carbonate grains were picked from five samples and analysed for their stable isotope ($\delta^{13}C$ versus $\delta^{18}O$) composition.

Table 11: List of minerals separated from stream sediments of the Møllneselva stream. "x" marks mineral phases identified and picked under a stereomicroscope, whereas green cells mark mineral compositions confirmed by SEM-EDS.

Sample	Mag	Hem-Ilm	Fe-oxy-hydroxide	Bn	Ccp	Py	Po	Cct	Carbonates
J013	x	x	x						
J014	x	x	x						
J015	x	x	x		x				
J017	x		x						
J018	x	x	x		x	x			x
J019	x	x		x			x		
J020	x	x	x	x	x	x			
J021	x	x	x		x	x			
J022	x	x	x						
J023	x	x	x						x
J024	x	x	x	x	x	x			
J025	x	x	x	x	x				
J026	x	x	x						
J027	x	x	x	x	x				
J032	x	x	x	x	x	x			
J033	x	x	x	x	x	x			
J034	x	x	x	x	x	x			
J035	x	x	x	x	x	x			
J036	x	x	x	x	x	x	x		

Table 12: List of minerals separated from stream sediments of the Annaselva stream

Sample	Mag	Hem-Ilm	Fe-oxy-hydroxide	Bn	Ccp	Py	Po	Cct	Carbonates
J001	x	x							
J003	x	x	x						
J004	x		x						
J005		x	x						
J006	x	x	x						
J007	x	x	x						
J008	x	x	x						
J009	x	x	x			x			
J010	x	x	x		x				
J011	x	x	x						
J012	x	x							
J002	x	x	x	x		x			x

Table 13: List of minerals separated from stream sediments of the Brakkelva stream

Sample	Mag	Hem-Ilm	Fe-oxy-hydroxide	Bn	Ccp	Py	Po	Cct	Carbonates
J028	x	x	x						
J029	x	x	x						
J030	x	x	x						
J031	x	x	x						
J037	x	x	x						
J038	x	x	x		x				
J039	x	x	x	x	x	x	x	x	
J040	x	x	x						
J041	x	x	x	x	x	x			
J042	x	x	x	x	x	x			
J043	x	x	x	x					
J044	x	x	x	x	x	x			x
J016	x	x	x						x

3.3.1 Major element composition of heavy minerals

The major element composition of separated heavy minerals was obtained from SEM-EDS analyses of mineral mounts. In total, more than 100 element maps and 350 spot analyses were collected to gather internal standards for laser ablation analyses (Appendix D).

3.3.1.1 Fe-oxides

In addition to containing varying amounts of Ti, many of the Fe-oxides have a heterogeneous elemental distribution. Exsolution lamellae of ilmenite and spots of Ti-enrichment are features commonly observed (Figure 22B). However, Fe-oxides with a more uniform elemental

distribution were favoured when selecting grains for LA-ICP-MS analyses (Figure 22, Table 14).

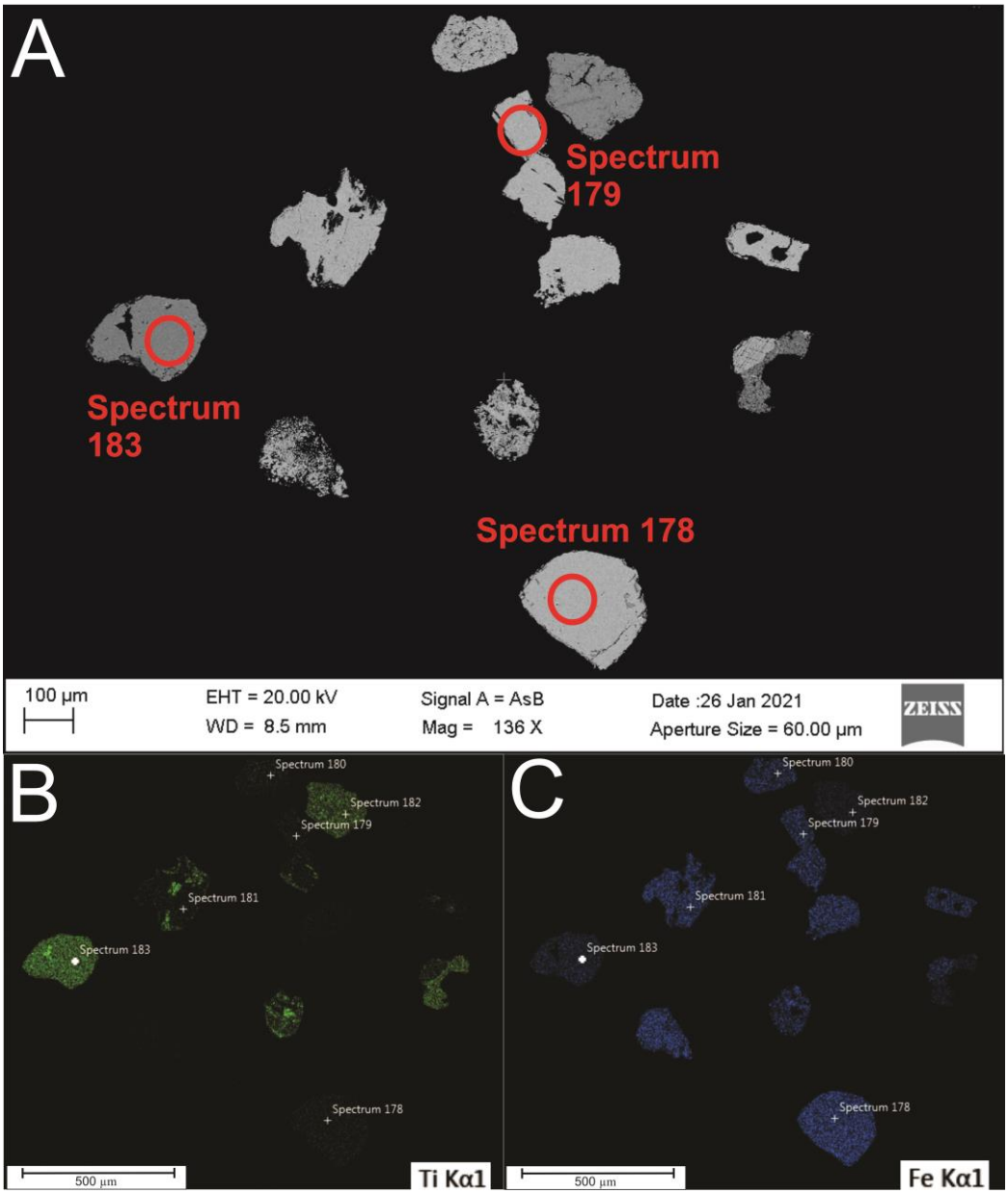

Figure 22: Images of Fe-oxides separated from sample J022. A: BSE image emphasizing the crystalline surface structure of the grains. Red circles mark areas analysed by EDS-spot method and which were further analysed by LA-ICP-MS. B and C: EDS-maps showing the distribution of Ti and Fe across the polished surface of the grains. Local enrichments of Ti is seen on some of the grains.

Table 14: Results of SEM-EDS spot analyses of grains from sample J022 which were selected for LA-ICP-MS (wt.% normalized to 100%). One of the grains, spectrum 183, has a composition of ilmenite.

Spectrum	O	Ti	Fe	Cr	Mn
178	27,9	3,38	68,72	-	-
179	27,67	3,36	68,69	0,29	-
183	31,11	32,12	35,88	-	0,89

3.3.1.2 Fe-oxy-hydroxides

The Fe-oxy-hydroxides were very fine-grained, appearing as brittle shells or porous mineral aggregates with a variable elemental composition (Figure 23, Table 15). Because variable amounts of OH groups in different types of Fe-oxy-hydroxides, the acquired EDS-data were not normalized to 100 wt.% and absolute concentrations of Fe were reported to be used as internal standard (Appendix D). Limitations of the SEM-EDS method in analyses of OH-bearing mineral phases have been discussed in section 2.5.3.

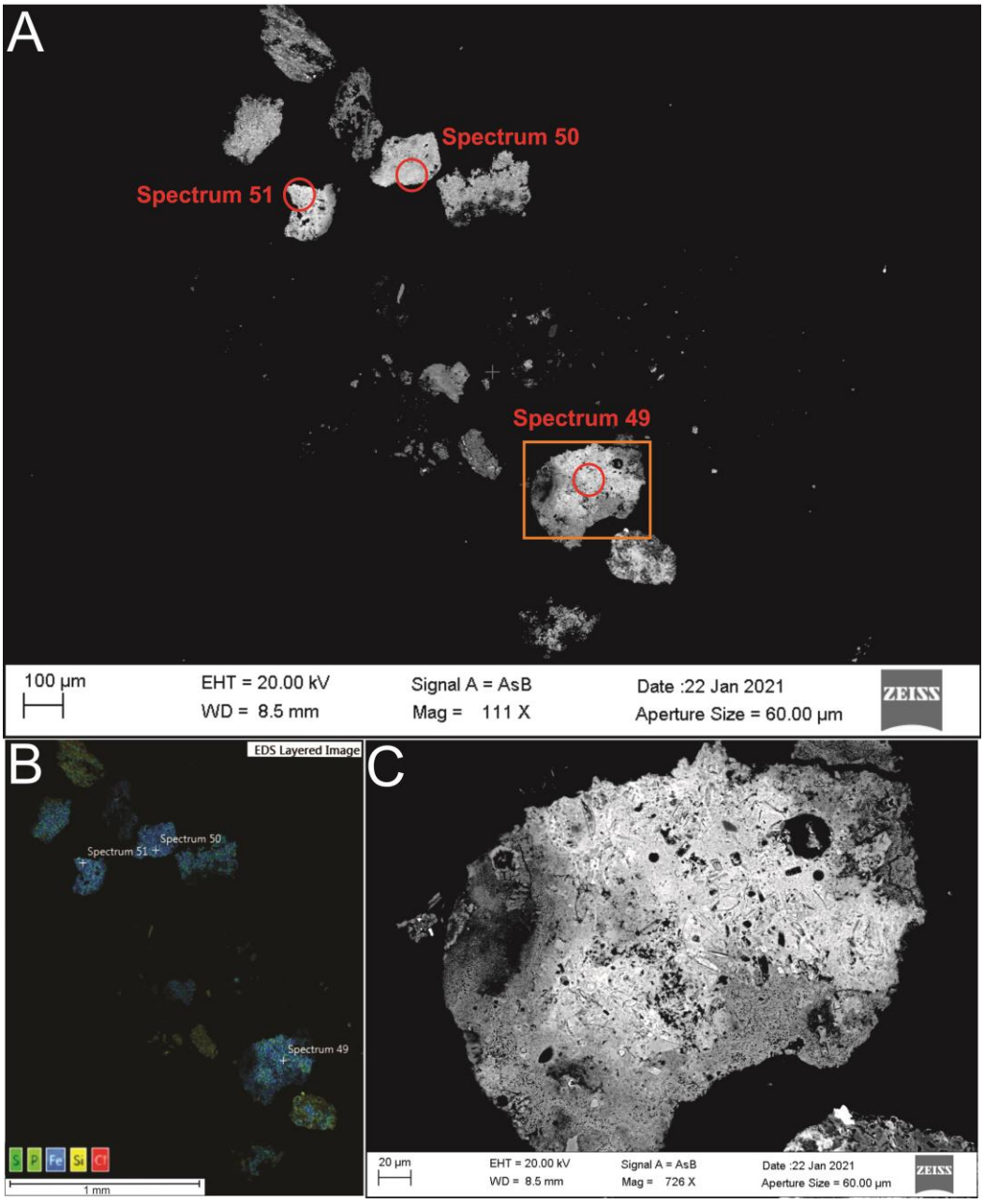

Figure 23: Images of Fe-oxy-hydroxides separated from sample J008. A: BSE image of the grouping of grains and spots analysed by SEM-EDS and which were further analysed by LA-ICP-MS. Orange inset marks area of Figure 23C. B: EDS layered image of the same grouping of grains. Blue and yellow areas indicate high concentrations of Fe and Si, respectively. C: High-magnification BSE image of a grain emphasizing the large variations on the crystalline surface structure.

Table 15: Results of SEM-EDS spot analyses of Fe-oxy-hydroxides from sample J008 which were selected for LA-ICP-MS (total absolute concentrations). As seen in the right row, total absolute concentration deviates from 100%.

Spectrum	O	Fe	Al	Si	P	Ca	Mn	Total wt.%
49	18,86	52,12	0,26	1,50	0,17	0,27	-	73,18
50	22,48	47,41	-	1,37	-	0,60	-	71,86
51	18,91	52,08	-	1,70	0,19	0,26	0,25	73,13

3.3.1.3 Pyrite and chalcopyrite

Grains of pyrite and chalcopyrite were for the most part homogenous in composition. A few of the grains had an oxidized rim, identified in the SEM by the presence of oxygen and lack of sulphur, and were not prioritized when selecting grains for laser ablation.

In general, the elemental composition of pyrite and chalcopyrite analysed in the SEM-EDS showed values very similar to their empirical formulas from the literature (Figure 24, Table 16). The small deviation is assumed to mainly derive from the margin of error which follows the method. Exceptions are spot analyses on two pyrite grains where 1-1.5 wt.% of nickel was recorded (Appendix D).

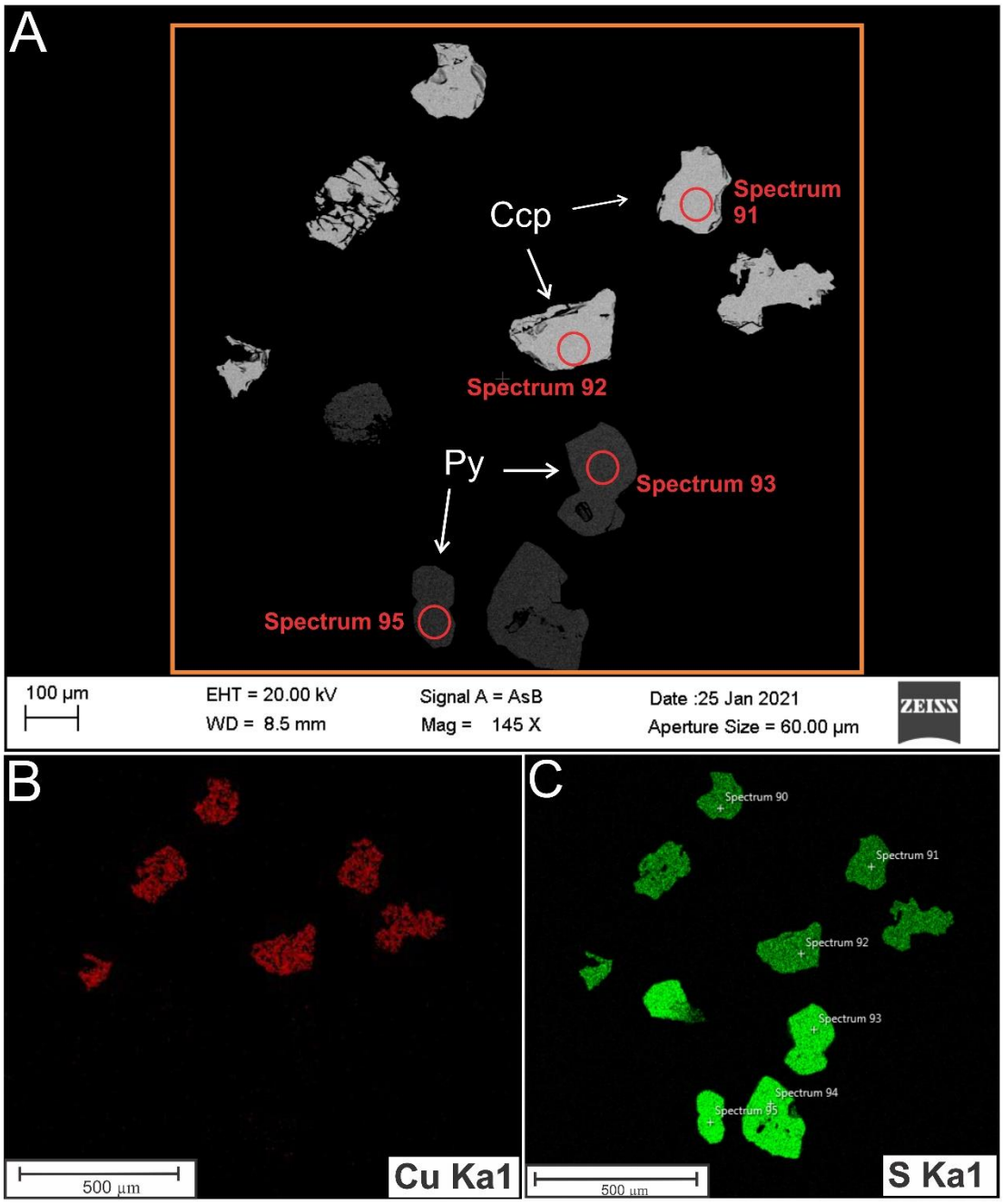

Figure 24: Images of pyrite and chalcopyrite separated from sample J032. A: BSE image of the grouping of sulphides. Red circles are spots analysed by both SEM-EDS and LA-ICP-MS. The inset marks area of Figure 24B and Figure 24C. B and C: EDS-maps showing the distribution of Cu and S. Only grains of Ccp are visible on the Cu EDS-map. Grains of Py gives a stronger positive S-signal than the Ccp.

Table 16: Results of SEM-EDS spot analyses of pyrite and chalcopyrite grains from sample J032 selected for LA-ICP-MS (wt.% normalized to 100%).

Spectrum	S	Fe	Cu
91	34,42	30,94	34,63
92	34,76	30,70	34,55
93	53,08	46,92	-
95	53,02	46,98	-

3.3.1.4 Pyrrhotite

Grains of pyrrhotite were only identified in sample J036. Pyrrhotite grains look more fractured than the other sulphides. Four EDS-spot analyses were performed on these grains (Figure 25, Table 17) and they show very similar compositions despite the varying chemical formula of pyrrhotite ($Fe_{(1-x)}S$, where x = 0-0.17). The same four spots have been analysed by LA-ICP-MS for their trace element composition.

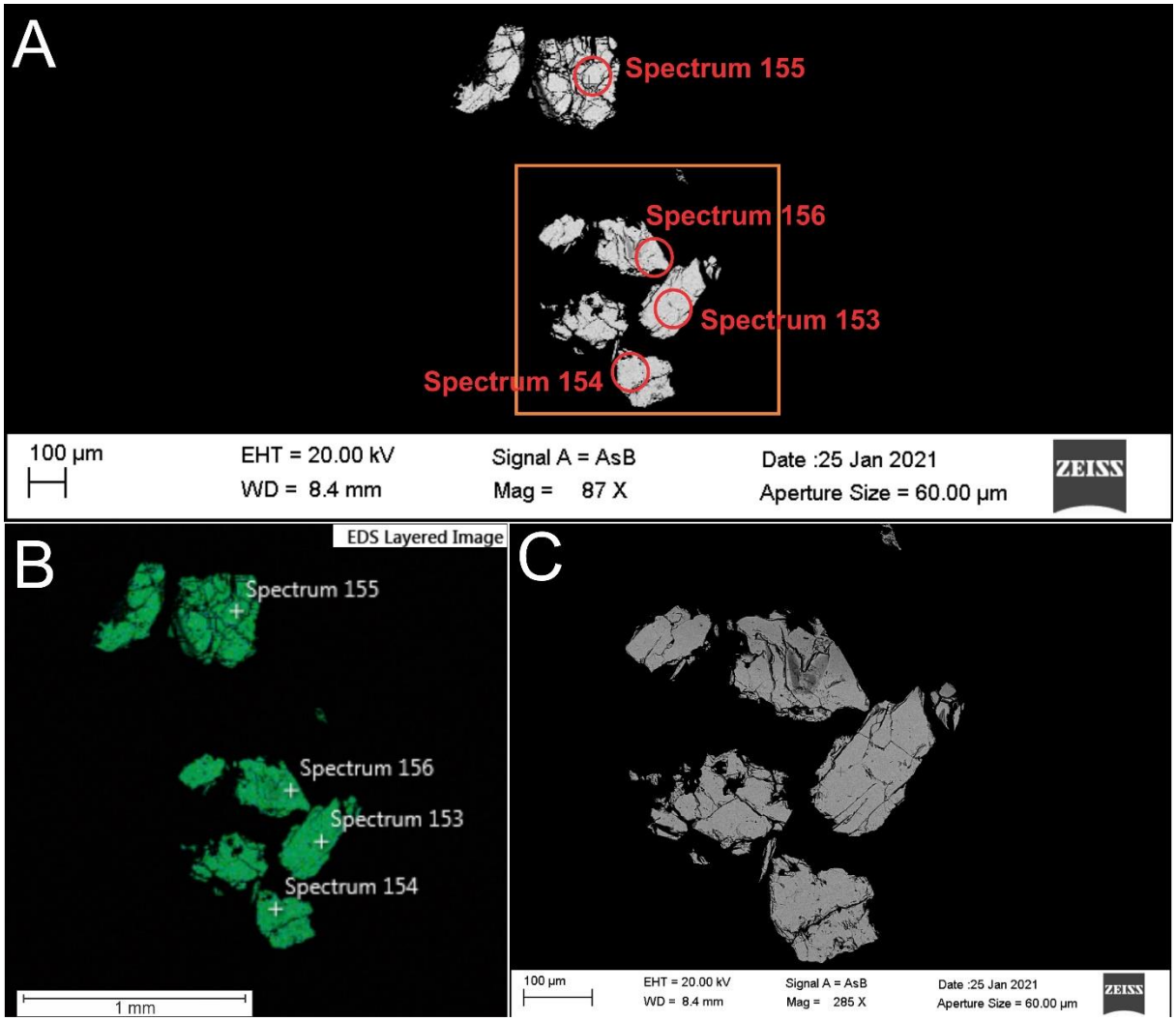

Figure 25: Images of pyrrhotite picked from sample J036. A: BSE image of the pyrrhotite grains with spots marked for LA-ICP-MS (red circles). The inset marks the area of Figure 25C. B: Layered EDS-image displaying no evident variable elemental distribution. C: High-magnification BSE image of pyrrhotite grains featuring the more deformed trend of these sulphides.

Table 17: Results of SEM-EDS spot analyses of pyrrhotite grains selected for LA-ICP-MS (wt.% normalized to 100%).

Spectrum	S	Fe
153	39,23	60,77
154	39,27	60,63
155	39,27	60,63
156	39,23	60,77

3.4 Minor and trace element composition of heavy minerals

The LA-ICP-MS technique was utilized to analyse the minor and trace element composition of selected heavy minerals. The results of the LA-ICP-MS of Fe-oxides, Fe-oxy-hydroxides and sulphides are listed in Appendix F.

3.4.1 Fe-oxides and Fe-oxy-hydroxides

LA-ICP-MS analyses of Fe-oxides and Fe-oxy-hydroxides determined concentrations of 35 elements. Descriptive statistics of a selection of elements with number of grains analysed of each mineral from the different streams are listed in Table 18 and is the basis of data presented in Figure 26. Note that the statistical power varies between the different heavy minerals due to difference in sample size.

Table 18: Summary statistics of a selection of minor and trace elements in Fe-oxy-hydroxides and Fe-oxides from LA-ICP-MS analyses. All concentrations are given in parts per million. Corresponding box-plots are shown in Figure 26. Med = median concentration, min = minimum concentration, max = maximum concentration, n = number of spots/grains analysed.

Fe-oxy-hydroxides

	The Møllneselva stream n = 39			The Annaselva stream n = 17			The Brakkelva stream n = 20			All streams n = 76		
	Med	Min	Max	Med	Min	Max	Med	Min	Max	Med	Min	Max
Mg	545	25.3	9809	480	65.3	5821	649	34.1	4064	589	25.3	9809
Mn	705	6.03	19225	2370	12.5	23470	907	15.1	14174	965	6.03	23470
Ca	2289	81.8	22959	4187	92.4	13855	2362	236	26342	3011	81.8	26342
Al	3103	0.04	54146	10470	288	55366	3782	0.05	45480	4160	0.04	55366
Sc	2.07	0.00	106	1.91	0.24	16.2	1.18	0.05	85.5	1.92	0.00	106
Ti	22.1	0.04	15972	305	6.12	4231	13.8	0.02	3846	35.4	0.02	15972
V	42.6	0.02	686	104	0.92	2937	36.1	0.00	2020	53.4	0.00	2937
Cr	25.2	1.26	1037	49.1	2.32	1414	12.9	0.64	8035	25.2	0.64	8035
Ni	121	1.10	3806	24.2	12.5	623	170	4.68	1592	99.9	1.10	3806
Mo	10.1	0.05	181	25.2	0.05	624	15.2	0.06	386	15.8	0.05	624
Co	56.0	0.06	11283	25.5	8.18	8912	54.7	5.88	9216	40.7	0.06	11283
Cu	112	0.58	3289	60.0	4.49	4846	105	1.91	4298	69.5	0.58	4846
Zn	81.5	0.03	3269	240	0.57	13450	176	0.43	1539	170	0.03	13450
As	150	0.86	13691	419	29.7	3037	201	0.66	5892	221	0.66	13691
Se	5.66	0.09	109	4.23	0.59	367	4.35	0.06	157	5.13	0.06	367
Sb	1.34	0.01	572	3.36	0.62	57.3	2.54	0.03	612	2.06	0.01	612
Pb	4.56	0.00	1072	39.4	0.85	495	13.4	0.00	1764	11.3	0.00	1764

Ilmenite

	The Møllneselva stream n = 7			The Annaselva stream n = 10			The Brakkelva stream n = 1			All streams n = 18		
	Med	Min	Max	Med	Min	Max	Med	Min	Max	Med	Min	Max
Mg	2469	363	9437	1073	294	5812	1337	1337	1337	1682	294	9437
Mn	17514	51.2	24040	8787	58.2	50809	14176	14176	14176	14125	51.2	50809
Ca	9.98	2.13	7913	119	2.80	6092	3.00	3.00	3.00	45.8	2.13	7913
Al	163	9.51	8944	180	12.6	5932	23.2	23.2	23.2	143	9.51	8944
Sc	14.6	2.79	29.0	6.70	1.65	81.4	4.79	4.79	4.79	7.03	1.65	81.4
Ti	302968	287818	356807	313405	259392	395790	338026	338026	338026	313405	259392	395790
V	543	95.6	1645	479	15.9	1910	252	252	252	513	15.9	1910
Cr	58.8	20.2	803	66.0	3.46	492	15.6	15.6	15.6	58.8	3.46	803
Ni	16.9	1.48	33.2	3.08	0.10	16.5	22.6	22.6	22.6	6.80	0.10	33.2
Mo	3.38	1.49	17.0	3.16	1.04	27.7	2.97	2.97	2.97	3.26	1.04	27.7
Co	55.1	1.52	83.2	14.0	1.70	40.7	74.9	74.9	74.9	28.8	1.52	83.2
Cu	5.31	4.74	6.77	5.46	4.42	10.4	5.21	5.21	5.21	5.32	4.42	10.4
Zn	102	14.3	687	83.4	14.8	2604	233	233	233	100	14.3	2604
As	1.14	0.27	4.31	1.07	0.69	63.4	0.74	0.74	0.74	1.05	0.27	63.4
Se	0.05	0.03	0.15	0.12	0.04	1.03	0.03	0.03	0.03	0.05	0.03	1.03
Sb	0.02	0.00	2.08	0.05	0.00	12.8	0.00	0.00	0.00	0.03	0.00	12.8
Pb	0.02	0.00	0.68	0.61	0.00	48.1	0.01	0.01	0.01	0.16	0.00	48.1

Hematite

	The Møllneselva stream n = 30			The Annaselva stream n = 7			The Brakkelva stream n = 22			All streams n = 59		
	Med	Min	Max	Med	Min	Max	Med	Min	Max	Med	Min	Max
Mg	248	7.33	2931	108	69.0	1982	325	17.1	2520	262	7.33	2931
Mn	114	0.93	1082	154	69.9	242	61.1	1.11	1113	109	0.93	1113
Ca	45.6	1.90	4465	175	30.7	340	29.7	1.91	4665	43.9	1.90	4665
Al	709	175	6682	1326	310	3467	392	11.4	1225	566	11.4	6682
Sc	2.97	0.13	110	1.76	0.92	68.7	2.11	0.01	44.3	2.09	0.01	110
Ti	8527	0.07	40197	15870	340	49673	1931	0.05	44680	7075	0.05	49673
V	626	9.66	5194	419	97.4	2264	146	2.41	1681	393	2.41	5194
Cr	370	0.10	3141	298	23.6	16671	289	0.09	3123	298	0.09	16671
Ni	13.7	0.05	108	25.8	3.05	441	4.78	0.09	1000	10.1	0.05	1000
Mo	0.38	0.00	60.8	0.82	0.05	9.90	0.15	0.00	4.07	0.34	0.00	60.8
Co	3.81	0.03	42.2	5.68	2.11	93.3	0.86	0.01	19640	2.89	0.01	19640
Cu	0.39	0.01	528	4.25	0.41	252	0.21	0.01	218	0.43	0.01	528
Zn	5.70	0.04	88.5	13.7	1.86	1896	0.80	0.05	15.1	2.76	0.04	1896
As	1.62	0.20	124	74.7	0.82	100	1.18	0.62	736	1.60	0.20	736
Se	0.12	0.03	6.48	0.05	0.03	1.00	0.11	0.02	28.0	0.11	0.02	28.0
Sb	0.57	0.00	28.0	17.1	0.07	34.9	0.18	0.00	41.0	0.51	0.00	41.0
Pb	0.86	0.00	184	69.7	2.21	137	0.01	0.00	183	0.42	0.00	184

Magnetite

	The Møllneselva stream n = 163			The Annaselva stream n = 83			The Brakkelva stream n = 105			All streams n = 351		
	Med	Min	Max	Med	Min	Max	Med	Min	Max	Med	Min	Max
Mg	163	9.65	20314	133	1.33	29100	82.0	5.67	9266	122	1.33	29100
Mn	255	2.72	10507	169	20.2	9178	234	8.44	16986	224	2.72	16986
Ca	44.4	1.44	5661	31.0	1.40	2338	39.6	1.38	35287	39.5	1.38	35287
Al	399	23.4	30436	999	50.0	92062	454	1.66	89768	482	1.66	92062
Sc	0.50	0.01	188	0.87	0.01	109	0.29	0.01	39.0	0.50	0.01	188
Ti	75.4	1.16	32382	643	46.1	43390	129	0.68	35023	140	0.68	43390
V	1009	0.45	3967	636	19.7	9327	1252	0.01	4805	972	0.01	9327
Cr	354	0.44	373343	539	0.12	440432	216	0.08	262892	374	0.08	440432
Ni	98.2	2.02	2789	130	0.23	3144	110	2.87	993	108	0.23	3144
Mo	0.05	0.00	361	0.12	0.00	21.6	0.05	0.00	6.80	0.06	0.00	361
Co	19.5	0.01	576	37.2	0.63	809	33.9	0.01	672	31.9	0.01	809
Cu	0.11	0.00	1791	0.42	0.01	257	0.08	0.01	107	0.11	0.00	1791
Zn	11.4	0.06	12958	26.9	0.49	84352	20.6	0.06	170968	21.0	0.06	170968
As	0.87	0.23	164	2.02	0.30	103	0.74	0.14	142	0.88	0.14	164
Se	0.06	0.01	7.48	0.06	0.02	5.22	0.05	0.02	4.26	0.06	0.01	7.48
Sb	0.03	0.00	54.6	0.14	0.00	21.0	0.01	0.00	36.8	0.03	0.00	54.6
Pb	0.06	0.00	113	0.98	0.00	286	0.02	0.00	243	0.09	0.00	286

There are marked variations in minor and trace element composition between the various Fe-oxide minerals and the Fe-oxy-hydroxides (Figure 26). Fe-oxy-hydroxides are enriched in most chalcophile elements (Cu, Zn, As, Se, Sb and Pb) relative to the Fe-oxides. The Fe-oxy-hydroxides also have the highest content of Ca, Al and Mo, but contains lower amounts of Ti, V and Cr.

Only 18 grains of ilmenite was identified across 44 samples. Ilmenite is enriched in Mg, Mn, Sc, Mo, Cu and Zn compared to hematite and magnetite. Hematite is slightly more enriched in most chalcophile elements (Cu, As, Se, Sb and Pb) comparing to magnetite. Perhaps the most striking contrast between hematite and magnetite is the difference in content of Ti, Ni and Co. Hematite has median Ti concentrations of 7075 ppm, whereas magnetite has a median Ti content of 140 ppm. The opposite is observed for Ni and Co. For magnetite, the median values of Ni and Co concentrations are 108 and 31.9 ppm, respectively, and they are approximately one order of magnitude greater than in hematite (Table 18).

Comparison of the median concentrations of Fe-oxides separated from the three different streams reveal that there are minor variations. Grains from the Møllneselva and Brakkelva streams seem to have similar minor and trace element compositions, whereas grains from the Annaselva stream often differs. Hematite and magnetite from the Annaselva stream have higher median concentrations of chalcophile elements than grains separated from the Møllneselva and Brakkelva streams. In addition, hematite and magnetite from Annaselva also have high contents of Al and Ni compared to similar minerals from the two other streams.

Some of the same characteristics can be seen for Fe-oxy-hydroxides. Most of the chaclcophile elements (Zn, As, Sb and Pb) show higher median concentrations in Fe-oxy-hydroxides from the Annaselva stream comparing to those from the Møllneselva and Brakkelva streams. Aluminium is also enriched in grains from Annaselva, but they have a low Ni content.

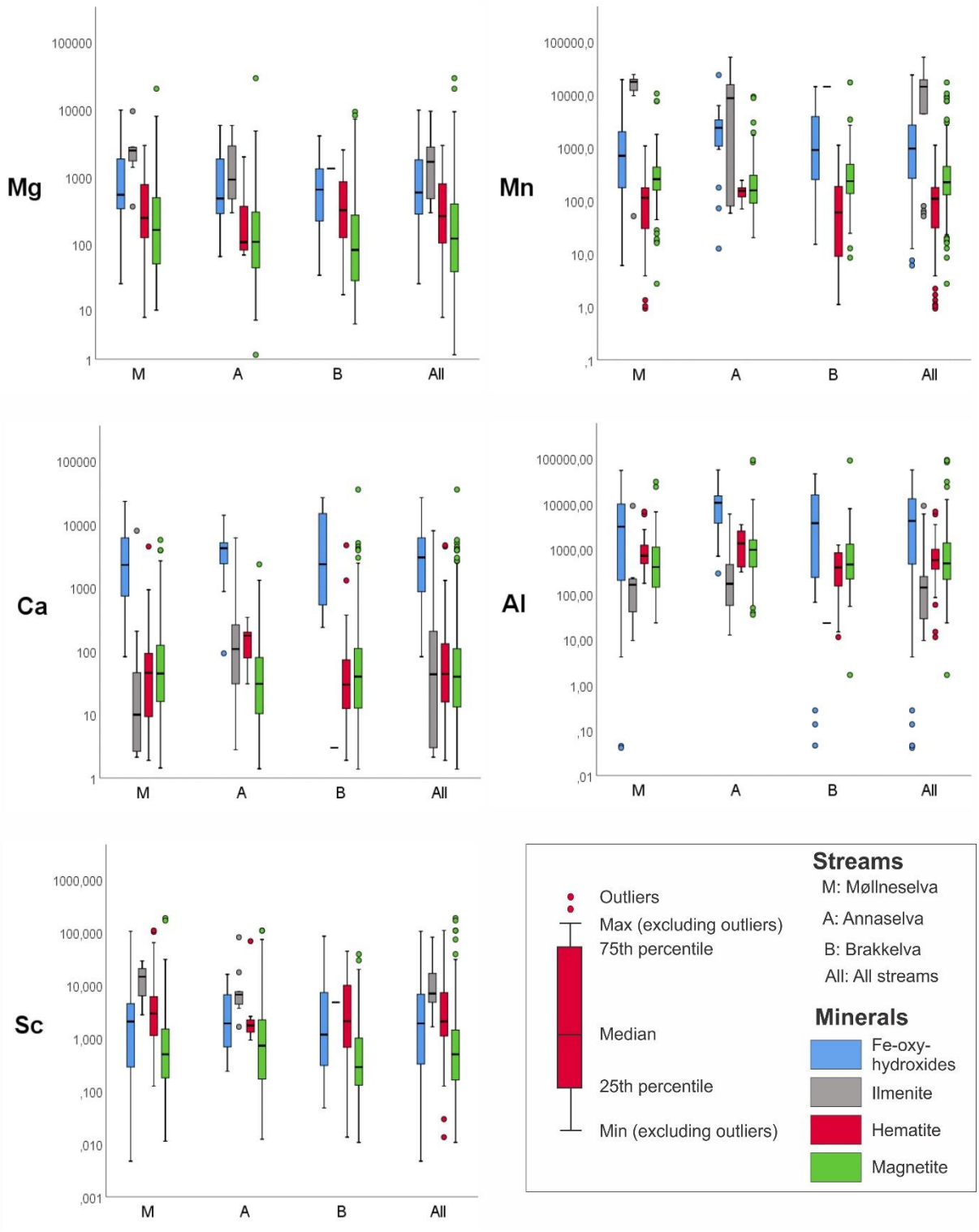

Figure 26: Log-scale boxplots of a selection of minor and trace elements in Fe-oxides and Fe-oxy-hydroxides. Concentrations of elements are in parts per million.

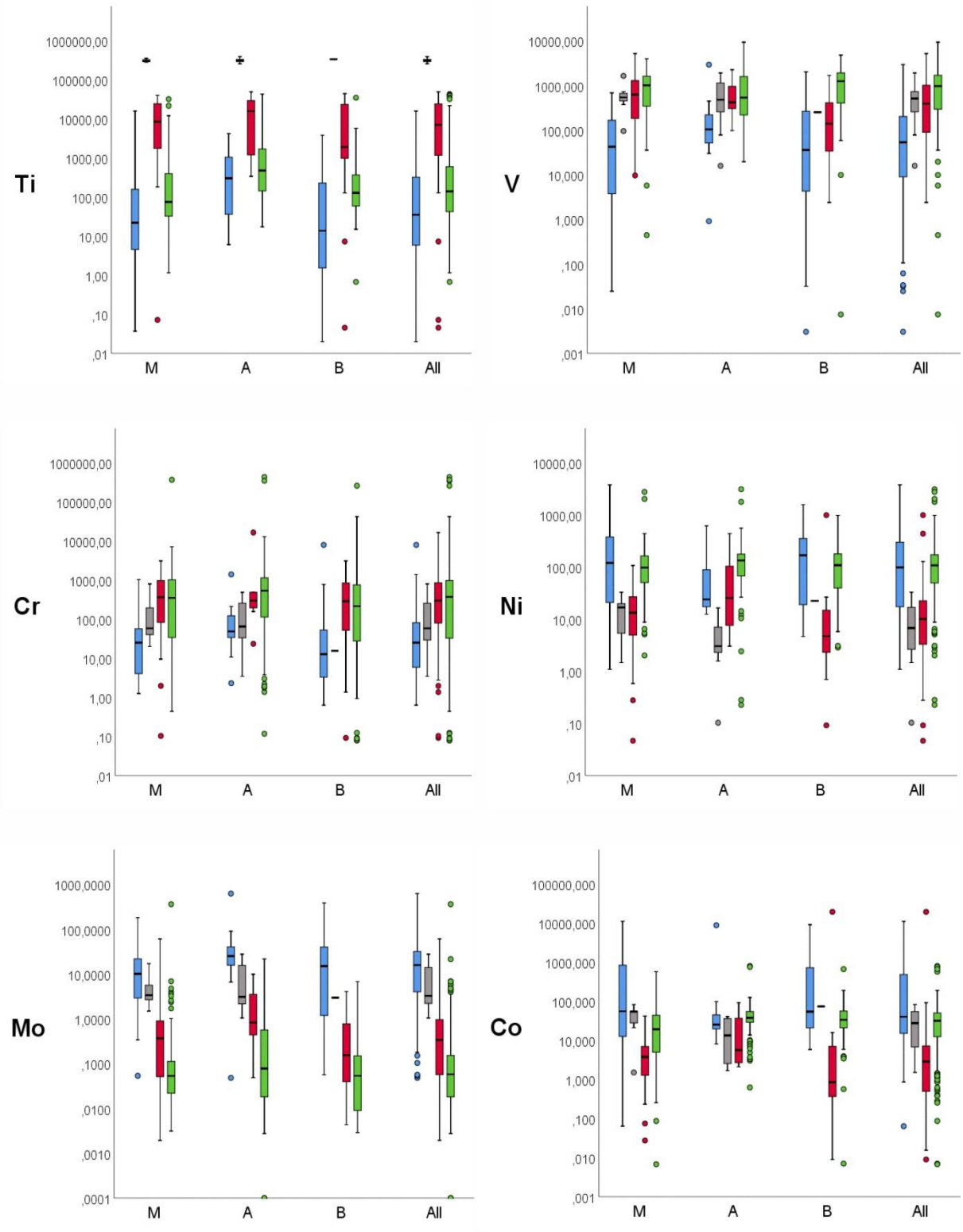

Figure 26: (Continued).

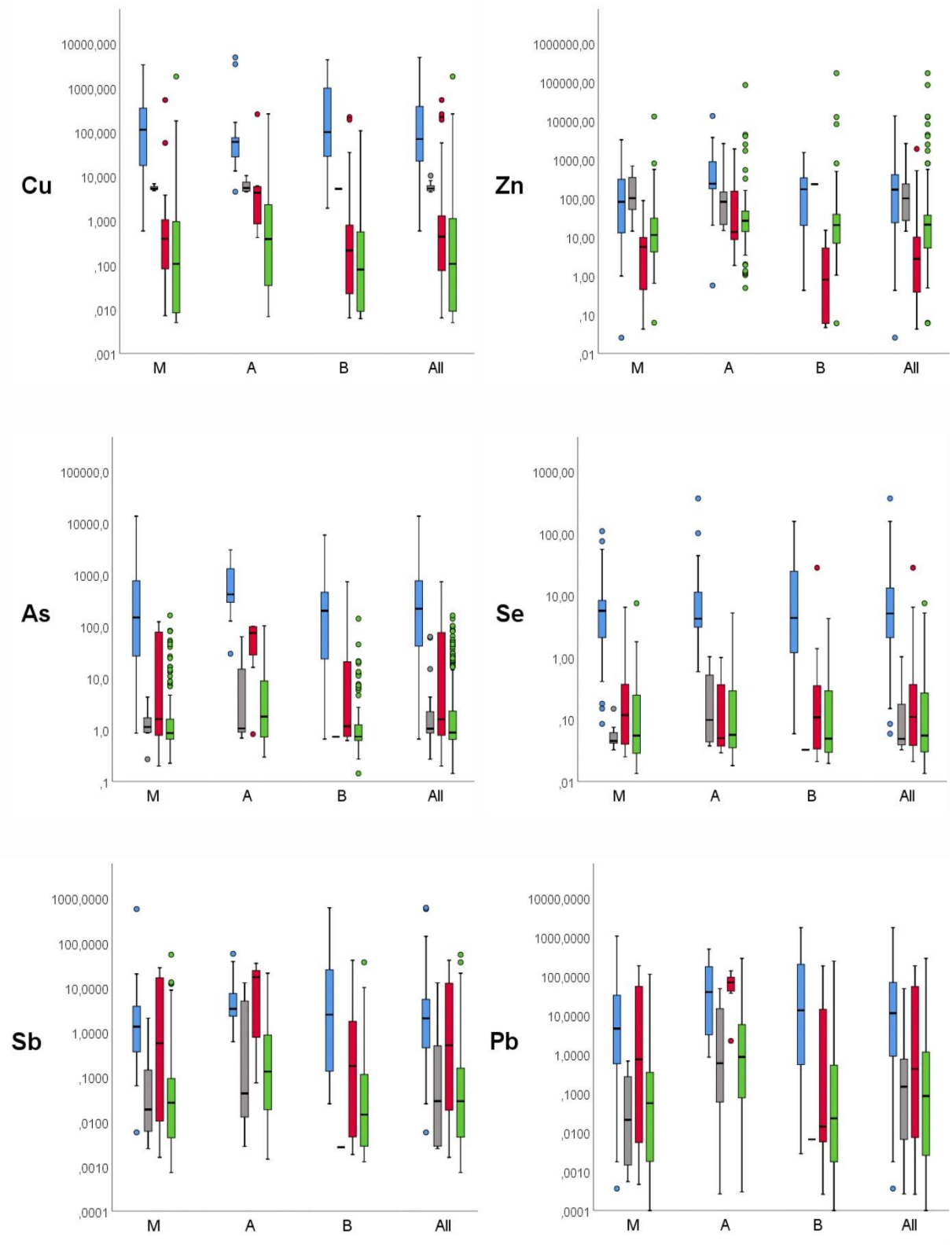

Figure 26: (Continued).

3.4.2 Sulphides

LA-ICP-MS analyses of chalcopyrite, pyrite and pyrrhotite resulted in the content of 39 isotopes covering 37 elements. 32 grains of chalcopyrite, 39 grains of pyrite and four grains of pyrrhotite, all separated from sediment samples where the streams drain the mafic rocks of the Kvenvik formation were analysed. Summary statistics of a selection of elements and their distribution in the analysed sulphides are listed in Table 19. The concentrations obtained of different sulphide minerals are illustrated as boxplots in Figure 27.

The Co content is higher in pyrite comparing to the values obtained for chalcopyrite and pyrrhotite. The median concentration of Co in pyrite is 1741.52 ppm. However, the range is large, extending from <1 ppm and up to >8700 ppm. Nickel shows a similar trend with a high, but variable concentration in pyrite. Molybdenum, V and Cr are quite evenly distributed in analysed sulphide minerals with few outlying values. Content of Au is generally low, with concentrations below the detection limit in most of analysed samples. Chalcopyrite is enriched in most of the chalcophile elements with higher median concentrations of Zn, Se, Ag, Cd, In, Sb, Te, Hg, Tl and Pb than in pyrite and pyrrhotite. In contrast, pyrite is more enriched in As.

Table 19: Descriptive statistics of a selection minor and trace elements in sulphides. Med = median concentration, min = minimum concentration, max = maximum concentration and n = number of spot analyses by LA-ICP-MS on individual grains. All concentrations are in parts per million.

	Chalcopyrite n = 32			Pyrite n = 39			Pyrrhotite n = 4		
	Med	Min	Max	Med	Min	Max	Med	Min	Max
Co	0.1585	0.00445	14.33	1741.52	0.196	8760.14	100.93	58.5	128.14
Ni	0.197	0.075	109.99	667.75	0.0765	13013	2004.875	1265.64	5802.63
Mo	0.01035	0.0035	2.06	0.0363	0.0017	6.42	0.0149	0.00655	2.84
V	0.04035	0.0033	7.59	0.0577	0.00235	19.23	0.153	0.0048	2.54
Cr	0.915	0.135	6.86	0.46	0.0515	91.1	1.845	1.42	4
Mn	0.3735	0.0225	55.66	2.06	0.28	151.54	3.75	1.52	337.14
Cu	307729	254837.2	328272.9	7.85	0.358	1401.22	0.5135	0.206	4.13
Au	0.00373	<DL	0.381	<DL	<DL	1.94	0.0054	<DL	0.64
Ge	0.595	0.035	1.44	0.63	0.135	1.51	0.421	0.045	1.1
Zn	16.93	0.12	422.2	0.43	0.05	11.24	0.31	0.074	5.13
As	0.323	0.0195	26.26	24.98	0.011	7035.02	0.2235	0.136	17.84
Se	167.86	10.26	468.89	53.35	0.733	449.27	154.65	105.5	199
Ag	1.1685	0.00225	30.73	0.0162	0.000885	6.48	1.0895	0.678	1.56
Cd	0.2235	0.00585	4.51	0.0147	0.0019	0.344	0.01355	0.00365	0.217
In	6.205	0.0899	35.6	0.00116	0.000215	8.25	0.000725	0.000335	0.00311
Sb	0.134	0.001354	4.89	0.0224	0.0007	124.58	2.67	0.58	6.5
Te	0.4185	0.01035	5.62	0.163	0.0057	6.13	7.99	0.768	59.08
Hg	0.555	0.025	6.25	0.16	0.009	4.58	0.36	0.18	0.49
Tl	0.009	0.0012	0.42	0.0043	0.000735	12.87	0.043	0.0016	0.69
Pb	1.297	0.00268	23.02	0.363	0.000448	124.04	84.83	16.48	147.38

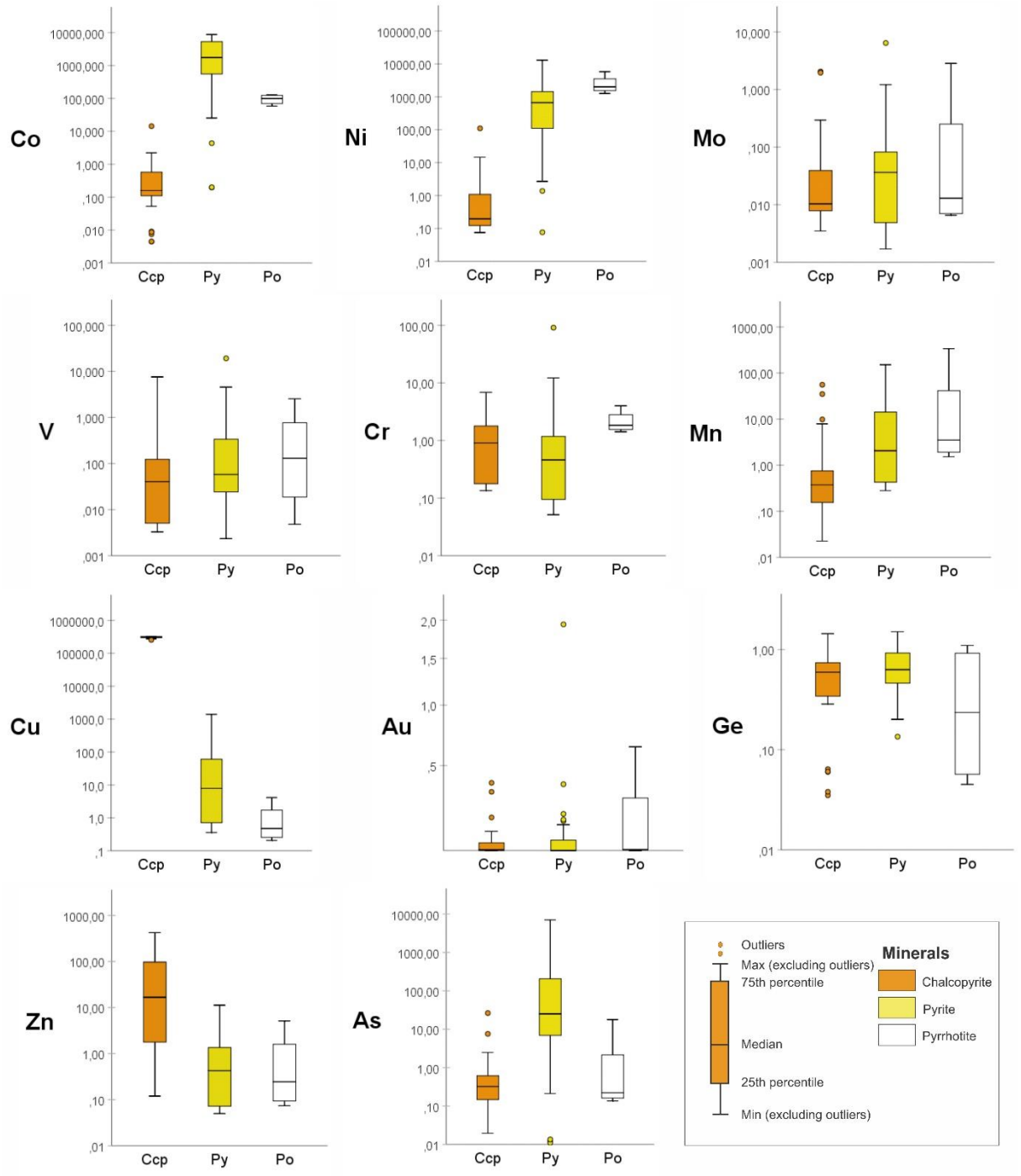

Figure 27: Log-scale boxplots of a selection of minor and trace elements in sulphides. Concentrations are in parts per million.

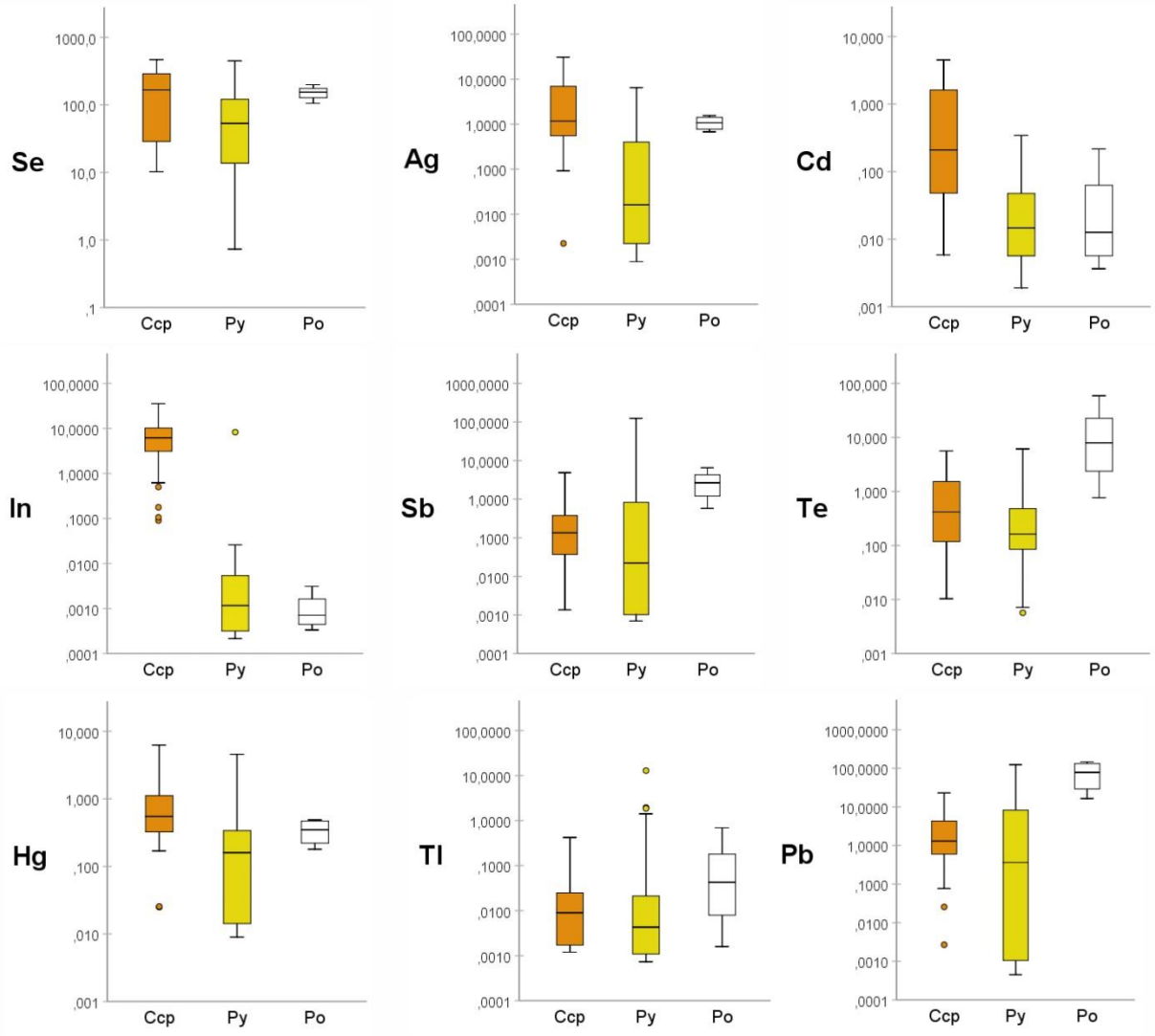

Figure 27: (Continued).

3.5 Carbonate stable isotopes

Stable isotope analyses ($\delta^{18}O$ and $\delta^{13}C$) were performed on pulverized carbonate grains separated from five stream sediment samples. The $\delta^{18}O$ and $\delta^{13}C$ values are listed in Table 20 and illustrated in Figure 28. Carbonates from sediment samples collected in close vicinity of the sedimentary Storviknes formation, samples J002 and J016, show $\delta^{13}C$ (VPDB) values between -3.94 to -0.83‰ and $\delta^{18}O$ (VSMOW) values in the range from 20.36 to 20.72‰. Samples J018 and J023, are according to the bedrock map from The Geological Survery of Norway (2021a), taken from the Møllneselva stream and downstream from the sedimentary Skoađđovárri and Storviknes formations. However, carbonates separated from these samples have similar isotopic compositions as carbonates from sample J044 which only drains the mafic rocks of the Kvenvik formation. They are therefore labelled as “Sediment sample,

draining Kvenvik" in Figure 28. Samples J018, J023 and J44 have $\delta^{13}C$ and $\delta^{18}O$ values ranging between 7.45 to 8.39‰ and 12.36 to 13.00‰, respectively.

Table 20: Stable isotope composition ($\delta^{13}C$ and $\delta^{18}O$) of carbonate grains separated from five different stream sediment samples.

Sample name	Sample type	$\delta^{13}C$ VPDB [‰]	$\delta^{18}O$ VPDB [‰]	$\delta^{18}O$ VSMOW [‰]
J002	Stream sediment	-3.94	-9.91	20.64
J002B	Stream sediment	-3.71	-9.84	20.37
J016	Stream sediment	-0.85	-10.18	20.72
J016B	Stream sediment	-0.83	-10.19	20.36
J018	Stream sediment	8.39	-17.95	12.36
J023	Stream sediment	7.57	-17.32	13
J044	Stream sediment	7.45	-17.38	12.94

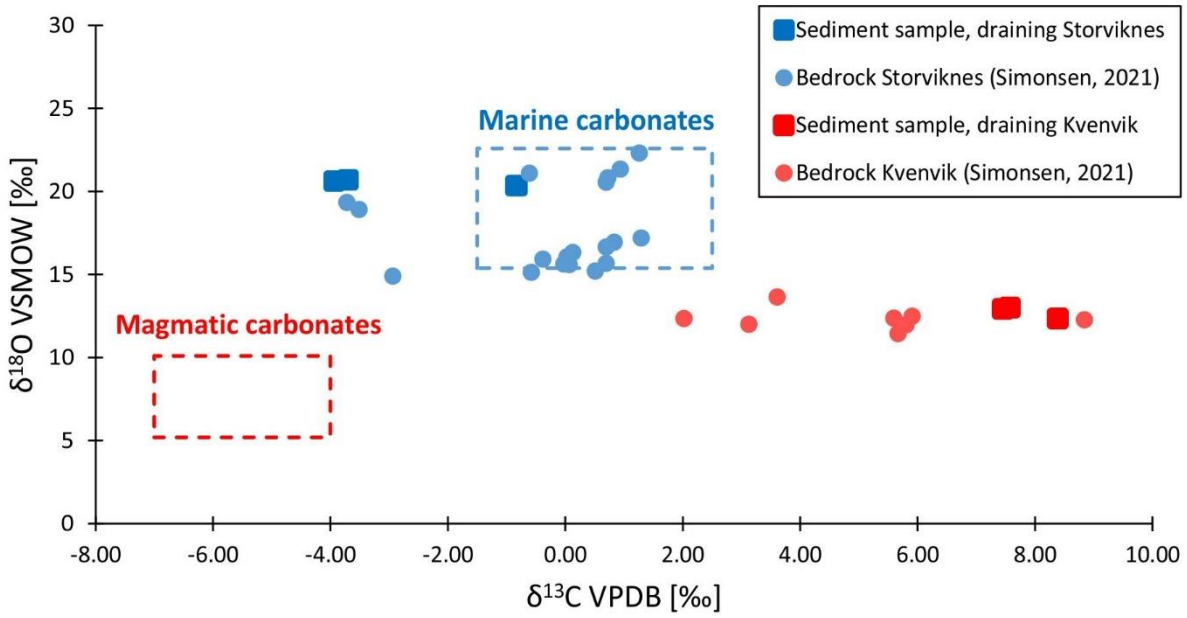

Figure 28: Scatter plot of $\delta^{13}C$ (VPDB) and $\delta^{18}O$ (VSMOW) obtained from the studied sediment samples (squares) and data obtained of the isotopic composition of carbonates found in the bedrock (dots) from Simonsen (2021). *Reference isotopic compositions of magmatic and marine carbonates from* Stakes & O'Neil (1982) *and* Veizer & Hoefs (1976).

.

4 Discussion

In this study, the results of the bulk chemistry of stream sediments and mineralogical, geochemical and stable isotope characteristics of individual mineral grains separated from the stream sediments have been combined in order to identify the geochemical footprint of the Cu mineralisation in the Kåfjord area of the Alta-Kvænangen Tectonic Window (Figure 1, Figure 4). Based on its host rock characteristics, the Cu mineralisation in the study area can be subdivided into two main types; (1) mafic rock-hosted Cu mineralisation and (2) sediment-hosted Cu mineralisation. Although, both types of Cu mineralisation occur mostly in forms of quartz-carbonate veins, they somewhat differ in terms of ore mineral assemblages and minor and trace element contents (Simonsen, 2021). The mafic hosted Cu mineralisation is characterized by relatively simple mineral assemblages, with chalcopyrite and pyrite as the main sulphide mineral phases. In contrast, mineral assemblages of the sediment-hosted Cu mineralisation are more complex and, in addition to chalcopyrite, consist of bornite, galena, covellite, tennantite, digenite, molybdenite, wittichenite and minor amounts of Ag- and Se-rich sulphide phases (Simonsen, 2021).

4.1 Bulk chemistry of stream sediments

The geochemistry of stream sediments is complex with a number of factors influencing abundance of elements. The main assumption for utilization of stream sediment geochemistry in exploration geology is that stream sediments represent a product of weathering of ore-bearing mineralisation located upstream of the sampling site (e.g. Carranza, 2011). However, anthropogenic activity can significantly affect the size and shape of natural geochemical anomalies (Selinus & Esbensen, 1995).

In the studied area, the <63 µm fraction is enriched in the great majority of analysed elements compared to the 125-250 µm fraction. This is believed to be related to the greater surface area to mass ratio of the fine fraction compared to the 125-250 µm fraction and the capability of grains to accumulate elements through surface reactions (e.g. Horowitz, 1991).

Sediments sampled from the Annaselva stream have the lowest content of Cu despite the fact that the stream runs parallel to the Cu mineralised Storviknes formation, and therefore one would expect a steady input of Cu along its river course (Figure 4, Figure 19). However, the enrichment of certain elements (Se, Bi, Pb, Mo, As) in sediments from the Annaselva stream compared to those from the Møllneselva and Brakkelva streams may be indicative of the more

complex mineralisation determined by Simonsen (2021). Additionally, the abundance of elements found in stream sediments can reflect the bedrock lithology in the catchment area (e.g. Halamić et al., 2001). Sediments from the Møllneselva and Brakkelva streams, which drain the Kvenvik formation display a mafic lithology signature with enrichment of V, Sc and Co compared to sediments from the Annaselva stream (Figure 19) (White & Klein, 2013).

The geochemistry of stream sediments is complex with a number of factors influencing abundance of elements. Anthropogenic activity is perhaps the most noticeable factor controlling the content of Cu in stream sediments in Kåfjord. The two major sources of human influence are the dams of the Mølleelva hydropower facility and the tailings of the abandoned mines. Sample J018 contains high amounts of Cu and is collected just downstream of the second dam in the Møllneselva stream where there has been extensive excavation work (Figure 29A). The tailings of the historical Cu mines consist of material with large erosional surfaces and anomalous concentrations of elements associated with the mineralisation. A few sampling locations (i.e. J007 and J039) are subjected to surface runoff and seepage from these waste material deposits. Hence, the concentration of Cu greatly increases downstream from the tailings (Figure 29B, Figure 29C).

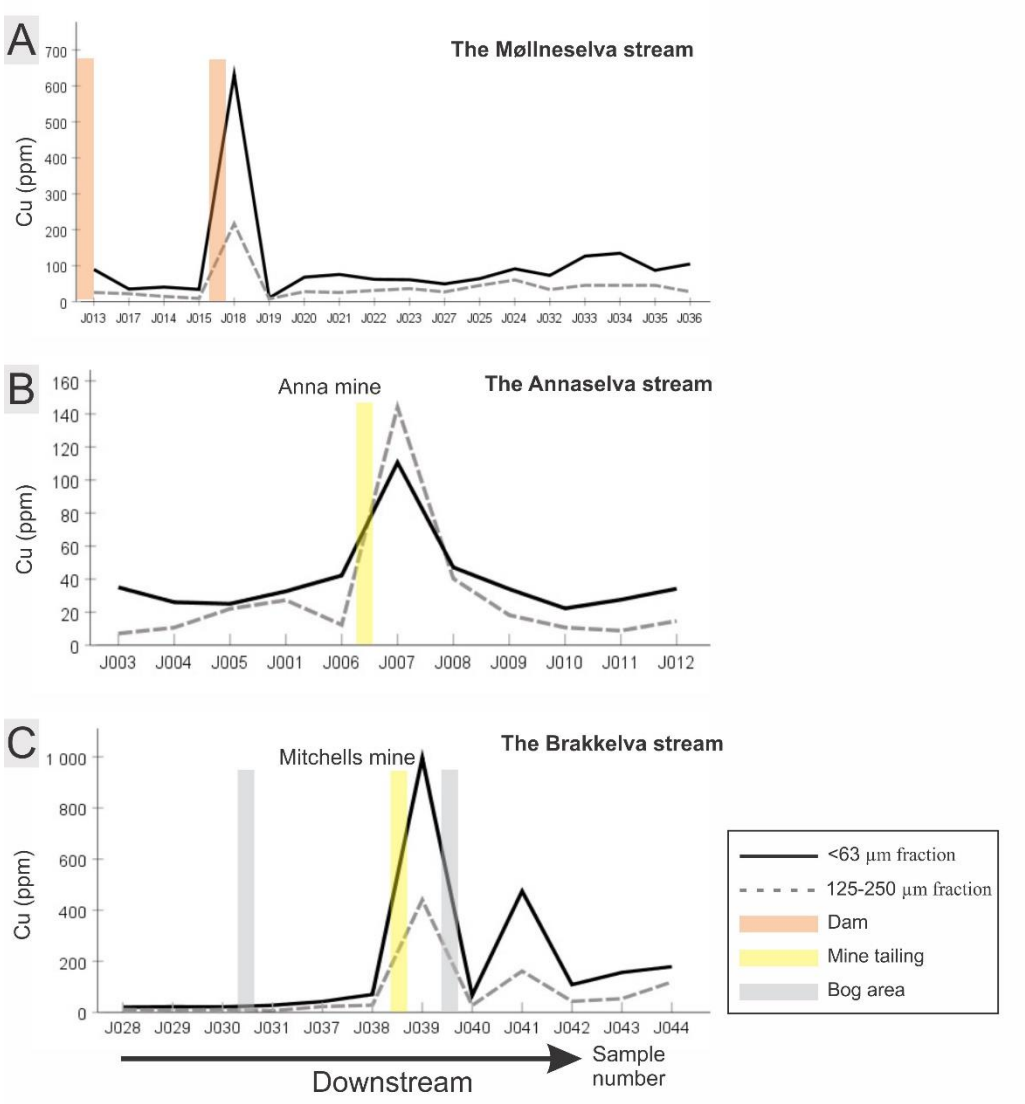

Figure 29: Longitudinal diagrams showing the distribution of Cu in stream sediment samples collected along the Møllneselva (A), Annaselva (B) and Brakkelva (C) streams in both the <63 and 125-250 µm fractions.

4.1.1 Statistical inference of the bulk chemistry of stream sediments

The linear relationship between elements is presented as correlation matrices in section 3.1.1 and can portray pathfinder elements for the different types of Cu mineralisation hosted by the Storviknes and Kvenvik formations.

A common feature for the three streams studied is the statistically significant positive correlation between Cu and chalcophile elements. In addition to chalcophile elements (Mo, Pb, Ag, Te and S), sediments of the <63 µm fraction from the Møllneselva stream show a positive correlation with the lithophile elements Fe, Sr, Ca, Cr, Mg, Ba, Ti, Na, Sc. The correlation between Cu and chalcophile elements is assumed to be related to the mineralisation of Cu sulphides, whereas the wide range of lithophile elements may represent

lithologies associated with the mineralisation. Alkaline earth metals (e.g. Sr, Mg, Ba) and divalent cations (e.g. Fe^{2+}) can substitute Ca in $CaCO_3$ can reflect that the Cu mineralisation occurs in carbonate-bearing veins and/or in carbonate-rich sediments. Chromium, Sc and Ti may reflect that much of the mineralisation is hosted by the mafic rocks of the Kvenvik formation. Sodium may be an indicator of evaporite dissolution and reflect the saline ore-forming fluids described by Simonsen (2021) in the AKTW, and by Mun et al. (2020a) in the nearby Repparfjord Tectonic-Window. However, because the Møllneselva steam runs through both the Cu mineralised Kvenvik and Storviknes formations, the correlation coefficients of Cu may be obscured due to the fact that different elements can be associated with Cu in the two systems. Additionally, no indicative results of the mineralisation are displayed in the correlation matrix of the 125-250 µm fraction from Møllneselva (Table 6).

In contrast, the correlation matrices of sediments from the Annaselva and Brakkelva streams show similar features with respect to Cu in the <63 µm and 125-250 µm fractions. Copper correlates with chalcophile elements in both streams (e.g. Zn, Ag, Bi). Furthermore, sediments from the Annaselva stream of the <63 µm fraction correlates with Ba and Sr which may be associated with the carbonate rocks hosting the Cu mineralisation of the Storviknes formation. Similarly, in the <63 µm fraction from Brakkelva Cu correlates with siderophile elements (Co, Ni, V) associated with the mafic host rock lithology.

The potential problem with applying a statistical analysis, which is based on the assumption of a normal data distribution, needs to be emphasised. Lilliefors corrected Kolmogorov-Smirnov test for normality (Appendix E) was performed on 44 samples of the <63 µm and 125-250 µm fractions in order to display the absence of normal distributed data. The majority of elements in both fractions does not seem to follow a normal distribution, though it should be noted that the statistical power of normality tests is strongly influenced by the sample size and does generally not perform well on such small sample sizes (Mohd Razali & Bee Wah, 2011). Different transformations could have been tested (e.g. ln-, log- or square-root-transformations) to potentially approach a normal distribution prior to carrying out the correlation analysis. However, as demonstrated by Reimann & Filzmoser (2000) such transformations of geochemical data rarely results in normal distributions.

Few measurements of the bulk chemistry of stream sediments are below the detection limit (Appendix C). In addition to the simple-substitution method for creating uncensored datasets, other options such as the maximum likelihood method could have been tested (e.g. Helsel &

Cohn, 1988; Sanford et al., 1993). However, as demonstrated by Carranza (2011), including up to c. 30% of samples with censored values (simple-substitution factor of ½ detection limit), does not impair geochemical anomalies reflecting the mineralisation. As mentioned, the 125-250 µm fraction is depleted in most analysed elements comparing to the <63 µm fraction. Additionally, it should be noted that a greater number of measurements of the 125-250 µm fraction are below the detection limit comparing to the fine-fraction.

4.2 Separation of heavy minerals

Magnetic separation followed by hand-picking of minerals seemed to be an efficient way of singling out Fe-oxides, Fe-oxy-hydroxides and sulphides from stream sediments. Fe-oxides and Fe-oxy-hydroxides were in the form of magnetite, hematite and FeO(OH)-species separated from almost all stream sediment samples. The samples in which sulphides were separated from, i.e. the lower stretches of the Møllneselva and Brakkelva streams, appeared to somewhat correspond with a high Cu concentration recorded by the bulk chemistry of the analysed stream sediments (Figure 20). In contrast, no sulphides were separated from any of the samples collected from the streams that drain the sediment-hosted Cu mineralisation of the Storviknes formation. Even in the sample J002, collected from the underwater tailing of The Lundstrøm mine, and which fraction <63 µm has the highest content of Cu of all samples (>1000 ppm), no sulphide minerals were identified suggesting that sulphide minerals have been weathered in this stream.

The oxidation of sulphide minerals is accelerated when exposed to oxygen dissolved in water (e.g. Blowes et al., 2013; Nordstrom et al., 2015). Hence, it is expected that a larger portion of the sulphides is oxidized within sediment samples with a higher redox potential. Sediments from Annaselva, the stream draining the Storviknes formation, were more oxidized than the samples from the Brakkelva and Møllneselva streams (Figure 21). Microbial activity has the potential to lower the redox potential in sediments through the consumption of oxygen. The amount of dissolved oxygen in pore waters can decrease as organic material is being decomposed and the supply of oxygen from the water column is limited (Søndergaard, 2009). There is only a thin cover of vegetation in areas of higher elevations (i.e. along the Annaselva stream). Thus, the waters are likely to be more oxidized as a consequence of lower amounts of organic component in the stream sediments. The more prominent vegetation along the streams at lower elevations indicates a higher microbial activity and lower redox potential, especially the lower stretches of the Brakkelva stream where the soil surrounding the stream channel is

waterlogged. Samples from the Brakkelva stream were measured to have the lowest redox potential.

In addition, the Cu-bearing mineral assemblages hosted by the sedimentary Storviknes formation are more complex than the mafic rock-hosted mineralisation of the Kvenvik formation (Simonsen, 2021). Galvanic reactions can occur when two or more sulphide minerals are in contact in a solution and promote the dissolution of sulphide minerals, even in near-neutral solutions (e.g. Kwong et al., 2003; Chopard et al., 2017; Mun et al., 2020b; Yang et al., 2021). Therefore, a complex mineralisation characterized by intergrowth and/or impurities of various sulphide minerals may result in galvanic reactions and promote the dissolution of sulphide phases.

4.3 Indicator minerals

The composition of minerals can differ with respect to the environment in which they are formed. By utilizing LA-ICP-MS, the distribution of trace elements in specific minerals can be determined and assist in uncovering spatial relationships which can be useful in mineral exploration. For instance, Fe-oxides and sulphides with well-documented minor and trace element distributions for a number of mineral systems have the potential to be used as indicator minerals (Cook et al., 2016, and references therein).

4.3.1 Magnetite

Magnetite is a widely used indicator mineral because of its abundance in many ore deposits and its variable composition which can be related to different formation conditions (e.g. magmatic or hydrothermal origin). Dare et al. (2014) has proposed plotting Ti versus Ni/Cr to discriminate between magnetite from magmatic and hydrothermal settings. The discriminant diagram reveals that both magmatic and hydrothermal magnetite are found in all three streams (Figure 30).

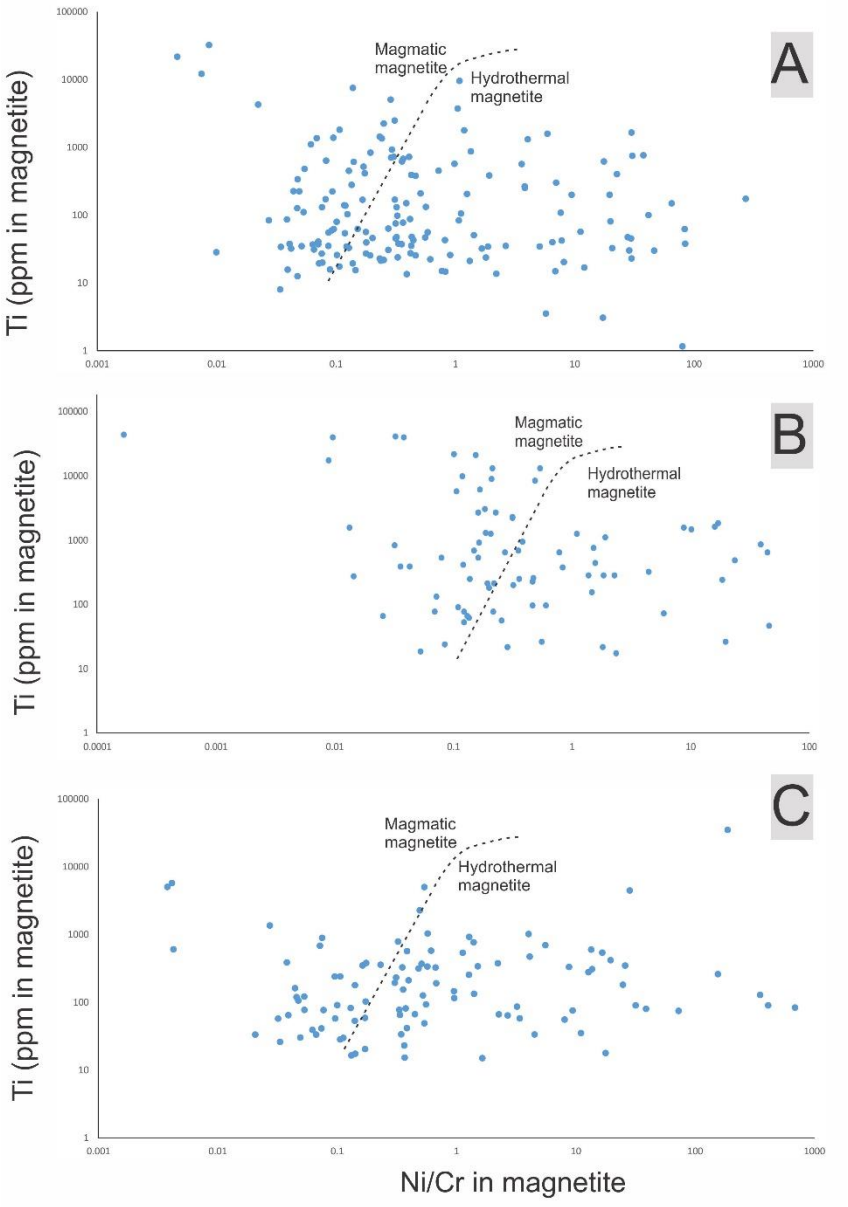

Figure 30: Scatter plots of Ti (ppm) versus Ni/Cr to discriminate between magmatic and hydrothermal magnetite separated from stream sediments (after Dare et al. 2014*). A: Magnetite grains from the Møllneselva stream; B: from the Annaselva stream and C: from the Brakkelva stream.*

Hydrothermal magnetite is commonly depleted in Ti and Al compared to magmatic magnetite (e.g. Dupuis & Beaudoin, 2011; Nadoll et al., 2012, 2014). Furthermore, Van Baalen (1993) demonstrated how some high field strength elements (HFSE), with high cationic charge relative to ionic radii, are immobile during hydrothermal alteration. Thus, these HFSE elements are expected to be depleted in hydrothermal magnetite compared to magmatic magnetite.

By defining each grain of magnetite to be of either hydrothermal or magmatic origin after the discrimination diagram proposed by Dare et al. (2014) and Figure 30, the mentioned

characteristics of magnetite regarding content of Ti, Al and HFSE, such as Zr and Hf, can be investigated. Grains of magnetite defined as hydrothermal and magmatic have similar concentrations of Ti, Al, Zr and Hf, and they plot within the same area (Figure 31). Only a slight depletion of these elements is observed in hydrothermal magnetite when comparing the median concentrations (illustrated by larger circles in Figure 31). Zr and Hf have almost identical physicochemical properties (charge, atomic radius and oxidation state) and are expected to have similar partitioning behaviour in magnetite, as seen by the strong positive correlation.

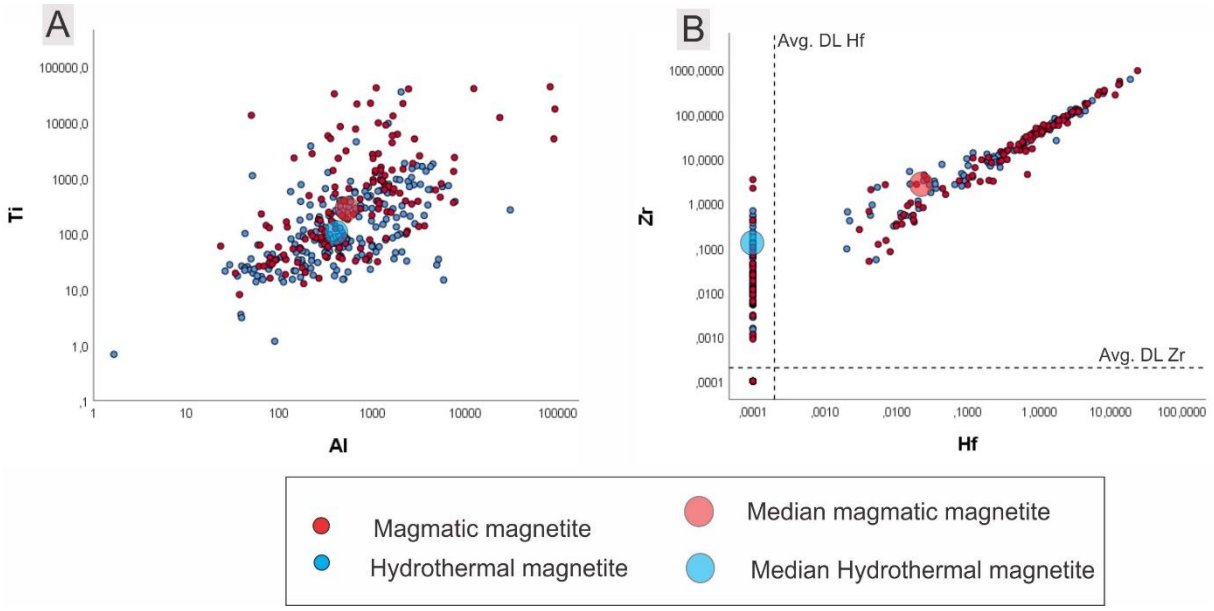

Figure 31: Scatter plots of Ti versus Al and Zr versus Hf in magnetite defined as magmatic or hydrothermal after Dare et al. (2014)*. Hydrothermal and magmatic magnetite has very similar contents of Ti, Al, Zr and Hf, and are not distinguishable based on these elements. Stippled lines are the average detection limits of Zr and Hf recorded in magnetite (Appendix F). Concentrations are in parts per million.*

Additionally, Figure 31B illustrates the importance in recognizing censored values below the detection limit and treating them accordingly. More than half of the grains defined as hydrothermal magnetite have concentrations of Hf below the DL, as seen by the median. If measurements below the detection limit had been excluded, bias towards higher concentrations would follow.

However, the great number of magnetite grains defined as both magmatic and hydrothermal from stream sediments (Figure 30) and the deficit of magnetite in ore parageneses described by Simonsen (2021) demonstrates the issues in using magnetite as an indicator mineral for the Cu mineralisation in Kåfjord. Because both magmatic and hydrothermal magnetite primarily

occurs in the mafic rocks, but not in the mineralised veins, it cannot be used as a reliable indicator for the Cu mineralisation.

4.3.2 Hematite and Fe-oxy-hydroxides

In contrast to magnetite, hematite has concentrations of Ti, Ni and Cr that reveal a more distinct signature (Figure 32). Fe-oxy-hydroxides have lower contents of Ti and greater Ni/Cr ratios than hematite. The high content of Ti and low Ni/Cr ratio in hematite may be indicative of a magmatic origin, whereas composition of Fe-oxy-hydroxides can reflect a hydrothermal origin. According to Dare et al. (2014), Ni has a higher solubility than Cr in hydrothermal fluids. Thus, hydrothermal magnetite, and perhaps other Fe-oxides or Fe-oxy-hydroxides, are thought to have a greater Ni/Cr ratio than those of magmatic origin.

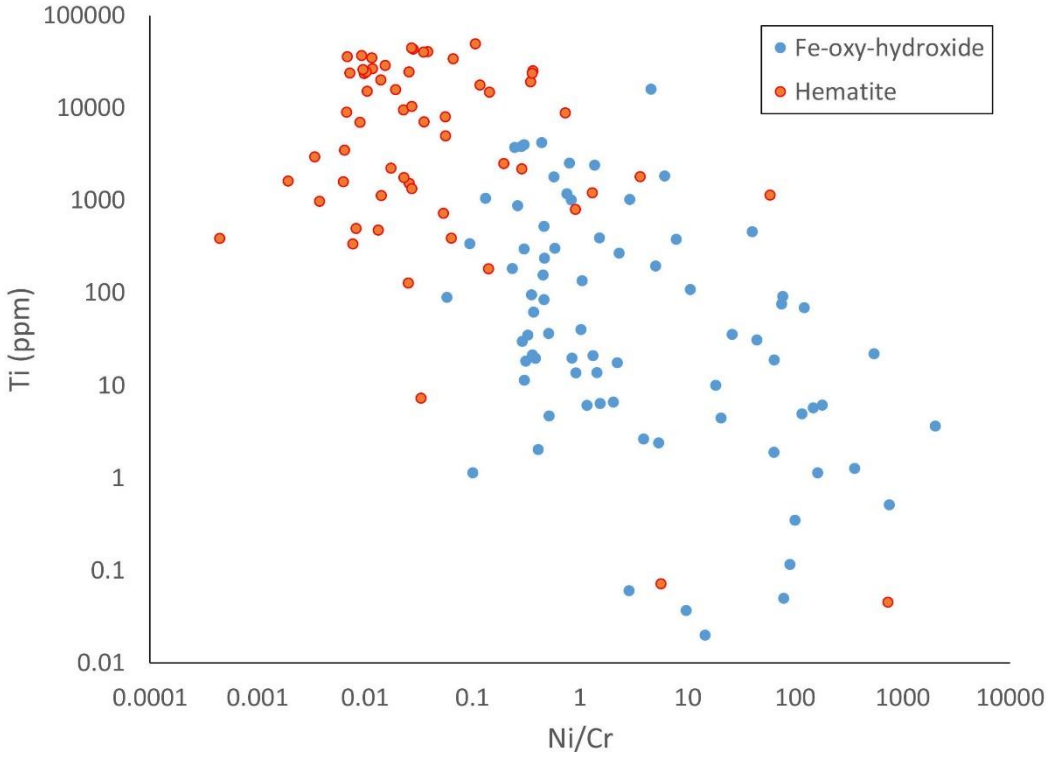

Figure 32: Scatter plot of Ti (ppm) versus Ni/Cr in hematite and Fe-oxy-hydroxides. Composition of hematite may indicate magmatic origin characterized by high content of Ti and a low Ni/Cr ratio. Fe-oxy-hydroxides have a more variable composition, but may be indicative of a composition resembling hydrothermal origin.

4.3.3 Sulphides and indicators for mineralisation

The Cu mineralisation in Kåfjord is found in close relation to quartz-carbonate veins and occur in the form of sulphides. Comparison of minor and trace element composition of heavy minerals indicates that the hydrothermal mineralisation is characterised by high contents of Ag and Se (Figure 33). In contrast, Ga is depleted in the minerals of hydrothermal origin, in comparison to Fe-oxides that display a stronger magmatic influence.

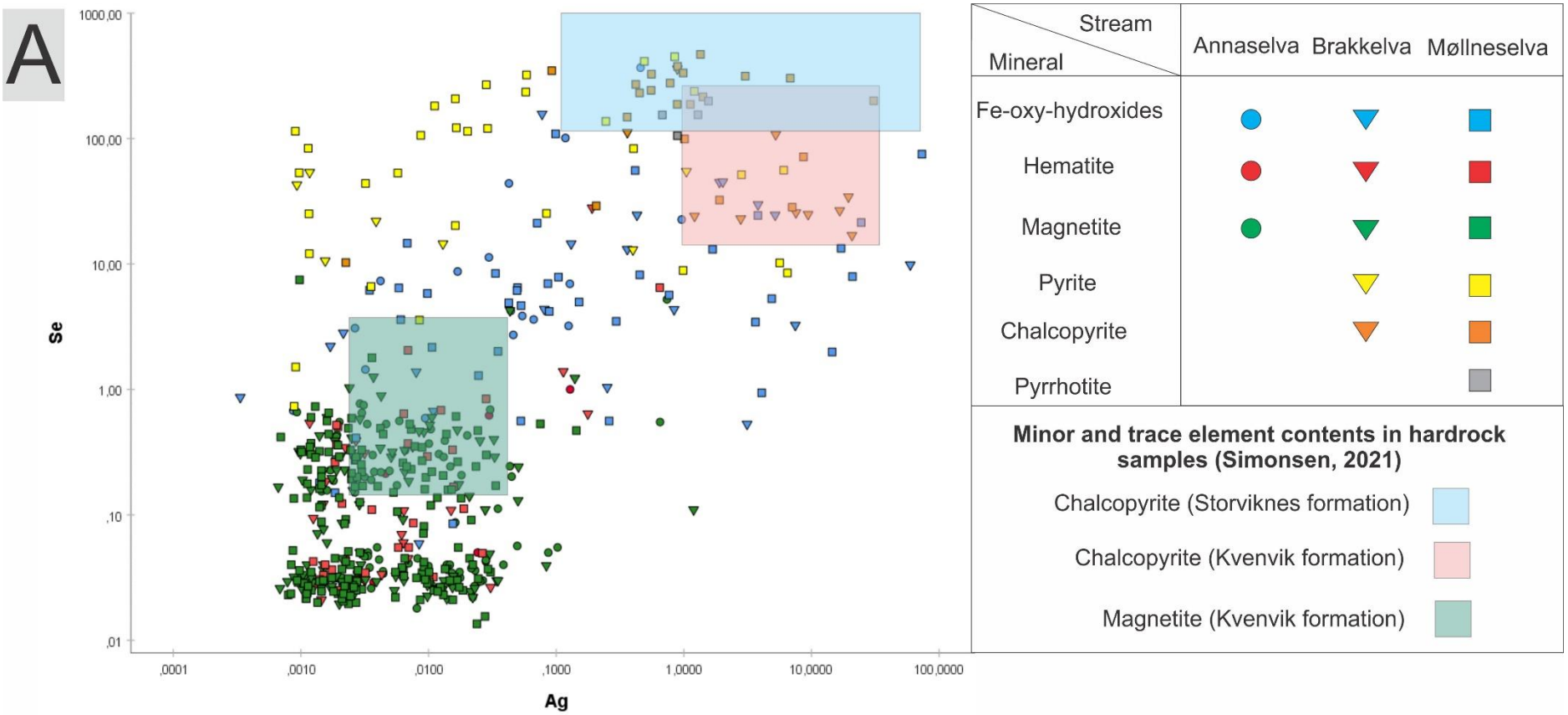

Figure 33: Scatter plots of Se, Ag, Ni and Ga content in heavy minerals separated from stream sediments. Symbols are discriminated by stream (circle, triangle or square) and mineral or mineral aggregates (colour). Additionally, the approximate composition of chalcopyrite and magnetite from lithological samples from Simonsen (2021) *are included.*

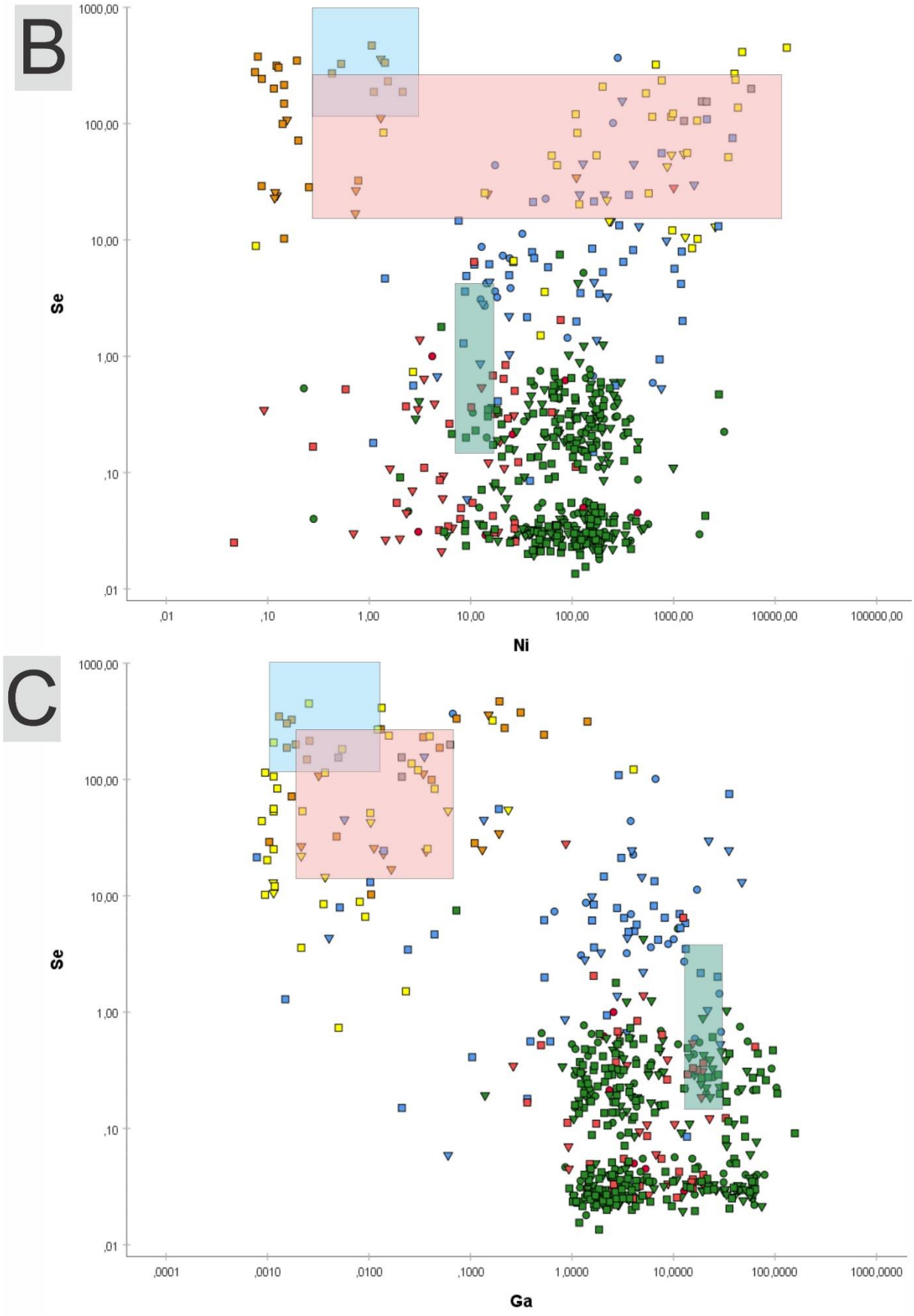

Figure 33: (Continued).

The high content of Se in chalcopyrite from the Storviknes formation (blue semi-transparent square, Figure 33) seems to have been preserved in stream sediments. Few measurements of chalcopyrite separated from the stream draining the Kvenvik formation (orange triangles, Figure 33) plot within the field of chalcopyrite from the Storviknes formation. Furthermore, the contents of Se, Ag and Ga in Fe-oxy-hydroxides resembles the geochemical signature of the hydrothermal sulphides.

Magnetite and hematite separated from stream sediments show more variable concentration of Se than magnetite from lithological samples. This is because a large number of measurements are below the detection limit (Appendix F).

4.4 Carbonate stable isotopes

Distinctive differences in stable isotope composition of carbonates, specifically $\delta^{13}C$, has been identified in carbonates from the Kvenvik and Storviknes formations (Figure 28). Furthermore, Melezhik et al. (2015) and Simonsen (2021) have recorded stable isotope compositions similar to those retrieved from stream sediments. Even though Melezhik et al. (2015) targeted the carbonate-siliciclastic sedimentary successions within the Kvenvik formation and Simonsen (2021) focused on the hydrothermal quartz-carbonate veins, they both recorded a typical range of $\delta^{13}C$ from be +4 to +10‰ (VPDB). In contrast, the carbonates of the Storviknes formation show a marked $\delta^{13}C$ depletion (often $\delta^{13}C$ around 0‰).

An excursion in the $\delta^{13}C$ isotope composition has been recorded in marine carbonates both from Fennoscandian and South African sedimentary successions of Paleoproterozoic age. These broadly correlative sedimentary successions are linked to the Lomagundi carbon isotope event (c. 2.32 - 2.06 Ga) when $\delta^{13}C$ isotope signatures in marine carbonates reached +10‰ (Karhu, 2005). Thus, the deposition of the Kvenvik formation, and its carbonates, are believed to be during this Lomagundi isotopic event, with the Storviknes formation deposited after 2.06 Ga (Melezhik et al., 2015).

The carbon in the quartz-carbonate veins of the Kvenvik formation could derive from the sedimentary carbonate successions lower in the stratigraphy (Figure 3). A minimal contribution from hydrothermal or organic sources could be considered, as suggested for the $\delta^{13}C$ values of carbonates in the Cu-bearing quartz-carbonates veins in the nearby Repparfjord Tectonic Window (Mun et al., 2020a).

Two distinctly different stable isotope compositions have been recorded in grains separated from stream sediments. Carbonates from samples J018 and J023 have $\delta^{13}C$ values of 8.39 and 7.57‰ (VPDB), respectively. Although these display compositions corresponding to carbonates of the Kvenvik formation, they are from samples collected in an area where the Møllneselva stream primarily drains the Skoađđovárri sandstone formation according to the bedrock map from The Geological Survery of Norway (2021a) (Figure 4; Figure 10). It should be noted that both these sampling locations are downstream from the second dam where extensive excavation work has been done. However, more detailed mapping of the bedrock and sediments within the drainage basins of these samples is necessary to determine the origin of these carbonates.

5 Conclusion

This study has been a part of MinExTarget: Enhanced Use of Heavy Mineral Chemistry in Exploration Targeting, a project aimed at developing and introducing a new exploration tool to provide more efficient targeting in the early stages of mineral exploration. To identify the geochemical footprint of the Cu mineralisation hosted by the Alta-Kvænangen Tectonic Window, Kåfjord, the bulk chemistry of stream sediments and mineralogical, geochemical and stable isotope characteristics of individual grains separated from the stream sediments were exploited. The main findings resulted in the following conclusions:

- The bulk chemistry of the <63 µm fraction is enriched in the great majority of analysed elements and has fewer measurements below the detection limit comparing to the 125-250 µm fraction.
- Untransformed data of the bulk chemistry of stream sediments including censored values replaced by ½ the detection limit, display statistically significant positive correlations between Cu and elements associated with the Cu mineralisation and the lithologies hosting the mineralisation. The hydrothermal signature of the mineralisation is displayed by the correlation between Cu and chalcophile elements in samples from all three streams. Copper correlates with alkaline earth metals (e.g. Sr, Ba) in sediments from the streams draining the Storviknes formation reflecting that the mineralisation occurs in a close relation to carbonate-rich lithologies. In sediments from the stream draining the mafic rock-hosted Cu mineralisation of the Kvenvik formation, Cu is associated with siderophile elements (Co, Ni, V). Additionally, in sediments from the Møllneselva stream Cu correlates with Na, which may reflect the highly saline hydrothermal fluids that circulated through the volcano-sedimentary sequences.
- Magnetic separation, followed by hand-picking seems to be an efficient way of singling out Fe-oxides, Fe-oxy-hydroxides and sulphides from stream sediments. The absence of sulphides in sediments from the stream draining the Storviknes formation is believed to be related to galvanic interactions in the complex sulphide mineral assemblages and/or the higher redox potential in the pore waters.
- Magnetite separated from stream sediments seem to be of magmatic and hydrothermal origin, and does not appear to be related to ore parageneses. Thus, magnetite cannot be used as a reliable proxy for Cu mineralisation in Kåfjord.

- The minor and trace element composition of hematite from stream sediments is indicative of its magmatic origin. Therefore, hematite cannot be used as a reliable indicator for the Cu mineralisation in Kåfjord.
- The hydrothermal Cu sulphide mineralisation is characterised by high contents of Ag and Se, but low concentrations of Ga. Additionally, the depletion of Se in sulphides from the Kvenvik formation compared to those from the Storviknes formation is preserved in sulphide grains separated from the stream sediments.
- Minor and trace element compositions of Fe-oxy-hydroxides indicate that the original hydrothermal signature is preserved resembling the signature of sulphide mineralisation.
- Carbonates separated from stream sediments preserve isotopic composition ($\delta^{18}O$ and $\delta^{13}C$) of hydrothermal carbonates associated with both sediment- and mafic rock-hosted Cu mineralisation.
- In conclusion, this work finds that stream sediments in the Kåfjord area can successfully be used to trace the Cu bedrock mineralisation and presents a novel approach in mineral exploration that combines bulk chemistry of stream sediments with major and trace element compositions of separated heavy minerals. Sulphide grains separated from the studied stream sediments preserve the original geochemical signature of Cu bedrock mineralisation. Additionally, geochemistry of Fe-oxy-hydroxides can potentially be used as an indicator of the Cu mineralisation for stream sediments in which sulphide minerals have been weathered.

6 Further research

Further investigations of the bedrock and Quaternary sediments with detailed mapping may provide a better insight to how the geochemical footprint and multi-element dispersion patterns are expressed in stream sediments in Kåfjord. A similar study on stream sediments in the broadly correlative Repparfjord Tectonic Window with the Nussir and Ulveryggen Cu deposits would contribute to a better understanding of the occurrence and distribution of chemical elements.

References

Bauer, A., & Velde, B. D. (2014). Geology and Chemistry at the Surface. In *Geochemistry at the Earth's Surface* (pp. 1–55). Springer, Berlin, Heidelberg. https://doi.org/10.1007/978-3-642-31359-2

Bergh, S. G., & Torske, T. (1986). The Proterozoic Skoadduvarri Sandstone Formation, Alta, Northern Norway: A tectonic fan-delta complex. *Sedimentary Geology*, *47*(1–2), 1–25. https://doi.org/10.1016/0037-0738(86)90068-0

Bergh, S. G., & Torske, T. (1988). Palaeovolcanology and tectonic setting of a proterozoic metatholeiitic sequence near the baltic shield margin, Northern Norway. *Precambrian Research*, *39*(4), 227–246. https://doi.org/10.1016/0301-9268(88)90021-6

Bingen, B., Andersson, J., Söderlund, U., & Möller, C. (2008). The Mesoproterozoic in the Nordic countries. *Episodes*, *31(1)*, *29*. https://doi.org/10.18814/epiiugs/2008/v31i1/005

Blowes, D. W., Ptacek, C. J., Jambor, J. L., Weisener, C. G., Paktunc, D., Gould, W. D., & Johnson, D. B. (2013). The Geochemistry of Acid Mine Drainage. In *Treatise on Geochemistry: Second Edition* (Vol. 11). Elsevier Ltd. https://doi.org/10.1016/B978-0-08-095975-7.00905-0

Brandon, D., & Kaplan, W. D. (2008). *Microstructural Characterization of Materials* (2nd ed.). John Wiley & Sons Ltd.

Carranza, E. J. M. (2011). Analysis and mapping of geochemical anomalies using logratio-transformed stream sediment data with censored values. *Journal of Geochemical Exploration*, *110*(2), 167–185. https://doi.org/10.1016/j.gexplo.2011.05.007

Chopard, A., Plante, B., Benzaazoua, M., Bouzahzah, H., & Marion, P. (2017). Geochemical investigation of the galvanic effects during oxidation of pyrite and base-metals sulfides. *Chemosphere*, *166*, 281–291. https://doi.org/10.1016/j.chemosphere.2016.09.129

Cook, N., Ciobanu, C. L., George, L., Zhu, Z.-Y., Wade, B., & Ehrig, K. (2016). Trace element analysis of minerals in magmatic-hydrothermal ores by laser ablation inductively-coupled plasma mass spectrometry: Approaches and opportunities. *Minerals*, *6*(4), 1–34. https://doi.org/10.3390/min6040111

Coplen, T. B., Qi, H., Révész, K., Casciotti, K. L., & Hannon, J. E. (2012). Determination of the δ 15 N of Nitrate in Water: RSIL Lab Code 2900 (slightly revised from the version released in 2007). In *Book 10, Methods of the Reston Stable Isotope Laboratory* (p. 35). U.S. Geological Survey.

Dare, S. A. S., Barnes, S.-J., Beaudoin, G., Méric, J., Boutroy, E., & Potvin-Doucet, C. (2014). Trace elements in magnetite as petrogenetic indicators. *Mineralium Deposita*, *49*(7), 785–796. https://doi.org/10.1007/s00126-014-0529-0

Davis, J. C. (2002). Elementary statistics. In *Statistics and Data Analysis in Geology* (3rd ed., pp. 11–119). Wiley.

Dupuis, C., & Beaudoin, G. (2011). Discriminant diagrams for iron oxide trace element fingerprinting of mineral deposit types. *Mineralium Deposita*, *46*(4), 319–335. https://doi.org/10.1007/s00126-011-0334-y

Eilu, P. (ed.). (2012). Mineral deposits and metallogeny of Fennoscandia. In *Geological Survey of Finland Special Paper 53*.

Fletcher, W. K. (1997). Stream Sediment Geochemistry in Today 's Exploration World. *Proceedings of Exploration*, *97*, 249–260.

Gaál, G., & Gorbatschev, R. (1987). An Outline of the precambrian evolution of the baltic shield. *Precambrian Research*, *35*, 15–52. https://doi.org/10.1016/0301-9268(87)90044-1

Garrels, R. M., & MacKenzie, F. T. (1967). Origin of the Chemical Compositions of Some Springs and Lakes. *Advances in Chemistry*, *67*, 222–242.

Gorbatschev, R., & Bogdanova, S. (1993). Frontiers in the Baltic Shield. *Precambrian Research*, *64*(1–4), 3–21. https://doi.org/10.1016/0301-9268(93)90066-B

Grunsky, E. C., & Smee, B. W. (1999). The differentiation of soil types and mineralization from multi-element geochemistry using multivariate methods and digital topography. *Journal of Geochemical Exploration*, *67*(1–3), 287–299. https://doi.org/10.1016/S0375-6742(99)00054-0

Halamić, J., Peh, Z., Bukovec, D., Miko, S., & Galovic, L. (2001). A Factor Model of the Relationship between Stream Sediment Geochemistry and Adjacent Drainage Basin Lithology, Medvednica Mt., Croatia. *Geologica Croatia*, *54*(1), 37–51.

Haldar, S. K. (2018). Exploration Geochemistry. In *Mineral Exploration: Principles and Applications* (2nd ed., pp. 85–101). Elsevier.

Helsel, D. R., & Cohn, T. A. (1988). Estimation of descriptive statistics for multiply censored water quality data. *Water Resources Research*, *24*(12), 1997–2004. https://doi.org/10.1029/WR024i012p01997

Hoefs, J. (2018). *Stable Isotope Geochemistry* (8th ed.). Springer International Publishing.

Horowitz, A. J. (1991). *A Primer on Sediment-Trace Element Chemistry* (Vol. 2). Lewis Publishers.

Hulkki, H., Taivalkoski, A., & Lehtonen, M. (2018). Signatures of Cu (-Au) mineralisation reflected in inorganic and heavy mineral stream sediments at Vähäkurkkio, north-western Finland. *Journal of Geochemical Exploration*, *188*, 156–171. https://doi.org/10.1016/j.gexplo.2018.01.012

Jaacks, J. A., Closs, G., & Coope, J. A. (2011). Geochemical Prospecting. In P. Darling (Ed.), *SME Mining Engineering Handbook* (3rd ed., pp. 127–141). Society for Mining, Metallurgy, and Exploration, Inc.

Karhu, J. A. (2005). Paleoproterozoic carbon isotope excursion. In *Precambrian geology of Finland - key to the evolution of the Fennoscandian shield* (pp. 669–680). Elsevier B.V.

Koch, J., & Günther, D. (2016). Laser ablation inductively coupled plasma mass spectrometry. In *Encyclopedia of Spectroscopy and Spectrometry* (3rd ed., pp. 526–532). Elsevier Ltd. https://doi.org/10.1016/B978-0-12-803224-4.00024-8

Koistinen, T., Stephens, M. B., Bogatchev, V., Nordgulen, Ø., Wennerström, M., & Korhonen, J. (2001). *Geological map of the Fennoscandian Shield 1: 2 000 000*. Espoo, Trondheim, Uppsala, Moscow.

Kwong, Y. T. J., Swerhone, G. W., & Lawrence, J. R. (2003). Galvanic sulphide oxidation as a metal-leaching mechanism and its environmental implications. *Geochemistry: Exploration, Environment, Analysis*, *3*(4), 337–343. https://doi.org/10.1144/1467-7873/03/013

Lahtinen, R., Garde, A. A., & Melezhik, V. A. (2008). Paleoproterozoic evolution of Fennoscandia and Greenland. *Episodes*. https://doi.org/10.18814/epiiugs/2008/v31i1/004

Lahtinen, R., Korja, A., & Nironen, M. (2005). Chapter 11 Paleoproterozoic tectonic evolution. In *Developments in Precambrian Geology* (Vol. 14, pp. 481–531). Elsevier B.V. https://doi.org/10.1016/S0166-2635(05)80012-X

Liu, Y. S., Hu, Z. C., Li, M., & Gao, S. (2013). Applications of LA-ICP-MS in the elemental analyses of geological samples. *Chinese Science Bulletin*, *58*(32), 3863–3878. https://doi.org/10.1007/s11434-013-5901-4

Lloyd, G. E. (1987). Atomic number and crystallographic contrast images with the SEM: a review of backscattered electron techniques. *Mineralogical Magazine*, *51*(359), 3–19. https://doi.org/10.1180/minmag.1987.051.359.02

Longerich, H. P., Jackson, S. E., & Günther, D. (1996). Laser ablation inductively coupled plasma mass spectrometric transient signal data acquisition and analyte concentration calculation. *Journal of Analytical Atomic Spectrometry*, *11*(9), 899–904.

https://doi.org/10.1039/JA9961100899
Mangerud, J., Gyllencreutz, R., Lohne, Ø., & Svendsen, J. I. (2011). Glacial history of Norway. In *Developments in Quaternary Science* (Vol. 15, pp. 279–298). Elsevier B.V. https://doi.org/10.1016/B978-0-444-53447-7.00022-2
Melezhik, V. A. (2006). Multiple causes of Earth's earliest global glaciation. *Terra Nova*, *18*(2), 130–137. https://doi.org/10.1111/j.1365-3121.2006.00672.x
Melezhik, V. A., Bingen, B., Sandstad, J. S., Pokrovsky, B. G., Solli, A., & Fallick, A. E. (2015). Sedimentary-volcanic successions of the Alta-Kvaenangen Tectonic Window in the northern Norwegian Caledonides: Multiple constraints on deposition and correlation with complexes on the Fennoscandian Shield. *Norwegian Journal of Geology*, *95*, 245–284. https://doi.org/10.17850/njg95-3-01
Melezhik, V. A., & Hanski, E. J. (2013). 3.1 The Early Palaeoproterozoic of Fennoscandia: Geological and Tectonic Settings. In *Reading the Archive of Earth's Oxygenation: Volume 1: The Palaeoproterozoic of Fennoscandia as Context for the Fennoscandian Arctic Russia - Drilling Early Earth Project* (pp. 33–38). Springer, Berlin, Heidelberg. https://doi.org/10.1007/978-3-642-29682-6_3
Misra, C. K. (2012). *Introduction to geochemistry: principles and applications*. John Wiley & Sons.
Moberg, A. (1968). *Kopparverket i Kåfjord: Ett bidrag til Nordkalottens historia*. Norrbottens Museum, Luleå.
Mohd Razali, N., & Bee Wah, Y. (2011). Power comparisons of Shapiro-Wilk, Kolmogorov-Smirnov, Lilliefors and Anderson-Darling tests. *Journal of Statistical Modeling and Analytics*, *2*(1), 21–33.
Mun, Y., Palinkas, S. S., Kullerud, K., Nilsen, K. S., Neufeld, K., & Bekker, A. (2020a). Evolution of metal-bearing fluids at the Nussir and Ulveryggen sediment-hosted Cu deposits, Repparfjord Tectonic Window, northern Norway. *Norwegian Journal of Geology*, *100*. https://doi.org/10.17850/njg100-2-5
Mun, Y., Palinkaš, S. S., Forwick, M., Junttila, J., Pedersen, K. B., Sternal, B., Neufeld, K., Tibljaš, D., & Kullerud, K. (2020b). Stability of Cu-sulfides in submarine tailing disposals: A case study from Repparfjorden, Northern Norway. *Minerals*, *10*(2). https://doi.org/10.3390/min10020169
Nadoll, P., Angerer, T., Mauk, J. L., French, D., & Walshe, J. (2014). The chemistry of hydrothermal magnetite: A review. *Ore Geology Reviews*, *61*, 1–32. https://doi.org/10.1016/j.oregeorev.2013.12.013
Nadoll, P., Mauk, J. L., Hayes, T. S., Koenig, A. E., & Box, S. E. (2012). Geochemistry of magnetite from hydrothermal ore deposits and host rocks of the mesoproterozoic Belt Supergroup, United States. *Economic Geology*, *107*(6), 1275–1292. https://doi.org/10.2113/econgeo.107.6.1275
Nash, W. P. (1992). Analysis of oxygen with the electron microprobe: Applications to hydrated glass and minerals. *American Mineralogist*, *77*(3–4), 453–457.
Nasuti, A., Roberts, D., Dumais, M.-A., Ofstad, F., Hyvönen, E., Stampolidis, A., & Rodionov, A. (2015). New high-resolution aeromagnetic and radiometric surveys in Finnmark and North Troms: linking anomaly patterns to bedrock geology and structure. *Norwegian Journal of Geology*, *95*(3–4), 217–243. https://doi.org/10.17850/njg95-3-10
Newbury, D. E., & Ritchie, N. W. M. (2013). Is Scanning Electron Microscopy/Energy Dispersive X-ray Spectrometry (SEM/EDS) Quantitative? *Scanning*, *35*, 141–168. https://doi.org/10.1002/sca.21041
Nordstrom, D. K., Blowes, D. W., & Ptacek, C. J. (2015). Hydrogeochemistry and microbiology of mine drainage: An update. *Applied Geochemistry*, *57*, 3–16. https://doi.org/10.1016/j.apgeochem.2015.02.008

Norges vassdrags- og energidirektorat. (2019). *NEVINA Beregninger av lavvannsindekser og flomverdier Brukerveiledning*.
Norges vassdrags- og energidirektorat. (2020). *Elvenettverk / ELVIS*. https://www.nve.no/karttjenester/kartdata/vassdragsdata/elvenettverk-elvis
Norges vassdrags- og energidirektorat. (2021a). *Nedlasting av fagdata fra NVE*. https://nedlasting.nve.no/gis/
Norges vassdrags- og energidirektorat. (2021b). *Vannkraftverk*. https://www.nve.no/energiforsyning/vannkraft/vannkraftdatabase/vannkraftverk/?id=1928
Norges vassdrags- og energidirektorat, Meteorologisk institutt, & Kartverket. (2021). *Klima*. http://www.senorge.no/index.html?p=klima
Patterson, C. G. (1999). oxidation-reduction. In *Encyclopedia of Geochemistry* (pp. 462–466). Springer. https://doi.org/10.1007/1-4020-4496-8_232
Reimann, C., & Filzmoser, P. (2000). Normal and lognormal data distribution in geochemistry: Death of a myth. Consequences for the statistical treatment of geochemical and environmental data. *Environmental Geology*, *39*(9), 1001–1014. https://doi.org/10.1007/s002549900081
Rose, A. W., Hawkes, H. E., & Webb, J. S. (1979). *Geochemistry in Mineral Exploration* (2nd ed.). Academic Press.
Rudnick, R. L., & Gao, S. (2003). Composition of the Continental Crust. In *Treatise on Geochemistry* (Vols. 3–9, pp. 1–64). Elsevier Inc. https://doi.org/10.1016/B0-08-043751-6/03016-4
Sam Rosenblum and Isabelie K. Brownfield. (2000). Magnetic susceptibilities of minerals. In *USGS Open-File Report 99-529*.
Sanford, R. F., Pierson, C. T., & Crovelli, R. A. (1993). An objective replacement method for censored geochemical data. *Mathematical Geology*, *25*(1), 59–80. https://doi.org/10.1007/BF00890676
Scheu, C., & Kaplan, W. D. (2012). Introduction to Scanning Electron Microscopy. In G. Dehm, J. M. Howe, & J. Zweck (Eds.), *In-situ Electron Microscopy* (pp. 3–37). Wiley-VCH.
Selinus, O. S., & Esbensen, K. (1995). Separating anthropogenic from natural anomalies in environmental geochemistry. *Journal of Geochemical Exploration*, *55*(1–3), 55–66. https://doi.org/10.1016/0375-6742(95)00034-8
Simonsen, S. S. (2021). *Geochemistry of sediment- and mafic rock-hosted Cu deposits in the Kåfjord area, Alta-Kvænangen Tectonic Window, Northern Norway*.
Singer, Philip, C., & Stumm, W. (1970). Acidic mine drainage: the rate-determining step. *Science*, *167*(3921), 1121–1123.
Søndergaard, M. (2009). Redox Potential Definitions and General Aspects. In E. G. Likens (Ed.), *Encyclopedia of Inland Waters* (pp. 852–859). Elsevier Inc.
Sorjonen-Ward, P., & Luukkonen, E. J. (2005). Archean rocks. In M. Lehtinen, P. A. Nurmi, & O. T. Rämö (Eds.), *Precambrian Geologi of Finland* (pp. 19–99). Elsevier.
Stakes, D. S., & O'Neil, J. R. (1982). Mineralogy and stable isotope geochemistry of hydrothermally altered oceanic rocks. *Earth and Planetary Science Letters*, *57*(2), 285–304. https://doi.org/10.1016/0012-821X(82)90151-0
Stroeven, A. P., Hättestrand, C., Kleman, J., Heyman, J., Fabel, D., Fredin, O., Goodfellow, B. W., Harbor, J. M., Jansen, J. D., Olsen, L., Caffee, M. W., Fink, D., Lundqvist, J., Rosqvist, G. C., Strömberg, B., & Jansson, K. N. (2016). Deglaciation of Fennoscandia. *Quaternary Science Reviews*, *147*, 91–121. https://doi.org/10.1016/j.quascirev.2015.09.016
The Geological Survery of Norway. (2021a). *Bedrock*. Digital Map Database.

https://www.ngu.no/en/topic/map-viewers
The Geological Survery of Norway. (2021b). *Sediments and marine limit*. Digital Map Database. https://www.ngu.no/en/topic/map-viewers
Van Actherbergh, E., E., R., C., Jackson, S., & Griffin, W. (2001). Data reduction software for LA-ICP-MS. In P. Sylvester (Ed.), *Laser Ablation-ICP-mass spectrometry in the earth sciences: principles and applications* (pp. 239–243). Mineralogical Society of Canada Short Course Series.
Van Baalen, M. R. (1993). Titanium mobility in metamorphic systems: a review. *Chemical Geology*, *110*(1–3), 233–249. https://doi.org/10.1016/0009-2541(93)90256-I
Veizer, J., & Hoefs, J. (1976). The nature of O18/O16 and C13/C12 secular trends in sedimentary carbonate rocks. *Geochimica et Cosmochimica Acta*, *40*(11), 1387–1395. https://doi.org/10.1016/0016-7037(76)90129-0
Vik, E. (1985). *En geologisk undersøkelse av kobbermineraliseringene i Alta–Kvænangenvinduet, Troms or Finnmark. PhD Thesis*.
White, W. M., & Klein, E. M. (2014). Composition of the Oceanic Crust. In *Treatise on Geochemistry: Second Edition* (Vol. 4). Elsevier Ltd. https://doi.org/10.1016/B978-0-08-095975-7.00315-6
Whitney, D. L., & Evans, B. W. (2010). Abbreviations for names of rock-forming minerals. *American Mineralogist*, *95*(1), 185–187. https://doi.org/10.2138/am.2010.3371
Wolfgong, W. J. (2016). Chemical analysis techniques for failure analysis: Part 1, common instrumental methods. In *Handbook of Materials Failure Analysis with Case Studies from the Aerospace and Automotive Industries* (pp. 279–307). Elsevier Inc. https://doi.org/10.1016/B978-0-12-800950-5.00014-4
Yang, B., Tong, X., Xie, X., & Huang, L. (2021). Insight into the effect of galvanic interactions between sulfide minerals on the floatability and surface characteristics of pyrite. *Physicochemical Problems of Mineral Processing*, *57*(2), 24–33. https://doi.org/10.37190/PPMP/132342
Zwaan, K. B., & Gautier, A. M. (1980). *Alta og Gargia Beskrivelse til de berggrunnsgeologiske kart 1834 I og 1934 IV -M 1:50000 (Med fargetrykte kart)*. https://urn.nb.no/URN:NBN:no-nb_digibok_2013070808023

Appendices

Appendix A: Catchment characteristics

Catchment characteristics for the Møllneselva stream.

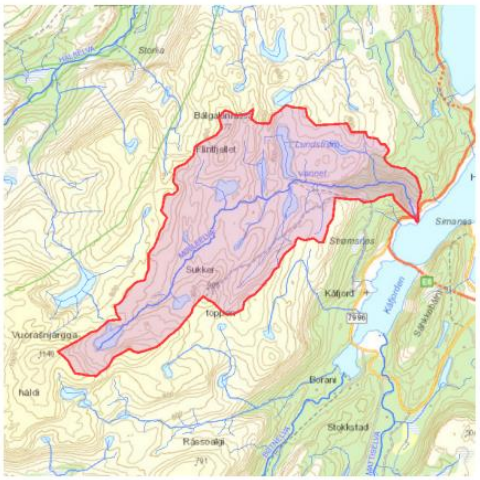

Norges vassdrags- og energidirektorat

Kartbakgrunn:	Statens Kartverk
Kartdatum:	EUREF89 WGS84
Projeksjon:	UTM 33N
Beregn.punkt:	807813 E 7780572 N

Nedbørfeltgrenser, feltparametere og lavvannsindekser er automatisk generert og kan inneholde feil. Resultatene må kvalitetssikres.

Lavvannindekser

Vassdragsnr.:	**212.3Z**
Kommune.:	**Alta**
Fylke.:	**Troms og Finnmark**
Vassdrag.:	**Mølleelva**

Feltparametere

Areal (A)	22.9	km²
Effektiv sjø (A_{SE})	2.03	%
Elvleengde (E_L)	11.7	km
Elvegradient (E_G)	70.4	m/km
Elvegradient $_{1085}$ ($E_{G,1085}$)	70.7	m/km
Helning	13.5	°
Dreneringstetthet (D_T)	1.4	km^{-1}
Feltlengde (F_L)	9.5	km

Arealklasse

Bre (A_{BRE})	0	%
Myr (A_{MYR})	0.2	%
Leire (A_{LEIRE})	0	%
Skog (A_{SKOG})	6.6	%
Sjø (A_{SJO})	6.3	%
Snaufjell (A_{SF})	86.6	%

Hypsografisk kurve

Høyde $_{MIN}$	6	m
Høyde $_{MAX}$	1088	m

Lavvannsindekser

Alminnelig lavvannføring	2.5	l/s*km²
5-persentil (år)	2.3	l/s*km²
5-persentil sommer (1/5-30/9)	2.4	l/s*km²
5-persentil vinter (1/10-30/4)	1.9	l/s*km²
Base flow	10.49	l/s*km²
Base flow index (BFI)	0.33	-

Klima- /hydrologiske parametere

Klimaregion	Finnmark	-
Lavvannsperiode	-	-
Avrenning 1961-90 (Q_N)	31.8	l/s*km²
Sommernedbør	239	mm
Vinternedbør	310	mm
Årstemperatur	-1.3	°C
Sommertemperatur	5.6	°C
Vintertemperatur	-6.2	°C
Temperatur juli	9.2	°C
Temperatur august	8.1	°C

Det er generelt stor usikkerhet i beregning av lavvannsindekser. Resultatene må verifiseres mot egne observasjoner eller sammenlignbare målestasjoner.

I nedbørfelt med høy breprosent eller stor innsjøprosent vil tørrværsavrenning (Base flow) ha store bidrag fra disse lagringsmagasinene.

Rapportdato: 2/16/2021 © nevina.nve.no

Catchment characteristics for the Annaselva stream.

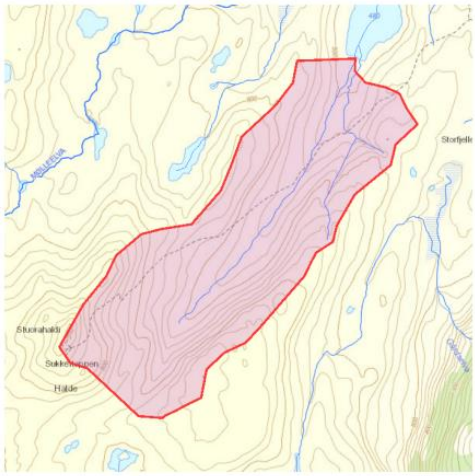

Norges vassdrags- og energidirektorat

Kartbakgrunn:	Statens Kartverk
Kartdatum:	EUREF89 WGS84
Projeksjon:	UTM 33N
Beregn.punkt:	804502 E 7780614 N

Nedbørfeltgrenser, feltparametere og lavvannsindekser er automatisk generert og kan inneholde feil. Resultatene må kvalitetssikres.

Lavvannindekser

Vassdragsnr.:	**212.3Z**
Kommune.:	**Alta**
Fylke.:	**Troms og Finnmark**
Vassdrag.:	**Mølleelva**

Feltparametere

Areal (A)	2.5	km^2
Effektiv sjø (A_{SE})	0	%
Elvleengde (E_L)	2.2	km
Elvegradient (E_G)	56.7	m/km
Elvegradent $_{1085}$ ($E_{G,1085}$)	52.6	m/km
Helning	16.6	°
Dreneringstetthet (D_T)	1.5	km^{-1}
Feltlengde (F_L)	2.8	km

Arealklasse

Bre (A_{BRE})	0	%
Myr (A_{MYR})	0	%
Leire (A_{LEIRE})	0	%
Skog (A_{SKOG})	0	%
Sjø (A_{SJO})	0	%
Snaufjell (A_{SF})	99.9	%

Hypsografisk kurve

$Høyde_{MIN}$	481	m
$Høyde_{MAX}$	901	m

Lavvannsindekser

Alminnelig lavvannføring	2.9	$l/s*km^2$
5-persentil (år)	2.7	$l/s*km^2$
5-persentil sommer (1/5-30/9)	3.1	$l/s*km^2$
5-persentil vinter (1/10-30/4)	2.3	$l/s*km^2$
Base flow	24.78	$l/s*km^2$
Base flow index (BFI)	0.77	-

Klima- /hydrologiske parametere

Klimaregion	Finnmark	-
Lavvannsperiode	-	-
Avrenning 1961-90 (Q_N)	32.2	$l/s*km^2$
Sommernedbør	235	mm
Vinternedbør	294	mm
Årstemperatur	-1.4	°C
Sommertemperatur	5.5	°C
Vintertemperatur	-6.4	°C
Temperatur juli	9.2	°C
Temperatur august	8.1	°C

Det er generelt stor usikkerhet i beregning av lavvannsindekser. Resultatene må verifiseres mot egne observasjoner eller sammenlignbare målestasjoner.

I nedbørfelt med høy breprosent eller stor innsjøprosent vil tørrværsavrenning (Base flow) ha store bidrag fra disse lagringsmagasinene.

Rapportdato: 2/16/2021 © nevina.nve.no

Catchment characteristics for the Brakkelva stream.

Norges vassdrags- og energidirektorat

Kartbakgrunn:	Statens Kartverk
Kartdatum:	EUREF89 WGS84
Projeksjon:	UTM 33N
Beregn.punkt:	806536 E 7779078 N

Nedbørfeltgrenser, feltparametere og lavvannsindekser er automatisk generert og kan inneholde feil. Resultatene må kvalitetssikres.

Lavvannindekser

Vassdragsnr.:	**212.410**
Kommune.:	**Alta**
Fylke.:	**Troms og Finnmark**
Vassdrag.:	**KYSTFELT**

Feltparametere

Areal (A)	2.2	km²
Effektiv sjø (A_{SE})	0	%
Elvleengde (E_L)	1.5	km
Elvegradient (E_G)	128.1	m/km
Elvegradent $_{1085}$ ($E_{G,1085}$)	129.9	m/km
Helning	20.1	°
Dreneringstetthet (D_T)	0.7	km^{-1}
Feltlengde (F_L)	2.0	km

Arealklasse

Bre (A_{BRE})	0	%
Myr (A_{MYR})	3.0	%
Leire (A_{LEIRE})	0.3	%
Skog (A_{SKOG})	55.5	%
Sjø (A_{SJO})	0	%
Snaufjell (A_{SF})	41.0	%

Hypsografisk kurve

Høyde $_{MIN}$	19	m
Høyde $_{MAX}$	569	m

Lavvannsindekser

Alminnelig lavvannføring	2.2	l/s*km²
5-persentil (år)	2.1	l/s*km²
5-persentil sommer (1/5-30/9)	1.7	l/s*km²
5-persentil vinter (1/10-30/4)	1.8	l/s*km²
Base flow	7.12	l/s*km²
Base flow index (BFI)	0.49	-

Klima- /hydrologiske parametere

Klimaregion	Finnmark	-
Lavvannsperiode	-	-
Avrenning 1961-90 (Q_N)	14.5	l/s*km²
Sommernedbør	226	mm
Vinternedbør	256	mm
Årstemperatur	-0.0	°C
Sommertemperatur	7.5	°C
Vintertemperatur	-5.3	°C
Temperatur juli	11.1	°C
Temperatur august	9.9	°C

Det er generelt stor usikkerhet i beregning av lavvannsindekser. Resultatene må verifiseres mot egne observasjoner eller sammenlignbare målestasjoner.

I nedbørfelt med høy breprosent eller stor innsjøprosent vil tørrværsavrenning (Base flow) ha store bidrag fra disse lagringsmagasinene.

Rapportdato: 2/16/2021 © nevina.nve.no

Appendix B: Mineral abbreviations

Mineral abbreviations after Whitney & Evans (2010*).*

Symbol	Mineral name
Mag	Magnetite
Hem	Hematite
Ilm	Ilmenite
Po	Pyrrhotite
Bn	Bornite
Ccp	Chalcopyrite
Cct	Chalcocite
Py	Pyrite
Cal	Calcite
Dol	Dolomite
Mgs	Magnesite

Appendix C: Bulk chemistry of stream sediments

Table C1: Bulk chemistry of stream sediments. By Bureau Veritas Mineral Laboratories, Vancouver, Canada, method AQ250 (Aqua Regia digestion, Ultratrace ICP-MS).

	Method	AQ250	AQ250	AQ250	AQ250	AQ250	AQ250	AQ250	AQ250	AQ250	AQ250	AQ250	AQ250	AQ250	AQ250	AQ250	AQ250	AQ250	AQ250	AQ250
	Analyte	Mo	Cu	Pb	Zn	Ag	Ni	Co	Mn	Fe	As	U	Au	Th	Sr	Cd	Sb	Bi	V	Ca
	Unit	PPM	PPM	PPM	PPM	PPB	PPM	PPM	PPM	%	PPM	PPM	PPB	PPM	PPM	PPM	PPM	PPM	PPM	%
	MDL	0.01	0.01	0.01	0.1	2	0.1	0.1	1	0.01	0.1	0.1	0.2	0.1	0.5	0.01	0.02	0.02	1	0.01
J001(63)	Sediment Pulp	1.69	32.67	8.64	38.9	42	27.3	10	499	1.63	36.2	12.9	4.4	0.9	14.2	0.16	0.26	0.25	18	0.27
J002(63)	Sediment Pulp	57.46	>10000	64.09	74.2	3549	60.2	24.7	>10000	4.73	47.4	2.7	57.9	3.6	24.7	0.31	1.59	11.85	19	7.02
J003(63)	Sediment Pulp	1.03	35.03	5.27	36	51	27.4	7.2	237	1.43	21.4	11	5.8	1.1	11.7	0.06	0.3	0.18	14	0.29
J004(63)	Sediment Pulp	4.23	26.01	6.15	26.2	20	25.1	9.4	252	2.4	56	3.7	14.1	1.2	9.7	0.02	0.23	0.19	26	0.2
J005(63)	Sediment Pulp	0.32	25.06	4.44	9.8	24	12.9	2.5	24	0.47	2.3	7.2	4.8	0.6	9.7	0.05	0.18	0.14	12	0.21
J006W(wet sieved)	Sediment Pulp	1.34	74.06	15.31	89.6	163	36	11.4	515	1.82	37.7	12.3	5.8	0.6	18.6	0.18	0.31	0.24	20	0.44
J006(63)	Sediment Pulp	1.21	42.18	12.14	57.2	67	29.3	10.5	449	1.74	37.3	11.8	16.5	0.6	15.5	0.15	0.29	0.22	19	0.27
J007(63)	Sediment Pulp	1.53	110.7	17.37	63.4	144	33.7	11.4	666	1.61	31.1	11.2	5.2	0.6	19.8	0.25	0.33	0.26	17	0.3
J008(63)	Sediment Pulp	1.48	47.08	16.94	62.4	67	37.9	11.6	762	1.51	23.1	10.3	5.7	0.5	15.7	0.33	0.29	0.24	16	0.3
J009(63)	Sediment Pulp	1.15	34.02	11.77	44.6	58	29.1	9.9	670	1.19	13	8	4.5	0.5	12.1	0.28	0.24	0.19	14	0.26
J010(63)	Sediment Pulp	0.61	22.31	7.41	32.8	30	21.8	8.2	377	1.2	8.2	3.7	4	0.4	9.1	0.13	0.19	0.15	18	0.23
J011(63)	Sediment Pulp	1.15	27.55	9.44	44.7	61	32.9	10.9	781	1.57	11.9	4.9	4.7	0.9	11.7	0.29	0.22	0.15	20	0.31
J012(63)	Sediment Pulp	2.31	34.22	10.73	48.2	67	38	13.5	832	1.89	22.4	12.2	13.9	0.9	13.9	0.16	0.25	0.21	21	0.33
J013(63)	Sediment Pulp	1.44	89.65	18.33	100.9	88	53.1	21.3	1665	2.81	21	8.3	4.2	1.1	9.4	0.99	0.24	0.23	52	0.35
J014(63)	Sediment Pulp	2.34	40.63	11.24	59.2	61	37.8	18.1	2330	2.02	21.3	4.7	1.8	3.8	10	0.61	0.21	0.17	25	0.27
J015(63)	Sediment Pulp	1.45	34.07	9.35	54.9	44	27.9	10.7	1157	1.47	27.6	5.5	3.7	1.6	11	0.36	0.2	0.16	20	0.32
J016(63)	Sediment Pulp	6.1	172.1	14.09	184.4	151	55.1	21.2	>10000	4.13	74.1	14.8	34.9	2.3	62.5	0.55	0.47	0.28	28	2.54
J017(63)	Sediment Pulp	0.46	35.07	5.87	39.7	37	25.5	10.5	602	1.5	14.2	4	9.8	2.1	7.5	0.23	0.16	0.12	21	0.23
J018(63)	Sediment Pulp	4.27	631.51	15.8	76.6	133	50.7	21.7	1778	2.87	18.8	4.6	4.9	4.4	28.9	0.38	0.31	0.18	30	1.36
J019(63)	Sediment Pulp	0.23	10.47	5.31	12.2	8	10.4	4.4	248	1.32	2.4	1.5	2.4	7	8.4	<0.01	0.19	0.13	10	0.17
J020(63)	Sediment Pulp	0.71	68.06	8.09	38.1	31	24.3	10.6	682	1.58	10.4	3.2	10.9	3.3	9.6	0.15	0.21	0.13	18	0.26
J021(63)	Sediment Pulp	1.2	75.69	7.65	29.2	21	23.5	9	674	1.35	5.9	2.2	1.7	3.5	10.7	0.16	0.2	0.15	15	0.29

Table C1: (Continued).

	Method	AQ250	AQ250	AQ250	AQ250	AQ250	AQ250	AQ250	AQ250	AQ250	AQ250	AQ250	AQ250	AQ250	AQ250	AQ250	AQ250	AQ250
	Analyte	P	La	Cr	Mg	Ba	Ti	B	Al	Na	K	W	Sc	Tl	S	Hg	Se	Te	Ga
	Unit	%	PPM	PPM	%	PPM	%	PPM	%	%	%	PPM	PPM	PPM	%	PPB	PPM	PPM	PPM
	MDL	0.001	0.5	0.5	0.01	0.5	0.001	20	0.01	0.001	0.01	0.1	0.1	0.02	0.02	5	0.1	0.02	0.1
J001(63)	Sediment Pulp	0.114	12.7	27.1	0.29	317.9	0.009	<20	0.98	0.004	0.17	<0.1	1.6	0.12	0.07	42	2.2	0.03	2.8
J002(63)	Sediment Pulp	0.047	16.2	40.5	4.14	398.7	0.014	<20	1.21	0.009	0.08	<0.1	6.9	0.09	0.02	4794	2.7	0.61	3
J003(63)	Sediment Pulp	0.094	13.3	26.9	0.32	244.5	0.01	<20	0.83	0.002	0.12	<0.1	1.4	0.09	0.05	30	0.9	<0.02	2.7
J004(63)	Sediment Pulp	0.091	16.7	31.5	0.36	219.9	0.012	<20	0.87	<0.001	0.14	<0.1	1.7	0.09	0.02	22	0.5	<0.02	3.4
J005(63)	Sediment Pulp	0.062	13.5	26.6	0.18	318.7	0.007	<20	0.96	<0.001	0.08	<0.1	1.2	0.12	0.11	38	1.3	<0.02	2.9
J006W(wet sieved)	Sediment Pulp	0.119	14.2	33.3	0.37	384.6	0.009	<20	1.23	0.063	0.18	<0.1	1.5	0.15	0.08	72	1.5	<0.02	3.7
J006(63)	Sediment Pulp	0.112	14.2	30.3	0.33	344.9	0.009	<20	1.09	0.003	0.16	<0.1	1.3	0.13	0.07	50	1.9	<0.02	3.5
J007(63)	Sediment Pulp	0.094	12.7	29.6	0.36	480.9	0.009	<20	0.98	0.002	0.14	<0.1	1.3	0.12	0.08	136	2.2	0.04	2.8
J008(63)	Sediment Pulp	0.1	12.6	30.5	0.35	259.9	0.01	<20	0.96	0.002	0.15	<0.1	1.1	0.11	0.08	120	2.7	0.04	2.8
J009(63)	Sediment Pulp	0.083	11.4	24.5	0.34	185	0.009	<20	0.8	0.002	0.13	<0.1	0.9	0.1	0.06	73	2.6	0.02	2.2
J010(63)	Sediment Pulp	0.078	14.4	25.1	0.37	130.9	0.011	<20	0.76	0.003	0.13	<0.1	1	0.07	0.05	25	1.7	<0.02	2.4
J011(63)	Sediment Pulp	0.084	14	38.1	0.52	133.3	0.012	<20	0.94	0.004	0.14	<0.1	1.1	0.09	0.06	42	2.4	0.05	2.6
J012(63)	Sediment Pulp	0.108	16.6	50.2	0.58	191.4	0.012	<20	1.11	0.004	0.15	<0.1	1.4	0.09	0.06	59	2.2	0.02	3.1
J013(63)	Sediment Pulp	0.091	16.4	52.3	0.86	162	0.03	<20	1.51	0.004	0.15	<0.1	3.5	0.17	0.07	63	1.7	0.05	4.4
J014(63)	Sediment Pulp	0.076	18.3	30.5	0.51	147.8	0.029	<20	0.86	0.004	0.1	<0.1	1.9	0.11	0.02	23	0.8	0.02	2.4
J015(63)	Sediment Pulp	0.087	16.5	26.9	0.46	146.4	0.021	<20	0.86	0.004	0.12	<0.1	1.5	0.1	0.04	38	1.1	0.02	2.2
J016(63)	Sediment Pulp	0.214	57.3	27.7	1.46	1110.4	0.015	<20	1.57	0.005	0.05	<0.1	6.5	0.09	0.14	161	5.4	0.06	2
J017(63)	Sediment Pulp	0.068	15.6	24.3	0.44	82.4	0.023	<20	0.73	0.001	0.09	<0.1	1.8	0.06	0.03	14	0.6	<0.02	2.1
J018(63)	Sediment Pulp	0.08	17.4	55.9	1.08	325.7	0.052	<20	1.21	0.01	0.14	0.1	6.6	0.11	0.12	49	1.7	0.12	3.2
J019(63)	Sediment Pulp	0.058	21.7	15.4	0.21	78.1	0.03	<20	0.36	0.002	0.08	<0.1	0.6	0.04	<0.02	<5	<0.1	0.03	1
J020(63)	Sediment Pulp	0.064	19.1	23.8	0.46	160.6	0.025	<20	0.79	0.004	0.13	<0.1	1.9	0.08	0.02	15	0.4	0.03	2.3
J021(63)	Sediment Pulp	0.057	18.4	24.5	0.4	174.7	0.026	<20	0.66	0.002	0.12	<0.1	1.4	0.09	0.02	15	0.3	0.02	1.9

Table C1: (Continued).

	Method	AQ250	AQ250	AQ250	AQ250	AQ250	AQ250	AQ250	AQ250	AQ250	AQ250	AQ250	AQ250	AQ250	AQ250	AQ250	AQ250	AQ250	AQ250	AQ250
	Analyte	Mo	Cu	Pb	Zn	Ag	Ni	Co	Mn	Fe	As	U	Au	Th	Sr	Cd	Sb	Bi	V	Ca
	Unit	PPM	PPM	PPM	PPM	PPB	PPM	PPM	PPM	%	PPM	PPM	PPB	PPM	PPM	PPM	PPM	PPM	PPM	%
	MDL	0.01	0.01	0.01	0.1	2	0.1	0.1	1	0.01	0.1	0.1	0.2	0.1	0.5	0.01	0.02	0.02	1	0.01
J022(63)	Sediment Pulp	0.54	62.05	8.02	33.8	24	21.9	9.4	638	1.29	6	2.6	7.1	3.3	9.8	0.21	0.2	0.22	15	0.25
J023(63)	Sediment Pulp	1.3	61.14	10.29	46	105	31.2	11.6	998	1.66	12.2	6	2.1	2.2	11.6	0.27	0.27	0.17	21	0.34
J024(63)	Sediment Pulp	2.14	91.41	12.88	80.3	91	47.3	19.4	1347	2.08	19	4.4	7.1	2.5	12	0.75	0.37	0.17	42	0.41
J025(63)	Sediment Pulp	0.58	64.06	10.22	55.1	77	29.8	14.5	803	1.74	13.9	3.7	13.6	2.2	11	0.49	0.27	0.18	32	0.32
J026S(63)	Sediment Pulp	3.33	254.28	44.63	380.3	338	107.5	57.2	3276	7.7	79.9	5.9	3.9	2.6	22.6	2.37	0.78	0.21	196	1.1
J027(63)	Sediment Pulp	0.53	49.35	7.77	33.2	36	22.4	9.8	1009	1.32	8.1	3.2	1.9	1.7	9	0.23	0.17	0.13	18	0.27
J028(63)	Sediment Pulp	1.48	20.82	7.91	38.1	31	22.7	9.2	905	1.38	9.8	2.7	2.4	3.1	17.8	0.1	0.25	0.13	13	0.34
J029(63)	Sediment Pulp	1.01	22.17	8.32	36.6	22	24.6	9.4	787	1.39	8.4	2.1	2.8	2.9	16	0.08	0.22	0.24	14	0.3
J030(63)	Sediment Pulp	0.48	21.79	6.34	38.7	33	18.7	8.2	481	1.22	5.7	1.8	93	2.8	13	0.12	0.25	0.15	13	0.28
J031(63)	Sediment Pulp	3.54	27.75	8.88	81.2	45	24.9	18.1	3433	4.44	43.5	4.3	2.8	3.3	21.9	0.6	0.25	0.16	34	0.49
J032(63)	Sediment Pulp	0.67	72.95	9.48	60.8	58	34.5	16.6	985	1.94	10.6	4.2	3.6	2.4	10.9	0.6	0.3	0.18	36	0.37
J033(63)	Sediment Pulp	1.33	126.62	11.74	66.7	101	47.1	23.5	1565	2.33	17.2	5	6.5	2.5	11.7	0.73	0.4	0.32	47	0.38
J034(63)	Sediment Pulp	1.96	134.84	8.56	110.7	61	56	24.3	1281	3.16	21.5	2.4	2.9	4.6	9.3	0.56	0.27	0.2	61	0.37
J035(63)	Sediment Pulp	1.16	87.14	6.88	65.6	65	53.5	19.1	799	2.28	12.7	2.2	4.8	3.6	9.8	0.53	0.3	0.19	42	0.62
J036(63)	Sediment Pulp	1.93	104.93	9.09	69.3	68	62.7	24.9	1320	2.84	17.4	4	3.4	3.9	11	0.45	0.36	0.29	51	0.44
J037(63)	Sediment Pulp	1.7	42.66	8.88	85.5	100	44	18.8	3523	2.79	19.5	3	1.2	4.5	25.5	0.65	0.22	0.15	29	0.71
J038(63)	Sediment Pulp	1.45	70.19	14.07	101.9	67	30.9	17	2083	2.47	19.7	4.3	2.9	3.3	26	0.34	0.27	0.16	33	0.72
J039(63)	Sediment Pulp	1.36	995.42	8.85	174.6	118	61.5	31.8	1639	3.65	16.7	2.1	54.2	4.3	18.9	0.37	0.21	0.34	83	0.64
J040(63)	Sediment Pulp	1.42	67.39	2.72	63.5	20	42.6	13.5	453	2.7	13.7	1.6	<0.2	4.6	12.8	0.03	0.14	0.09	26	0.27
J041(63)	Sediment Pulp	5.74	474.81	11.19	220.7	146	64.7	25.1	5927	6.34	106.9	11.1	4.1	3.8	47.4	0.82	0.4	0.24	55	1.26
J042(63)	Sediment Pulp	2.17	108.47	10.97	78.7	42	35.6	18.2	1557	3.06	20.6	4.2	2	4.9	23.4	0.11	0.11	0.09	43	0.59
J043(63)	Sediment Pulp	0.8	156.38	3.98	26.1	144	14.9	7	432	1.2	13.8	24	6.9	1.6	27.3	0.02	0.17	0.09	19	0.79
J044(63)	Sediment Pulp	2.03	178.89	7.59	77.6	58	52	31.6	1289	3.79	16.8	2.2	2.8	4.1	23.6	0.13	0.1	0.09	74	1.04

Table C1: (Continued).

	Method	AQ250	AQ250	AQ250	AQ250	AQ250	AQ250	AQ250	AQ250	AQ250	AQ250	AQ250	AQ250	AQ250	AQ250	AQ250	AQ250	AQ250	AQ250
	Analyte	P	La	Cr	Mg	Ba	Ti	B	Al	Na	K	W	Sc	Tl	S	Hg	Se	Te	Ga
	Unit	%	PPM	PPM	%	PPM	%	PPM	%	%	%	PPM	PPM	PPM	%	PPB	PPM	PPM	PPM
	MDL	0.001	0.5	0.5	0.01	0.5	0.001	20	0.01	0.001	0.01	0.1	0.1	0.02	0.02	5	0.1	0.02	0.1
J022(63)	Sediment Pulp	0.064	19.5	20.2	0.39	175.2	0.024	<20	0.63	0.002	0.11	<0.1	1.4	0.09	0.02	12	0.4	<0.02	1.8
J023(63)	Sediment Pulp	0.082	18.3	32.8	0.55	197.8	0.022	<20	0.93	0.005	0.16	<0.1	1.9	0.1	0.04	19	1.5	0.02	2.4
J024(63)	Sediment Pulp	0.074	17.6	47	0.87	207.5	0.029	<20	1.16	0.007	0.16	<0.1	3.6	0.14	0.06	44	1.6	0.05	3.5
J025(63)	Sediment Pulp	0.078	16.5	29.8	0.66	166.3	0.025	<20	0.94	0.005	0.14	<0.1	2.7	0.09	0.05	27	1.5	0.06	2.7
J026S(63)	Sediment Pulp	0.067	14.8	122.3	3.6	287.7	0.101	<20	3.3	0.007	0.14	<0.1	20.7	0.22	0.18	135	2.7	0.17	10.7
J027(63)	Sediment Pulp	0.06	14.4	21.1	0.43	175.7	0.019	<20	0.72	0.002	0.11	<0.1	1.2	0.09	0.03	10	0.8	0.02	1.9
J028(63)	Sediment Pulp	0.057	18.2	27	0.5	356.4	0.026	<20	0.74	0.006	0.13	4.5	1.3	0.09	0.02	13	0.7	0.03	2
J029(63)	Sediment Pulp	0.056	19.6	25.1	0.45	341.7	0.026	<20	0.81	0.006	0.16	3.3	1.4	0.1	<0.02	17	0.5	0.03	2.1
J030(63)	Sediment Pulp	0.055	17.2	20.4	0.35	252.4	0.03	<20	0.64	0.005	0.12	2.7	1.4	0.09	0.02	12	0.7	0.02	1.9
J031(63)	Sediment Pulp	0.076	20.6	25.7	0.37	332.1	0.026	<20	0.93	0.005	0.11	2.1	1.8	0.14	0.07	36	2.8	0.04	2.1
J032(63)	Sediment Pulp	0.071	16.3	32.7	0.71	165.6	0.03	<20	0.99	0.003	0.13	<0.1	2.7	0.11	0.06	46	1.5	0.06	2.8
J033(63)	Sediment Pulp	0.078	15.6	43.9	0.89	185	0.033	<20	1.16	0.005	0.15	<0.1	3.6	0.13	0.09	56	2.2	0.08	3.3
J034(63)	Sediment Pulp	0.069	14.3	60.7	1.18	201.8	0.06	<20	1.34	0.005	0.12	<0.1	4.7	0.1	0.06	22	0.9	0.07	4.2
J035(63)	Sediment Pulp	0.061	12.9	44.5	0.83	133.1	0.041	<20	1.01	0.005	0.11	<0.1	3.1	0.1	0.07	17	1.1	0.16	3
J036(63)	Sediment Pulp	0.072	15	55.5	0.95	151.2	0.049	<20	1.2	0.01	0.16	0.1	4	0.11	0.13	31	2	0.11	3.8
J037(63)	Sediment Pulp	0.084	19.8	28.4	1.45	381.7	0.028	<20	1.44	0.007	0.14	2.3	4.5	0.15	0.08	52	2.6	0.07	3.8
J038(63)	Sediment Pulp	0.081	22.3	37.1	0.66	367	0.037	<20	1.21	0.009	0.2	3.8	3	0.22	0.08	62	3	0.05	3
J039(63)	Sediment Pulp	0.067	15.2	61.3	1.06	287.7	0.092	<20	1.52	0.009	0.22	1.1	5.5	0.21	0.12	29	1.8	0.07	5.1
J040(63)	Sediment Pulp	0.076	16.9	36	1.45	112.4	0.039	25	1.22	0.009	0.08	<0.1	2.8	0.06	0.02	6	0.2	<0.02	3.4
J041(63)	Sediment Pulp	0.121	33.3	44	0.64	729.7	0.028	<20	1.84	0.008	0.14	1.2	5.4	0.18	0.17	134	6.2	0.09	3.2
J042(63)	Sediment Pulp	0.077	23.1	43	0.88	273.1	0.096	<20	1.38	0.011	0.31	0.2	3.5	0.32	0.04	17	0.8	0.03	4.7
J043(63)	Sediment Pulp	0.112	43.2	31.8	0.44	183.2	0.018	<20	1.1	0.007	0.09	<0.1	3.3	0.12	0.09	177	2.2	<0.02	2.7
J044(63)	Sediment Pulp	0.072	14.5	130.3	1.53	242.9	0.111	<20	1.51	0.011	0.24	0.2	7.5	0.22	0.06	25	0.9	0.03	6.3

Table C1: (Continued).

	Method	AQ250	AQ250	AQ250	AQ250	AQ250	AQ250	AQ250	AQ250	AQ250	AQ250	AQ250	AQ250	AQ250	AQ250	AQ250	AQ250	AQ250	AQ250	AQ250
	Analyte	Mo	Cu	Pb	Zn	Ag	Ni	Co	Mn	Fe	As	U	Au	Th	Sr	Cd	Sb	Bi	V	Ca
	Unit	PPM	PPM	PPM	PPM	PPB	PPM	PPM	PPM	%	PPM	PPM	PPB	PPM	PPM	PPM	PPM	PPM	PPM	%
	MDL	0.01	0.01	0.01	0.1	2	0.1	0.1	1	0.01	0.1	0.1	0.2	0.1	0.5	0.01	0.02	0.02	1	0.01
J001(125-250)	Sediment Pulp	1.01	27.29	6.63	32.9	68	18.9	8.2	244	1.32	28.3	6.2	0.8	0.9	7.1	0.04	0.19	0.12	14	0.18
J002(125-250)	Sediment Pulp	44.05	>10000.00	16.45	53.5	4004	51.2	16.3	5852	3.28	15.7	1.8	20.7	3	24.5	0.12	0.59	17.1	13	6.45
J003(125-250)	Sediment Pulp	0.23	7.09	1.95	12.9	37	9.7	2.8	46	0.73	5.2	1.1	1.7	2.4	3.7	<0.01	0.14	0.07	6	0.07
J004(125-250)	Sediment Pulp	1.1	10.66	2.66	14	34	11.8	4.7	88	1.25	19.9	1	4.8	3.7	2.9	<0.01	0.2	0.08	12	0.06
J005(125-250)	Sediment Pulp	0.13	22.04	2.6	13.1	47	14.5	2.8	26	0.56	1.7	3	0.8	1.5	4.2	0.02	0.15	0.08	7	0.16
J006(125-250)	Sediment Pulp	0.35	12.33	5.3	27.6	35	11.6	4.6	114	0.96	13.6	2.4	1.3	1.1	4.2	0.02	0.15	0.07	10	0.09
J007(125-250)	Sediment Pulp	0.62	144.11	9.2	43	119	21.8	8.2	267	1.28	18.2	4.6	6.4	1	11.7	0.1	0.43	0.15	12	0.16
J008(125-250)	Sediment Pulp	0.32	40.34	8	37.1	45	21.6	7.5	290	1.22	10.9	4.1	<0.2	0.8	6.1	0.13	0.21	0.12	12	0.16
J009(125-250)	Sediment Pulp	0.29	18.24	5.64	26.2	39	16.3	5.5	209	1	6.9	3	<0.2	1.2	4.9	0.08	0.2	0.08	10	0.12
J010(125-250)	Sediment Pulp	0.17	10.7	3.18	17.6	39	12.1	4.4	87	0.9	4.7	1	<0.2	2	3.4	<0.01	0.15	0.05	10	0.08
J011(125-250)	Sediment Pulp	0.21	8.8	3.18	20.3	28	14.4	6.5	152	1.14	4	0.8	<0.2	2.8	3.3	<0.01	0.13	0.04	10	0.07
J012(125-250)	Sediment Pulp	0.31	14.66	4.17	23.8	27	16.5	6.4	205	1.59	6.9	2.1	0.2	3.3	4.8	0.02	0.18	0.09	15	0.11
J013(125-250)	Sediment Pulp	0.43	25.71	3.94	29.4	62	20.1	7.3	385	1.11	8.1	2.1	<0.2	2.5	5.4	0.16	0.18	0.07	12	0.14
J014(125-250)	Sediment Pulp	0.28	14.66	2.57	19.6	33	13.9	5.3	336	0.91	4.2	1	<0.2	3.4	4.1	0.08	0.14	0.06	7	0.09
J015(125-250)	Sediment Pulp	0.14	9.07	2.7	17.5	36	11.8	4	134	1	6.5	1.1	<0.2	3.9	5.8	0.02	1.44	0.06	10	0.11
J016(125-250)	Sediment Pulp	1.84	104.11	4.5	66.1	86	27	9.7	3790	1.86	23.9	4.3	1.8	2.1	18.5	0.17	0.19	0.32	15	1.34
J017(125-250)	Sediment Pulp	0.22	22.04	2.72	21.8	36	15.6	5.9	215	0.88	7.4	1.8	<0.2	2.7	4.3	0.09	0.13	0.04	9	0.1
J018(125-250)	Sediment Pulp	0.3	216.99	16.66	19	43	14.6	9.6	262	1.03	4.4	0.9	2.5	3	5.4	0.02	0.13	0.05	9	0.29
J019(125-250)	Sediment Pulp	0.07	8.01	2.26	10.6	34	10.3	3.8	112	0.84	1.4	0.7	<0.2	4.1	3.7	<0.01	0.13	0.07	7	0.07
J020(125-250)	Sediment Pulp	0.17	27.87	2.95	17.6	45	12.7	4.8	180	1.13	2.6	1	<0.2	4.3	6.2	0.02	0.19	0.06	11	0.1
J021(125-250)	Sediment Pulp	0.19	25.6	3.17	15.6	33	12.8	5.2	143	1.2	2.3	1	0.2	4.4	6.2	<0.01	0.18	0.08	12	0.11
J022(125-250)	Sediment Pulp	0.09	31.22	2.68	16.4	44	12.8	4.8	161	0.88	2	0.9	<0.2	3.9	5	0.02	0.16	0.05	9	0.1

Table C1: (Continued).

	Method	AQ250	AQ250	AQ250	AQ250	AQ250	AQ250	AQ250	AQ250	AQ250	AQ250	AQ250	AQ250	AQ250	AQ250	AQ250	AQ250	AQ250
	Analyte	P	La	Cr	Mg	Ba	Ti	B	Al	Na	K	W	Sc	Tl	S	Hg	Se	Te	Ga
	Unit	%	PPM	PPM	%	PPM	%	PPM	%	%	%	PPM	PPM	PPM	%	PPB	PPM	PPM	PPM
	MDL	0.001	0.5	0.5	0.01	0.5	0.001	20	0.01	0.001	0.01	0.1	0.1	0.02	0.02	5	0.1	0.02	0.1
J001(125-250)	Sediment Pulp	0.067	13.5	18.6	0.24	209	0.01	<20	0.7	0.008	0.15	<0.1	1.3	0.11	0.03	21	1	<0.02	2.4
J002(125-250)	Sediment Pulp	0.021	7.2	30.4	4.32	302.1	0.006	<20	1.03	0.019	0.06	<0.1	4	0.04	0.11	735	5.3	0.38	2.7
J003(125-250)	Sediment Pulp	0.019	11.6	9.1	0.2	43.9	0.012	<20	0.3	0.005	0.11	<0.1	0.6	0.04	<0.02	<5	<0.1	<0.02	0.9
J004(125-250)	Sediment Pulp	0.022	12.8	13.2	0.2	47.6	0.016	<20	0.37	0.005	0.13	<0.1	0.9	0.05	<0.02	<5	0.1	<0.02	1.2
J005(125-250)	Sediment Pulp	0.028	10.4	14.5	0.22	115.6	0.009	<20	0.55	0.002	0.08	<0.1	0.9	0.07	0.05	14	0.6	<0.02	1.6
J006(125-250)	Sediment Pulp	0.024	10.8	12.3	0.2	122	0.011	<20	0.48	0.005	0.12	<0.1	0.9	0.06	<0.02	<5	0.3	<0.02	1.6
J007(125-250)	Sediment Pulp	0.044	12.4	18.5	0.3	335.3	0.011	<20	0.63	0.005	0.13	<0.1	1	0.08	0.04	47	0.8	<0.02	1.8
J008(125-250)	Sediment Pulp	0.042	11.9	18	0.28	126.6	0.012	<20	0.6	0.004	0.14	<0.1	0.9	0.07	0.03	49	1	<0.02	1.7
J009(125-250)	Sediment Pulp	0.03	12.5	15.4	0.24	91.6	0.013	<20	0.48	0.003	0.12	<0.1	1	0.06	<0.02	14	0.8	<0.02	1.6
J010(125-250)	Sediment Pulp	0.017	12.2	12.4	0.24	53.4	0.014	<20	0.41	0.004	0.12	<0.1	0.8	0.05	<0.02	<5	0.1	<0.02	1.3
J011(125-250)	Sediment Pulp	0.016	12.5	18.5	0.33	42.4	0.015	<20	0.48	0.003	0.12	<0.1	0.8	0.05	<0.02	<5	<0.1	<0.02	1.4
J012(125-250)	Sediment Pulp	0.025	13.5	26.3	0.38	70.8	0.017	<20	0.61	0.004	0.15	<0.1	0.9	0.06	<0.02	<5	0.4	<0.02	1.8
J013(125-250)	Sediment Pulp	0.034	12.3	16.1	0.35	49.6	0.016	<20	0.52	0.006	0.12	<0.1	1.2	0.06	<0.02	6	0.3	<0.02	1.3
J014(125-250)	Sediment Pulp	0.026	11.9	11.9	0.27	39.3	0.015	<20	0.35	0.003	0.08	<0.1	0.6	0.03	<0.02	<5	<0.1	<0.02	1
J015(125-250)	Sediment Pulp	0.027	11.7	12.4	0.24	44.8	0.02	<20	0.37	0.005	0.12	<0.1	0.8	0.04	<0.02	<5	0.2	<0.02	1
J016(125-250)	Sediment Pulp	0.094	17	13.8	1.09	310.5	0.012	<20	0.77	0.005	0.06	<0.1	2.4	0.03	0.09	38	1.5	<0.02	1.6
J017(125-250)	Sediment Pulp	0.027	12.1	12.6	0.3	50.5	0.015	<20	0.45	0.004	0.11	<0.1	1.1	0.05	<0.02	8	0.1	<0.02	1.3
J018(125-250)	Sediment Pulp	0.026	11	11.5	0.35	60.4	0.016	<20	0.37	0.004	0.08	<0.1	1.4	0.04	0.05	<5	0.5	0.02	1
J019(125-250)	Sediment Pulp	0.019	13.2	10	0.21	38.5	0.017	<20	0.31	0.004	0.12	<0.1	0.7	0.04	<0.02	<5	<0.1	<0.02	0.8
J020(125-250)	Sediment Pulp	0.023	14.5	15.6	0.28	97.6	0.023	<20	0.43	0.007	0.15	<0.1	1	0.06	<0.02	<5	<0.1	<0.02	1.1
J021(125-250)	Sediment Pulp	0.024	14.5	15.8	0.27	90.8	0.027	<20	0.43	0.008	0.15	<0.1	1	0.05	<0.02	<5	<0.1	<0.02	1.2
J022(125-250)	Sediment Pulp	0.02	12.9	12	0.29	83.3	0.018	<20	0.44	0.006	0.15	<0.1	1.1	0.05	<0.02	<5	<0.1	<0.02	1.1

Table C1: (Continued).

	Method	AQ250	AQ250	AQ250	AQ250	AQ250	AQ250	AQ250	AQ250	AQ250	AQ250	AQ250	AQ250	AQ250	AQ250	AQ250	AQ250	AQ250	AQ250	AQ250
	Analyte	Mo	Cu	Pb	Zn	Ag	Ni	Co	Mn	Fe	As	U	Au	Th	Sr	Cd	Sb	Bi	V	Ca
	Unit	PPM	PPM	PPM	PPM	PPB	PPM	PPM	PPM	%	PPM	PPM	PPB	PPM	PPM	PPM	PPM	PPM	PPM	%
	MDL	0.01	0.01	0.01	0.1	2	0.1	0.1	1	0.01	0.1	0.1	0.2	0.1	0.5	0.01	0.02	0.02	1	0.01
J023(125-250)	Sediment Pulp	0.15	36.32	2.97	16.1	47	12.5	5.4	189	1.3	2.4	1	<0.2	4.5	6.8	<0.01	0.19	0.07	13	0.11
J024(125-250)	Sediment Pulp	0.59	60.53	3.88	40.6	74	23.5	9.2	287	1.56	27.8	2.1	34.7	4.3	6.6	0.11	0.25	0.78	26	0.2
J025(125-250)	Sediment Pulp	0.26	45.12	3.73	33.3	47	21.5	9.4	221	1.72	7.7	1.6	0.8	3.9	6.2	0.06	0.21	0.06	28	0.16
J026S(125-250)	Sediment Pulp	1.15	201.12	15.4	174.4	197	78.6	40.8	1195	6	39.4	1.4	1.2	2.5	12	0.6	0.54	0.08	145	0.79
J027(125-250)	Sediment Pulp	0.11	27.18	2.42	15.8	50	12.3	4.9	134	0.99	2.1	0.9	2.7	3.2	5	0.04	0.17	0.12	10	0.1
J028(125-250)	Sediment Pulp	0.3	10.84	2.8	15.6	60	12.1	5.1	154	0.96	2.6	0.8	2	3.7	6.8	<0.01	0.17	0.1	9	0.11
J029(125-250)	Sediment Pulp	0.2	9.24	2.96	13.6	49	9.9	3.6	157	1.05	2.6	0.9	3.2	3.8	6.3	0.02	0.18	0.08	10	0.1
J030(125-250)	Sediment Pulp	0.15	10.89	2.32	15.9	31	10	3.5	136	0.68	2.7	0.7	1.5	2.8	4.4	0.02	0.14	0.17	6	0.11
J031(125-250)	Sediment Pulp	0.35	6.77	2.55	14.8	25	7.3	3.4	221	1.11	5	0.8	3.7	3	4.8	0.04	0.15	0.07	10	0.09
J032(125-250)	Sediment Pulp	0.14	33.68	3.25	25.7	50	19.4	9.9	214	1.54	5.2	1.2	1.7	3.6	5.4	0.05	0.19	0.06	24	0.13
J033(125-250)	Sediment Pulp	0.27	45.54	3.09	29.9	56	21	9.6	256	1.74	5.6	1.4	1	3.4	4.4	0.09	0.18	0.06	29	0.14
J034(125-250)	Sediment Pulp	0.2	45.36	2.86	24.4	30	18	9.4	216	1.32	4.9	0.7	1.8	3.5	4	0.06	0.16	0.12	20	0.11
J035(125-250)	Sediment Pulp	0.23	45.5	3.07	27.5	76	28.4	9.8	214	1.59	4.8	0.8	3	3.3	4.5	0.04	0.21	0.09	27	0.18
J036(125-250)	Sediment Pulp	0.2	27.45	2.83	27.8	41	25.5	11.5	247	1.98	7.5	0.9	5.5	3.7	4.7	<0.01	0.27	0.12	31	0.15
J037(125-250)	Sediment Pulp	0.25	22.93	4.25	21	111	14.7	5.3	428	1.21	3.8	0.7	2.5	10.4	6.6	0.03	0.17	0.09	12	0.18
J038(125-250)	Sediment Pulp	0.27	28.25	3.77	26.6	62	13.6	8.2	256	1.75	4.1	1	2.7	4.1	8.5	<0.01	0.13	0.08	26	0.2
J039(125-250)	Sediment Pulp	0.24	440.47	2.95	40	70	24.5	14.2	321	2.11	4.8	0.7	8.4	3.7	8	0.03	0.13	0.14	39	0.22
J040(125-250)	Sediment Pulp	0.4	27.28	1.38	23.1	25	16.1	5	149	1.05	3.7	0.7	<0.2	3.1	5.5	<0.01	0.09	0.06	11	0.11
J041(125-250)	Sediment Pulp	0.88	161.66	2.05	39.2	48	20	7.3	864	1.57	11.4	1.6	<0.2	2.6	7	0.11	0.11	0.08	23	0.21
J042(125-250)	Sediment Pulp	0.42	43.24	4.8	25.1	44	16.1	7.9	318	1.62	5.3	1	<0.2	3.7	15.5	0.02	0.07	0.05	29	0.25
J043(125-250)	Sediment Pulp	0.29	53.79	2.04	12.6	71	9.2	4.4	222	0.83	5.1	6.7	2.4	1.7	9.8	0.02	0.11	0.05	12	0.27
J044(125-250)	Sediment Pulp	0.26	118.91	3.23	23.5	72	30.7	34.7	301	5.48	5.9	0.8	1.2	3.6	13.8	<0.01	0.1	0.05	110	0.3

Table C1: (Continued).

	Method	AQ250	AQ250	AQ250	AQ250	AQ250	AQ250	AQ250	AQ250	AQ250	AQ250	AQ250	AQ250	AQ250	AQ250	AQ250	AQ250	AQ250	AQ250
	Analyte	P	La	Cr	Mg	Ba	Ti	B	Al	Na	K	W	Sc	Tl	S	Hg	Se	Te	Ga
	Unit	%	PPM	PPM	%	PPM	%	PPM	%	%	%	PPM	PPM	PPM	%	PPB	PPM	PPM	PPM
	MDL	0.001	0.5	0.5	0.01	0.5	0.001	20	0.01	0.001	0.01	0.1	0.1	0.02	0.02	5	0.1	0.02	0.1
J023(125-250)	Sediment Pulp	0.032	14	17.3	0.26	76.5	0.027	<20	0.37	0.006	0.12	<0.1	0.8	0.05	<0.02	<5	<0.1	<0.02	0.9
J024(125-250)	Sediment Pulp	0.031	12.2	26.2	0.63	75	0.036	<20	0.7	0.008	0.15	<0.1	2.7	0.07	0.02	10	0.3	0.03	2.2
J025(125-250)	Sediment Pulp	0.031	10.4	24.1	0.6	72	0.036	<20	0.65	0.005	0.11	<0.1	2.4	0.05	0.03	<5	0.4	<0.02	2.1
J026S(125-250)	Sediment Pulp	0.032	7	94.4	3.22	129.7	0.095	<20	2.66	0.008	0.08	<0.1	14.1	0.11	0.19	32	0.6	0.09	8.8
J027(125-250)	Sediment Pulp	0.028	12.3	12.7	0.28	52.6	0.021	<20	0.39	0.006	0.12	<0.1	1	0.06	<0.02	<5	<0.1	<0.02	1.1
J028(125-250)	Sediment Pulp	0.022	11.5	15.3	0.28	126.4	0.024	<20	0.4	0.009	0.13	0.2	0.9	0.06	<0.02	<5	<0.1	<0.02	1.1
J029(125-250)	Sediment Pulp	0.021	11.7	14.9	0.22	106.7	0.025	<20	0.36	0.008	0.13	1.2	0.9	0.06	<0.02	6	<0.1	0.02	0.9
J030(125-250)	Sediment Pulp	0.021	9.9	9.8	0.2	63.4	0.015	<20	0.28	0.005	0.07	0.6	0.7	0.04	<0.02	<5	0.2	0.02	0.8
J031(125-250)	Sediment Pulp	0.018	10.8	10	0.19	57.9	0.023	<20	0.26	0.008	0.07	0.2	0.6	0.04	<0.02	<5	<0.1	<0.02	0.7
J032(125-250)	Sediment Pulp	0.025	12	21.8	0.48	79.2	0.034	<20	0.59	0.009	0.14	<0.1	1.8	0.07	0.04	<5	0.2	0.03	1.7
J033(125-250)	Sediment Pulp	0.027	10.4	23.2	0.59	65	0.033	<20	0.64	0.007	0.11	<0.1	2	0.05	0.04	<5	0.2	0.02	2
J034(125-250)	Sediment Pulp	0.023	9.4	18.5	0.47	59.3	0.031	<20	0.52	0.006	0.1	<0.1	1.6	0.05	0.03	<5	0.1	<0.02	1.7
J035(125-250)	Sediment Pulp	0.025	10.6	23.5	0.52	73.6	0.043	<20	0.65	0.009	0.16	<0.1	2.2	0.06	0.03	<5	0.2	0.03	2
J036(125-250)	Sediment Pulp	0.025	10.6	26.9	0.49	56.8	0.044	<20	0.62	0.006	0.15	<0.1	2.3	0.07	0.15	<5	0.9	0.05	1.8
J037(125-250)	Sediment Pulp	0.023	8.6	13.2	0.56	58.7	0.023	<20	0.55	0.007	0.11	0.1	1.8	0.05	0.03	<5	0.1	0.02	1.5
J038(125-250)	Sediment Pulp	0.025	13.5	21.2	0.29	53.9	0.043	<20	0.45	0.012	0.11	0.2	1.6	0.06	<0.02	8	0.3	<0.02	1.7
J039(125-250)	Sediment Pulp	0.022	8.9	27.4	0.55	63.8	0.073	<20	0.7	0.013	0.13	0.1	2.5	0.07	0.15	<5	0.2	0.04	2.3
J040(125-250)	Sediment Pulp	0.023	9.1	13.9	0.53	49.9	0.022	<20	0.5	0.006	0.07	<0.1	1.1	0.05	<0.02	<5	0.1	0.03	1.4
J041(125-250)	Sediment Pulp	0.024	8.9	19	0.43	113.8	0.035	<20	0.57	0.008	0.07	<0.1	1.6	0.06	<0.02	10	0.3	0.03	1.7
J042(125-250)	Sediment Pulp	0.024	11.5	21.6	0.38	74.8	0.078	<20	0.63	0.026	0.16	<0.1	2.4	0.1	<0.02	<5	0.2	<0.02	2.3
J043(125-250)	Sediment Pulp	0.039	16.8	13.2	0.22	64.5	0.015	<20	0.45	0.008	0.08	<0.1	1.7	0.06	0.03	41	0.7	<0.02	1.2
J044(125-250)	Sediment Pulp	0.028	9.3	198.3	0.63	143.2	0.078	<20	0.7	0.024	0.13	<0.1	3.1	0.06	0.18	<5	0.5	0.04	3

Appendix D: SEM-EDS analyses of heavy minerals separated from stream sediments

(Appendix is available in an electronic form at https://munin.uit.no/)

Appendix E: K-S test for normality

Table E1: Results from Lilliefors corrected Kolmogorov-Smirnov test for normal distribution. Values in red are where $\rho > 0.05$ and elements follow normal distribution at the significance level of $\alpha = 0.05$.

Fraction <63 µm				Fraction 125-250 µm			
Element	Statistic	n	K-S p	Element	Statistic	n	K-S p
Mo	0.195	41	0.000	Mo	0.242	41	0.000
Cu	0.325	41	0.000	Cu	0.346	41	0.000
Pb	0.128	41	0.087	Pb	0.266	41	0.000
Zn	0.162	41	0.009	Zn	0.129	41	0.084
Ag	0.173	41	0.003	Ag	0.195	41	0.000
Ni	0.128	41	0.087	Ni	0.138	41	0.049
Co	0.195	41	0.000	Co	0.223	41	0.000
Mn	0.193	41	0.001	Mn	0.153	41	0.017
Fe	0.173	41	0.004	Fe	0.211	41	0.000
As	0.259	41	0.000	As	0.256	41	0.000
U	0.242	41	0.000	U	0.278	41	0.000
Au	0.341	41	0.000	Au	0.337	41	0.000
Th	0.110	41	,200*	Th	0.182	41	0.002
Sr	0.215	41	0.000	Sr	0.196	41	0.000
Cd	0.148	41	0.023	Cd	0.248	41	0.000
Sb	0.086	41	,200*	Sb	0.383	41	0.000
Bi	0.124	41	0.115	Bi	0.323	41	0.000
V	0.212	41	0.000	V	0.261	41	0.000
Ca	0.273	41	0.000	Ca	0.209	41	0.000
P	0.120	41	0.143	P	0.224	41	0.000
La	0.198	41	0.000	La	0.083	41	,200*
Cr	0.209	41	0.000	Cr	0.390	41	0.000
Mg	0.181	41	0.002	Mg	0.216	41	0.000
Ba	0.158	41	0.011	Ba	0.211	41	0.000
Ti	0.258	41	0.000	Ti	0.184	41	0.001
Al	0.121	41	0.135	Al	0.098	41	,200*
Na	0.166	41	0.006	Na	0.253	41	0.000
K	0.199	41	0.000	K	0.152	41	0.018
Sc	0.233	41	0.000	Sc	0.224	41	0.000
Tl	0.218	41	0.000	Tl	0.217	41	0.000
S	0.114	41	0.200	S	0.317	41	0.000
Hg	0.176	41	0.003	Hg	0.373	41	0.000
Se	0.110	41	,200*	Se	0.228	41	0.000
Te	0.210	41	0.000	Te	0.403	41	0.000
Ga	0.116	41	0.188	Ga	0.109	41	,200*

** This is a lower bound of true significance*

Appendix F: LA-ICP-MS analyses of heavy minerals separated from stream sediments

(Appendix is available in an electronic form at https://munin.uit.no/)

.